Semi-Annual Technical Report No. 2

1 April 1979 - 30 September 1979

(1)

ARPA Order:	3291-21
Program Code:	9D60
Contractor:	Saint Louis University
Effective Date of Contract:	1 October 1978
Contract Expiration Date:	30 September 1980
Amount of Contract:	$165,000
Contract Number:	F49620-79-C-0025
Principal Investigators:	Otto W. Nuttli Brian J. Mitchell
Phone:	314-658-3124 or 3123
Program Manager:	Brian J. Mitchell
Phone:	314-658-3123
Short Title:	Research in Seismology

Sponsored by

Advanced Research Projects Agency (DOD)

ARPA Order No. 3291-21

Monitored by AFOSR under Contract #49620-79-C-0025

The views and conclusions contained in this document are those of the authors and should not be interpreted as necessarily representing the official policies, either expressed or implied, of the Defense Advanced Research Projects Agency of the U.S. Government.

Table of Contents

Technical Report Summary

Research done during the time period covered by this report was concerned with observational and theoretical aspects of the attenuation of short-period seismic phases in the eastern United States and southern Asia, and of the corresponding Q structure of the earth's crust.

The attenuation of the short-period fundamental-mode Rayleigh waves in the eastern United States can be explained either by a frequency-independent or frequency-dependent model of shear wave internal friction. However, in order to fit the observed value of 1 to 10-sec period, first higher-mode Rayleigh waves, a frequency-dependent model is required. Additional higher-mode observational data at periods between 1 and 4 sec are required to determine the exact form of the frequency dependence.

Stochastic inversion techniques were applied to Rayleigh wave data to determine Q_β models for three regions of the United States. The results of this study indicate that upper crustal Q_β values in the western United States are significantly lower than in the eastern United States. Colorado Plateau values are intermediate between those of the Basin and Range and the eastern United States.

Iranian earthquakes recorded by short-period seismographs located in Iran were used to study the excitation and attenuation of the first P arrival (Pn or refracted P) and the crustal phases Pg, Sn and Lg. The latter three appear as trains of waves whose attenuation is shown to be similar to that of dispersed surface waves. By equalizing all the data to that of an $m_b = 5.0$ earthquake (using m_b determinations from

teleseismic P waves), data from a small number of stations but a large number of earthquakes are adequate to obtain attenuation curves of the various phases at distances of 100 to 1500 km. For 1-sec period waves the excitation of the Pg and Lg phases is about equal, and twice that of Sn. The excitation of 3-sec period Lg waves is approximately three times greater than that of 1-sec period Lg waves. The amplitude of the first P arrival is one of more orders of magnitude smaller than that of the other crustal phases to distances of 500 km, but comparable in amplitude at distances of 1000 to 1500 km. Furthermore, the first P wave is the only phase with a sharp onset, necessary for the accurate location of events. The coefficient of attenuation of 1-sec period Pg, Sn and Lg waves in Iran is approximately 0.0045 km^{-1}, similar to that found for southern California.

A generalized inversion method was applied to Tibetan group velocity and attenuation data to obtain a velocity and Q model. The velocity model gives a good fit to the group-velocity data over the range of observed periods, about 10 to 60 sec. The Q_β model has crustal values intermediate between those of the western and eastern United States.

Frequency Dependence of Shear Wave Internal Friction in the Continental Crust of eastern North America

by

Brian J. Mitchell

Department of Earth and Atmospheric Sciences
Saint Louis University
St. Louis, Missouri 63156

ABSTRACT

Fundamental-mode Rayleigh wave attenuation data for eastern North America can be explained by a frequency-independent model of shear wave internal friction (Q_β^{-1}) as well as by numerous frequency-dependent models of the crust. Assuming that $Q_\beta^{-1}(\omega, z) = C(z)\omega^{-\zeta}$, fundamental-mode Rayleigh wave data were inverted to obtain several frequency-dependent Q_β^{-1} models corresponding to different distributions of ζ. Limiting values of ζ were then sought by computing attenuation coefficients for the higher Rayleigh models for the various models. The calculated attenuation coefficients were compared to reported values for Lg and the first higher Rayleigh mode as observed at periods between 1 and 10 seconds in eastern North America. If it is assumed that ζ is constant over the entire period range between 1 and 40 seconds, then its most likely value lies between 0.3 and 0.5. The frequency-independent case ($\zeta = 0.0$) can definitely be rejected. Better fits to the data can be achieved by allowing ζ to vary with period, increasing relatively rapidly with decreasing period at periods of 4 seconds and less. It is possible that a peak in Q_β^{-1} occurs at periods between 1 and 4 seconds. Additional higher-mode data will be needed in that range; however, the existence of such a peak can be verified or rejected.

INTRODUCTION

Recent years have seen a marked increase in the quantity of surface wave attenuation data for various regions of the Earth and determinations of shear wave internal friction (Q_β^{-1}) models which are consistent with those data (e.g. Mitchell, 1973b, 1975; Lee and Solomon, 1975, 1978; Herrmann and Mitchell, 1975; Mitchell et al., 1977; Canas and Mitchell, 1979). Internal friction models are usually obtained under the assumption that Q is independent of frequency. That assumption is made largely because it is thought that the magnitude of the frequency dependence of Q in the seismic frequency band is small (Knopoff, 1964; Liu et al., 1976). Since it is, apparently, small, and the nature of the variation with frequency has not been known, it has been reasonable to obtain Q models using computationally convenient methods which assume that Q is independent of frequency.

Most mechanisms of seismic dissipation which are thought to pertain to the crust and upper mantle predict, however, that Q should have a dependence on frequency (Gordon and Nelson, 1966; Jackson and Anderson, 1970). In order to reconcile the frequency dependence of Q predicted by theory with the lack of significant frequency dependence thought to be observable in seismic data, it has been proposed that the intrinsic Q of the Earth can be explained by a distribution of relaxation mechanisms (Liu et al., 1966; O'Connell and Budiansky, 1977). This distribution is thought to be due to a spectrum of relaxation times, grain sizes, crack geometries, etc., which occur in the rocks of the Earth.

Although a spectrum of relaxation mechanisms probably occur in the

Earth, it is not likely that they will produce Q values which are perfectly frequency-independent over the entire seismic frequency band. Some body wave studies have, in fact, indicated that it is possible to detect a variation of Q with frequency for waves travelling through the mantle. (Solomon, 1972; Der and McElfresh, 1977; Sipkin and Jordan, 1979). All of these studies suggest that Q increases with increasing frequency in the body wave band. In a study combining the attenuation of shear waves from deep earthquakes with fundamental-mode surface wave attenuation results, Aki (1979) has obtained evidence for a peak in shear wave internal friction at periods of 2 or 3 seconds.

The present study will employ both fundamental- and higher-mode Rayleigh waves to investigate the existence, and nature of, frequency dependence of Q_β in the crust of eastern North America. By analyzing the fundamental mode, as well as several higher modes, it is possible to separate the depth dependence and frequency dependence of Q_β in this region having a relatively stable and uniform continental crust.

DATA

The most extensive set of surface wave attenuation coefficient data for a region which might be considered to have relatively uniform anelastic properties was obtained by Herrmann and Mitchell (1975) for a region of North America east of the Rocky Mountains. Love and Rayleigh wave data were obtained in the period range between 4 and 40 seconds and were used to obtain a frequency-independent Q_β^{-1} model of the crust in eastern North America. The present study will use the Rayleigh wave data of Herrmann and Mitchell (1975), supplemented by a data point at a period of 0.4 seconds (Kurz and Redpath, 1968) to invert for Q_β^{-1} models of the crust assuming various types of frequency dependence (Figure 1). Although not critical to the main conclusions of this study, the short-period data point permits the determination of a model with smaller upper crustal standard deviations than has been previously possible. The uncertainty of the determination by Kurz and Redpath was not given; consequently, a large standard deviation (10×10^{-3} km^{-1}) has arbitrarily been assigned to that value for use in all inversion attempts.

Other data to be employed are higher-mode attenuation coefficient values of various studies (Figure 2). Data at periods between 4 and 10 seconds are from Mitchell (1973a) and Herrmann (1973). Those values are taken to correspond to the first higher Rayleigh mode. Data at a period of about one second have been obtained in four studies (Nuttli, 1973; Street, 1976; Pomeroy, 1977; Bollinger, 1979) in regions of the central and eastern United States. All of those studies involved time domain measurements using vertical-component instruments to determine the attenuation of the phase Lg, a superposition of several higher-mode

Rayleigh waves. Pomeroy (1977) indicated that his measurements pertained to periods of 1-2 Hz, whereas the other data pertain more closely to 1 Hz. Although the authors assigned no confidence limits to these 1-second data, the distribution of points at values between 0.6 and 1.1 x 10^{-3} km^{-1} is taken in the present study to give an indication of the uncertainties of measurement of Lg attenuation at that period.

Data obtained by Nuttli and Dwyer (1978) at higher frequencies (2 Hz to 10 Hz) are also plotted. The computational procedures described in the following section do not permit the incorporation of data at periods much below 1 second. The data of Nuttli and Dwyer (1978) have been plotted, however, to illustrate that attenuation coefficient values apparently increase monotonically with increasing frequency over the internal 1 to 10 Hz. If those attenuation coefficient values can be taken to represent dissipation due to intrinsic anelasticity in the crust, and are not caused by scattering or other effects unrelated to intrinsic Q, they place important constraints on the nature of the frequency dependence of Q_β.

It is important to emphasize that in order to obtain information on the nature of the frequency dependence of Q_β using surface waves, is necessary to obtain high-quality attenuation data, both for the fundamental mode and the higher modes. High-quality attenuation data is notoriously difficult to obtain, being subject to such factors as scattering, lateral refraction, and multipathing, as well as to intrinsic anelasticity. The data of this study are characterized by relatively small standard deviations, both for the fundamental mode and for the first higher mode at periods between 4 and 10 seconds.

Attenuation coefficient values for 1-second Lg show substantial similarity among the four studies cited. The data therefore appear to be of a quality which are useful for this study. It will be assumed in the following sections that all of the attenuation coefficient values at periods between 1 and 40 seconds are governed entirely by intrinsic anelasticity of the crust.

METHOD

Higher-mode surface waves often appear as a conspicuous phase on seismograms generated by earthquakes in eastern North America. Figure 3 presents seismograms produced at four stations by the southeastern Missouri earthquake of 21 October 1965. The higher modes often appear as an impulsive phase as illustrated by the seismograms from stations MDS and ATL of that figure. Group velocities of five higher modes calculated for an eastern United States velocity model (Mitchell and Herrmann, 1979) appear in Figure 4 for periods between 1 and 10 seconds. At periods less than about 5 seconds there is an overlap among various modes. At shorter and shorter periods observed waveforms consist of larger and larger numbers of modes coalescing to form the phase Lg (Oliver and Ewing, 1957; Knopoff et al., 1973). The superposition of several modes with group velocity minima of about 3.5 km/sec explains the impulsive character often observed on long-period seismograms.

Although higher-mode group velocities often overlap, especially at shorter periods, the extent to which any mode contributes to the seismogram depends upon how well it was excited. Figure 5 presents the theoretical spectra corresponding to four central United States earthquakes as recorded at various stations. In most cases the contribution of the first higher mode is substantially greater than that of the second of higher order modes for periods greater than about 3 seconds. In computations of higher mode attenuation, it will be assumed that observed attenuation coefficient values at periods of 3 seconds and larger consist of only the first higher mode, that the

value at 2 seconds is the average of the first and second higher mode values, and that at a period of 1 second, the observed value is the average of the attenuation coefficient values for the first four higher modes. Since differences in the attenuation coefficient values among the various modes are not great, the results of this study do not depend critically upon the number of modes employed at any period.

The ability to separate the effects of frequency-dependence of Q_β from that of depth-dependence is possible because higher modes sample a different depth interval in the crust than does the fundamental mode for a given period. Figure 6 presents normalized amplitudes as a function of depth of the eigenfunctions of Rayleigh waves for the eastern United States model of Mitchell and Herrmann (1979). The amplitude of the fundamental mode at a period of 1 second is insignificant at depths below 2 or 3 km. The higher modes, however, sample the same depth interval as that sampled by the fundamental mode at a period of 6 seconds (about 20 km). Likewise, the first higher mode at a period of 6 seconds samples a depth interval similar to that sampled by the fundamental mode at a period of 25 seconds (about 60 km).

The initial step in the procedure employed is to invert the fundamental mode data of Figure 1 using the equations of Anderson et al. (1965) as modified by Mitchell (1975) to incorporate attenuation coefficient values. If it is assumed that compressional wave Q values, Q_α, are twice as large as Q_β, then the Rayleigh waves attenuation coefficient values, γ_R, are related to Q_β^{-1} and the elastic properties by:

$$\gamma_R = \frac{\pi}{T} \sum_{\ell=1}^{N} \left[\left(\frac{\beta_\ell}{C_R^2} \frac{\partial C_R}{\partial \beta_\ell} \right)_{\omega\rho\alpha} + \frac{1}{2} \left(\frac{\alpha_\ell}{C_R^2} \frac{\partial C_R}{\partial \alpha_\ell} \right)_{\omega\rho\beta} \right] Q_\beta^{-1} \qquad (1)$$

where α and β are compressional and shear wave velocities, C_R is Rayleigh wave phase plus velocity, T is period, and ℓ is a layer index. The subscripts ω, α, β, and ρ refer to frequency, compressional velocity, shear velocity, or density being held constant. The assumption that $Q_\alpha = 2Q_\beta$ has little effect on our results since surface wave attenuation is so slightly affected by Q_α. The above equation is usually employed assuming that Q_β is independent of frequency. In the present study, however, it will be assumed that Q_β depends upon both depth and frequency, so that in each layer, ℓ,

$$Q_{\beta\ell}(\omega) = C_\ell \, \omega^\zeta \qquad (2)$$

where ζ can be constant through the entire frequency range of interest or can vary with frequency. Note that if $\zeta = 0$, then Q_β is independent of frequency in the commonly assumed way.

The fundamental-mode data are inverted assuming various values for ζ. The fits of the theoretical curves to the data of Figure 1 for $\zeta = 0.0$ and 0.5 indicate that the fundamental mode data can be explained equally well by a wide range of modes corresponding to different ζ values. This situation occurs because variations in frequency dependence represented by different values of ζ in (1) can be offset by variations in values of C at different depths in the model.

The models obtained can now be used to compute attenuation coefficient values for the higher modes with a forward calculation using equation (1). The resulting values can then be compared with the higher mode data of Figure 2.

RESULTS

The results of computations for five values of ζ, between 0.0 and 1.0 appear in Figure 7. It is immediately clear that a frequency-independent model ($\zeta = 0.0$) does not even come close to explaining the 1-second Lg data. Although ζ values between 0.3 and 0.5 provide better fits, none of these curves for which ζ is constant over the entire frequency range provide very good fits to the entire data set between 1 and 10 seconds.

It is interesting to note that all curves for ζ between 0.0 and 0.3 are consistent with the data at periods of 4 seconds and more. This consistency supports the frequency-independent internal friction models of Mitchell (1973b) and Herrmann and Mitchell (1975) as being representative of the crust in eastern North America. It can also be seen that small negative values of ζ would also explain the data at periods greater than 4 seconds.

Further calculations were performed in which ζ was allowed to vary with period. Figure 8 presents the results of computations where $\zeta = 0$ at periods greater than 4 seconds and takes on larger values at shorter periods. The curve for which ζ jumps abruptly to 0.5 at a period of 4 seconds provides a very good fit to the data, but the abrupt change in ζ is probably unrealistic. Other cases assumed that ζ increases gradually from 0 at a period of 4 seconds to values ranging from 0.4 to 0.75 at 1 second. The case in which ζ increases to 0.5 provides an excellent fit to the data; however, it does not have the upward curvature to be consistent with the high-frequency data of Nuttli and Dwyer (1978) shown in Figure 2.

Figure 9 presents the results of further computations in which ζ was set at non-zero values at longer periods. Three cases in which ζ was set at 0.2 for periods greater than 4 seconds appear as curves 1, 2, and 3. The case in which ζ changes gradually between 0.5 and 0.2 at periods between 1 and 4 seconds provides an excellent fit to the data, and also provides the upward curvature needed to explain the data of Nuttli and Dwyer (1978).

An additional case in which ζ was set at -0.2 at periods greater than 4 seconds and more was also considered (curve 4 of Figure 9). If ζ varies smoothly between -0.2 and +0.6 as the period decreases between 4 seconds and 1 second, an excellent fit to the data is achieved, but a peak occurs at a period of about 2 seconds. In addition, the curvature is downward, rather than upward.

Models for which ζ is constant over the entire period range appear in Figure 10. Although it does not adequately explain the higher-mode data, a frequency-independent model ($\alpha = 0.0$) is presented, along with its standard deviations. Figure 11 presents resolving kernels for the same model. The standard deviations and resolving kernels for all of the frequency-dependent models are similar to those of the frequency-independent case, so are not plotted. From the magnitude of the standard deviations and the widths of the resolving kernels it is apparent that little can be said concerning the frequency-dependence of Q_β^{-1} in the lower crust. Therefore all of the conclusions regarding the frequency dependence of Q_β^{-1} must be restricted to the upper crust.

Figure 10 also presents a model for the case where ζ assumes the constant value of 0.3 at all periods. Other models, for cases where ζ

increases with decreasing period, appear in Figure 12. All of those models indicate that 1-second shear waves will undergo little attenuation as they traverse the crust. Longer period waves will be attenuated a great deal more. The model in which $\zeta = 0.2$ at periods greater than 4 seconds and increases to 0.5 with decreasing period to a period of 1 second is probably the model which best fits all of the presently available data. The higher-mode attenuation coefficients for that model explain the data very well and include an upward curvature at short periods as suggested by the data of Nuttli and Dwyer (1978). It should be noted, however, that none of the models, including this one, predicts as rapid an increase in attenuation with increasing frequency between 1 and 10 Hz as that predicted by the Nuttli and Dwyer data. There are at least two possible reasons for this discrepancy: (1) the attenuation of the high-frequency data of Nuttli and Dwyer (1978) is strongly affected by scattering or other effects not related to intrinsic Q in the crust, or (2) the parameter ζ takes on smaller values at frequencies greater than 1 Hz. There is no way to distinguish between these possibilities at the present time.

The final model, for which $\alpha = -0.2$ at periods greater than 4 seconds and increases to +0.6 with decreasing period to a period of 1 second is shown in Figure 13. As stated earlier, this model provides an excellent fit to the higher-mode data, but produces a peak in the theoretical values centered at a period of about 2 seconds and a downward curvature at shorter periods. The Q_β^{-1} model differs from all of the other models by having a maximum in Q_β^{-1} at a period near 3 seconds. This result is similar to that obtained by Aki (1979) in a combined study of the attenuation of shear waves from deep earth-

quakes in Japan and of reported surface waves attenuation values at longer periods. Although this agreement between two studies using different methods is intriguing, it is not possible to verify the existence of an internal friction peak with the higher-mode data presently available. Reliable attenuation data at periods between 1 and 4 seconds can be expected to resolve this question if it can be obtained.

The computations of the present study indicate that Q_β^{-1} in the crust in eastern North America is frequency dependent. Several possible models can, however, explain fundamental- and higher-mode Rayleigh wave attenuation coefficient data at periods of 1 second and greater. The models differ in the nature of their dependence upon frequency. One reason for the non-uniqueness of the results is the occurrence of a gap in the higher-mode data at periods between 1 and 4 seconds. If reliable data can be obtained for that range, it would be possible to exclude one of more of the models discussed above. For instance, if attenuation coefficient values between 1 and 4 seconds decreased monotonically with increasing period, models corresponding to negative values of ζ at the longer periods, and peaks in internal friction, could be rejected. If a large peak in the attenuation coefficient curve occurs, however, models with negative values of ζ at long periods and positive values at shorter periods, yielding a peak in internal friction, would be favored.

DISCUSSION

It has been possible to place limits on the nature and severity of the frequency dependenxe of Q_β in the continental crust. Higher-mode data is critically needed in the period range between 1 and 4 seconds before surface waves can be used to place further constraints on the nature of the frequency dependence of Q_β^{-1} and to infer the existence or absence of peaks in values of Q_β^{-1} in that range as inferred by Aki (1979).

Laboratory measurements of seismic attenuation have indicated that pore fluid attenuation mechanisms are dominant in the upper crust (Winkle and Nur, 1979). That result is in agreement that with the suggestion by Mitchell (1975) that enhancement in the content of interstitial fluids produces a greater observed attenuation of surface waves in western North America than in eastern North America.

It is of interest that fluid-flow models of energy dissipation in the crust (Mavko and Nur, 1975; O'Connell and Budiansky, 1977) predict peaks in Q_β^{-1} such as that inferred by one of the models of this study, if the distribution of crack geometries in the crust does not vary greatly. If the crust is characterized by a wide range of crack geometries, however, O'Connell and Budiansky (1977) show that there would be no narrow peaks and Q_β^{-1} could be nearly independent of frequency. Assuming that the fluid-flow model is applicable to the upper crust, then the availability of reliable attenuation data at periods between 1 and 4 seconds should permit us to estimate the distribution of aspect rations of fluid-filled cracks in the crust.

CONCLUSIONS

Higher-mode Rayleigh wave attenuation coefficient data in combination with fundamental-mode data indicate that Q_β is frequency dependent over at least part of the period range between 1 and 40 seconds. Several frequency-dependent Q_β^{-1} models have been presented which are consistent with all of the data and, undoubtedly, several other reasonable models could also be found.

If the exponent of frequency, ζ, for these models is assumed to be constant over the entire period range, then its value appears to be between 0.3 and 0.5. Better agreement with the higher-mode data can, however, be achieved if ζ varies with period, having zero or small values at longer periods (greater than about 4 seconds) and increasing values as period decreases to 1 second.

ACKNOWLEDGMENT

I wish to thank Otto Nuttli for providing several references on high-frequency attenuation data, Keiiti Aki for providing a copy of his manuscript prior to publication, and Robert Herrmann for providing computer programs for calculating surface wave eigenfunctions and spectra. This research was supported by the Advanced Research Projects Agency of the Department of the Defense and was monitored by the Air Force Office of Scientific Research under Contract No. F49620-79-C-0025.

REFERENCES

Aki, K., Attenuation of shear waves in the lithosphere for frequencies from 0.05 to 25 Hz, Phys. Earth Planet. Int., in press, 1979.

Anderson, D.L., A. Ben-Menahem, and C.B. Archambeau, Attenuation of seismic energy in the upper mantle, J. Geophys. Res., 70, 1441-1448, 1965.

Bollinger, G.A., Attenuation of the Lg phase and the determination of m_b in the Southeastern United States, Bull. Seism. Soc. Am., 69, 45-63, 1979.

Canas, J.A., and B.J. Mitchell, Lateral variation of surface-wave anelastic attenuation across the Pacific, Bull. Seism. Soc. Am., 68, 1637-1650, 1978.

Der, Z.A., and T.W. McElfresh, The relation between anelastic attenuation and regional amplitude anomalies of short-period P waves in North America, Bull. Seism. Soc. Am., 67, 1303-1317, 1977.

Gordon, R.B., and C.W. Nelson, Anelastic properties of the earth, Rev. Geophys., 4, 457-474, 1966.

Herrmann, R.B., Surface wave generation by the south central Illinois earthquake of November 9, 1968, Bull. Seism. Soc. Am., 63, 2121-2134, 1973.

Herrmann, R.B., and B.J. Mitchell, Statistical analysis and interpretation of surface wave anelastic attenuation data for the stable interior of North America, Bull. Seism. Soc. Am., 65, 1115-1128, 1975.

Jackson, D.D., and D.L. Anderson, Physical mechanisms of seismic wave attenuation, Rev. Geophys. Space Phys., 8, 1-63, 1970.

Knopoff, L., Q, Rev. Geophys., 2, 625-660, 1964.

Knopoff, L., F. Schwab, and E. Kausel, Interpretation of Lg, Geophys. J. Roy. Ast. Soc., 33, 389-404, 1973.

Kurz, M.K., Jr., and B.B. Redpath, Project Pre-Gondola, Seismic site calibration, Rpt. PNE-1100, May 1968, U.S. Army Nuclear Cratering Group, CE, Livermore, Cal., 71 pp., 1968.

Lee, W.B., and S.C. Solomon, Inversion schemes for surface wave attenuation and Q in the crust and the mantle, Geophys. J. Roy. Ast. Soc., 43, 47-71, 1975.

Lee, W.B., and S.C. Solomon, Simultaneous inversion of surface wave phase velocity and attenuation: Love waves in western North America, J. Geophys. Res., 83, 3389-3400, 1978.

Liu, H.-P., D.L. Anderson, and H. Kanamori, Velocity dispersion due to anelasticity; implications for seismology and mantle composition, Geophys. J.R. Astron. Soc., 47, 41-58, 1976.

Mavko, G., and A. Nur, Melt squirt in the asthenosphere, J. Geophys. Res., 80, 1444-1448, 1975.

Mitchell, B.J., Radiation and attenuation of Rayleigh waves from the southeastern Missouri earthquake of 21 October 1965, J. Geophys. Res., 78, 886-899, 1973a.

Mitchell, B.J., Surface wave attenuation and crustal anelasticity in central North America, Bull. Seism. Soc. Am., 63, 1057-1071, 1973b.

Mitchell, B.J., Regional Rayleigh wave attenuation in North America, J. Geophys. Res., 80, 4904-4916, 1975.

Mitchell, B.J., and R.B. Herrmann, Shear velocity structure in the eastern United States from the inversion of surface wave group and phase velocities, Bull. Seism. Soc. Am., 69, 1133-1148, 1979.

Mitchell, B.J., N.K. Yacoub, and A.M. Correig, A summary of seismic surface wave attenuation and its regional variation across continents and oceans, Geophys. Mono. 20, The Earth's Crust, edited by J.G. Heacock, 405-425, AGU, Washington, D.C., 1977.

Nuttli, O.W., Seismic wave attenuation and magnitude relations for eastern North America, J. Geophys. Res., 78, 876-885, 1973.

Nuttli, O.W., and J. Dwyer, Attenuation of high-frequency seismic waves in the central Mississippi Valley, 75 pp., Waterways Exp. Sta., Corps of Eng., Vicksburg, Miss., 1978.

O'Connell, R.J., and B. Budiansky, Viscoelastic properties of fluid-saturated cracks, J. Geophys. Res., 82, 5719-5735, 1977.

Oliver, J., and M. Ewing, Higher modes of continental Rayleigh waves, Bull. Seism. Soc. Am., 47, 187-204, 1957.

Pomeroy, P.W., Aspects of seismic wave propagation in eastern North America, A preliminary report, Roundout Associates, 1977.

Sipkin, S.A., and T.H. Jordan, Frequency dependence of Q_{ScS}, Bull. Seism. Soc. Am., 69, 1055-1079, 1979.

Solomon, S.C., On Q and seismic discrimination, Geophys. J. Roy. Ast. Soc., 31, 1055-1079, 1979.

Street, R.L., Scaling northeastern United States/southeastern Canada earthquakes by their Lg waves, Bull. Seism. Soc. Am., 66, 1525-1537, 1976.

Winkler, K., A. Nur, Pore fluids and seismic attenuation in rocks, Geophys. Res. Ltrs., 6, 1-4, 1979.

FIGURE CAPTIONS

Figure 1. Fundamental-mode Rayleigh wave attenuation coefficient data and theoretical values corresponding to two internal friction models obtained from inversions of the data. The open circles and vertical bars are the mean values and standard deviations of Herrmann and Mitchell (1975) for eastern North America. The closed circle is a data point from Kurz and Redpath (1968) inferred to correspond to the fundamental Rayleigh mode for a path in eastern Montana.

Figure 2. Higher-mode Rayleigh wave attenuation coefficient values for eastern North America. The values at periods between 4 and 10 seconds correspond to the first higher Rayleigh mode and the values at periods of 1 second and less correspond to Lg, a superposition of several higher modes.

Figure 3. Example seismograms from four stations for the southeastern Missouri earthquake of 21 October 1965. The approximate onset times of the higher and fundamental modes are indicated by H and F, respectively.

Figure 4. Theoretical group velocities of the first five higher modes at periods between 1 and 10 seconds for the eastern United States model of Mitchell and Herrmann (1979).

Figure 5. Theoretical amplitude spectra corresponding to the fundamental (F) and six higher modes for four events and stations in the eastern United States.

Figure 6. Rayleigh wave eigenfunctions for the fundamental, first, and fourth higher modes at a period of 1 second; for the fundamental and first higher mode at a period of 6 seconds; and for the fundamental mode at a period of 25 seconds.

Figure 7. Higher-mode Rayleigh wave attenuation coefficient data and theoretical values obtained for various frequency-dependent internal friction models for which the exponent of frequency (ζ) is assumed to be uniform over the entire frequency range.

Figure 8. Higher-mode Rayleigh wave attenuation coefficient data and theoretical values obtained for various frequency-dependent internal friction models for which ζ is assumed to vary with frequency and is equal to 0.0 at periods greater than 4 seconds. At periods between 1 and 4 seconds, $\zeta = 0.5$ for curve 1, ζ varies smoothly between 0.4 and 0.0 for curve 2, ζ varies smoothly between 0.5 and 0.0 for curve 3, and ζ varies between 0.75 and 0.0 for curve 4.

Figure 9. Higher-mode Rayleigh wave attenuation coefficient data and theoretical values obtained for various frequency-dependent internal friction models for which ζ is assumed to vary with frequency and is non-zero at periods greater than 4 seconds. For curve 1, ζ varies between 0.4 and 0.2 at periods between 1 and 4 seconds and $\zeta = 0.2$ at greater periods. For curve 2, ζ varies between 0.5 and 0.2 at periods between 1 and 4 seconds and $\zeta = 0.2$ at greater periods. For curve 3, ζ varies between 0.7 and 0.2 between 1 and 4 seconds and $\zeta = 0.2$ at greater periods. For curve 4, ζ varies between 0.6 and -0.2 between 1 and 4 seconds and $\zeta = 0.2$ at greater periods.

Figure 10. (Left) A frequency-independent model of internal friction for eastern North America. The horizontal bars represent one standard deviation.
(Right) A frequency-dependent model of internal friction for which ζ is constant and equal to 0.3 over the entire period range. The standard deviations have about the same values as those for the frequency-independent model.

Figure 11. Resolving kernels at four depths for the frequency-independent internal friction model of Figure 10. All of the frequency-dependent models in this report have resolving kernels with similar shapes and widths.

Figure 12. Three frequency-dependent internal friction models which satisfy both fundamental-mode and higher-mode Rayleigh wave attenuation coefficient data in eastern North America.

Figure 13. A frequency-dependent internal friction model which satisfies eastern North American attenuation coefficient data and which exhibits a peak in Q_β^{-1} at intermediate periods.

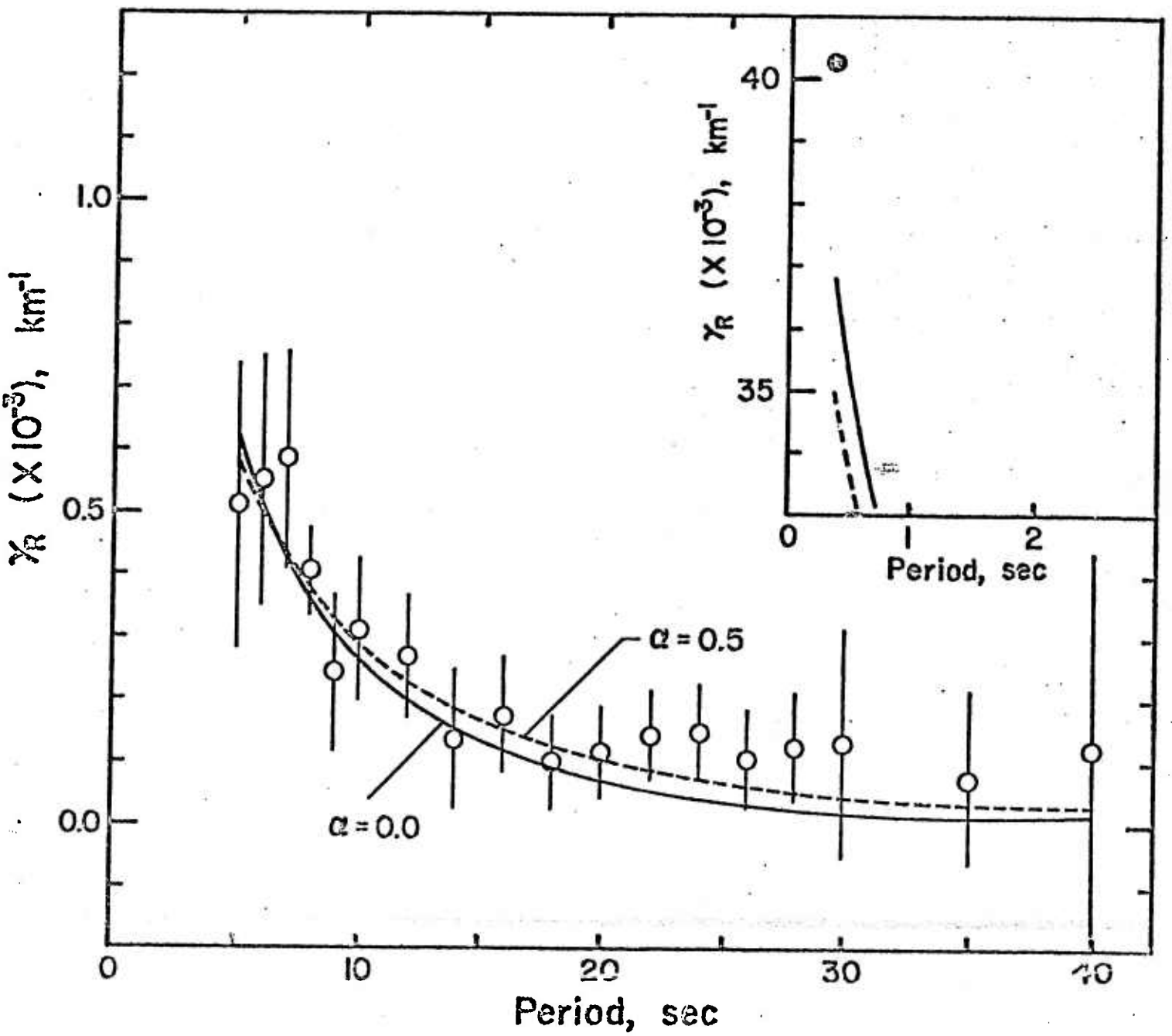
1.0
0.5
0.0
γ_R (X 10^{-3}), km^{-1}
0
10
20
30
40
Period, sec
α = 0.5
α = 0.0
40
35
γ_R (X 10^{-3}), km^{-1}
0
1
2
Period, sec

Figure 1

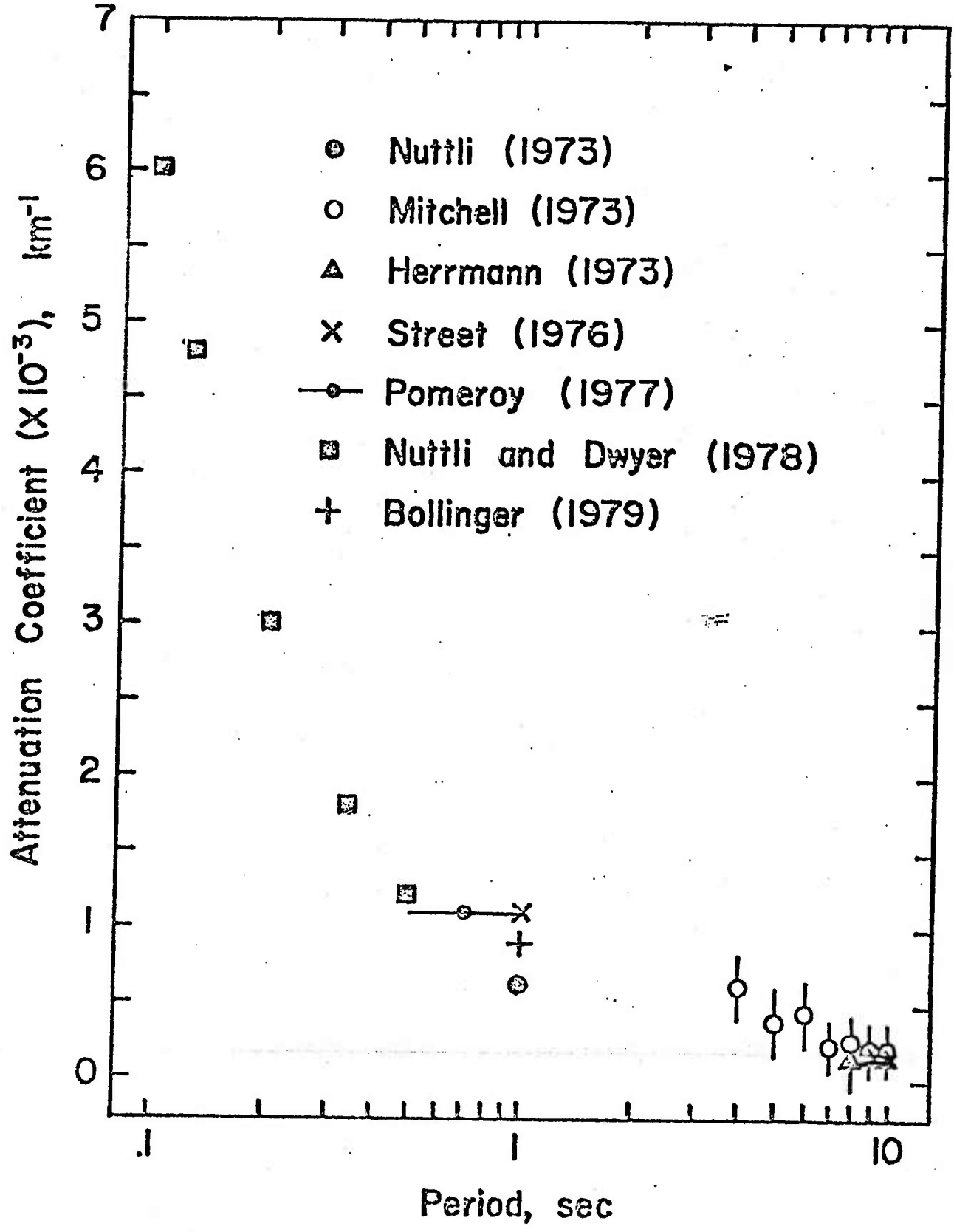
Attenuation Coefficient (X 10⁻³), km⁻¹
Period, sec
Nuttli (1973)
Mitchell (1973)
Herrmann (1973)
Street (1976)
Pomeroy (1977)
Nuttli and Dwyer (1978)
Bollinger (1979)
0
1
2
3
4
5
6
7
.1
1
10

Figure 2

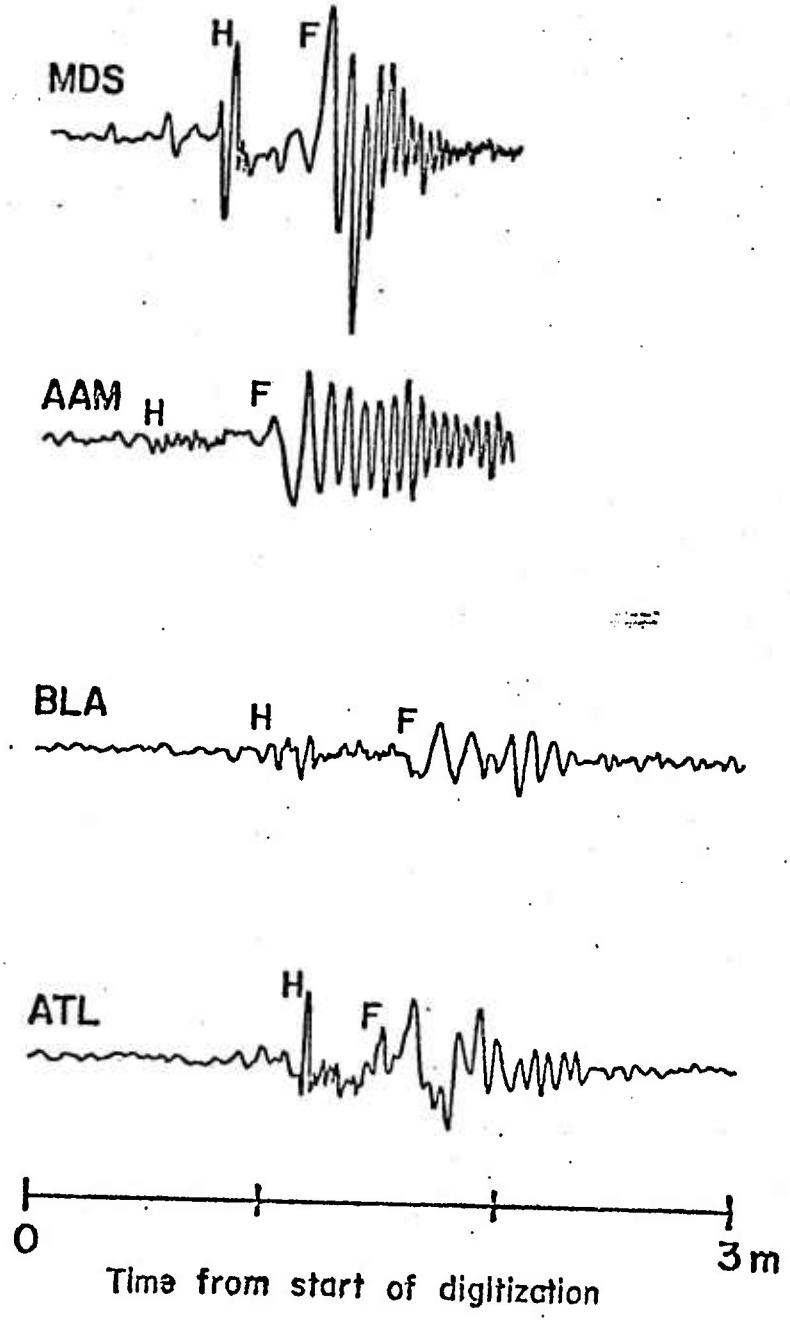
MDS
H
F
AAM
H
F
BLA
H
F
ATL
H
F
0
3 m
Time from start of digitization

Figure 3

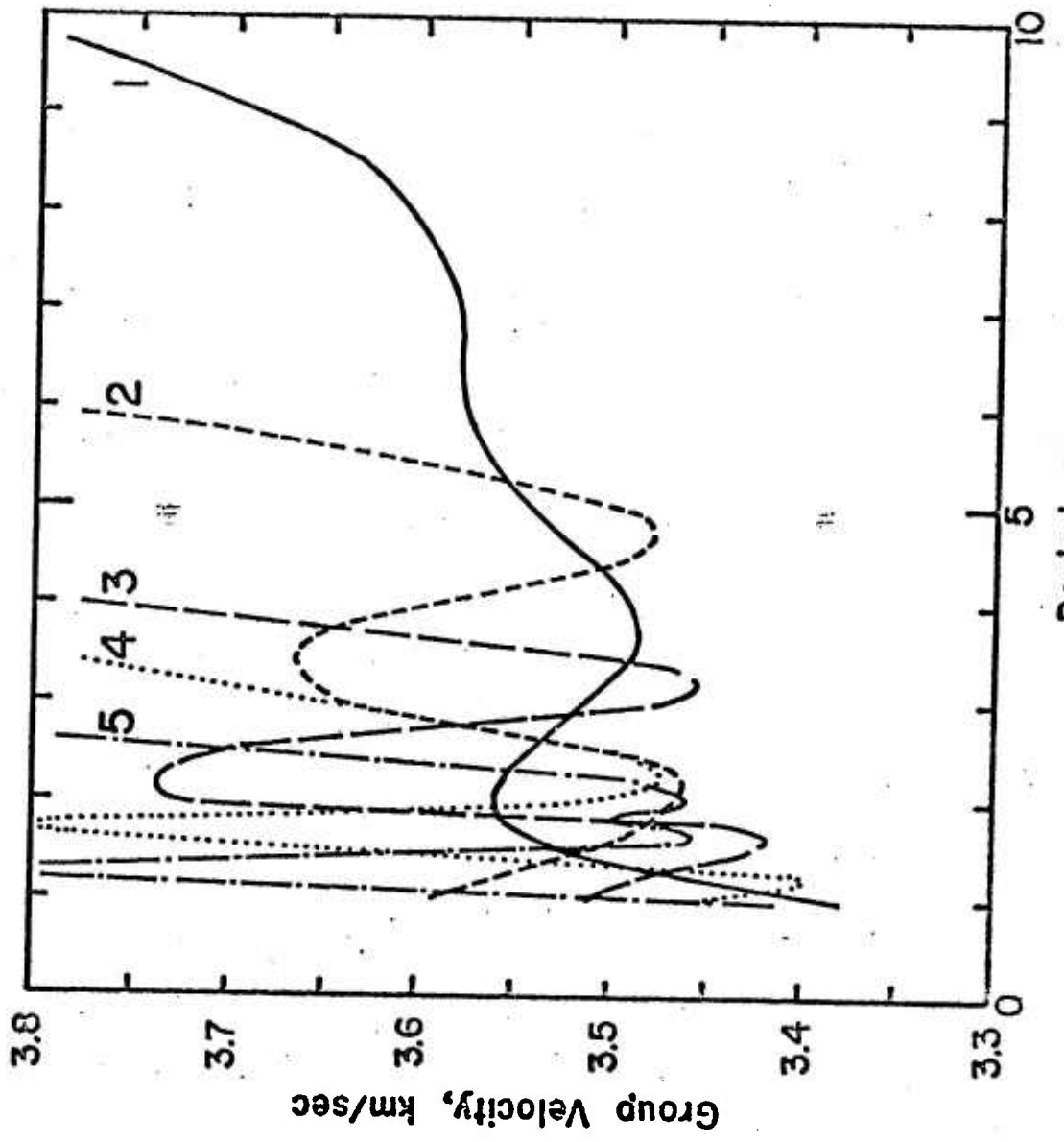

Figure 4

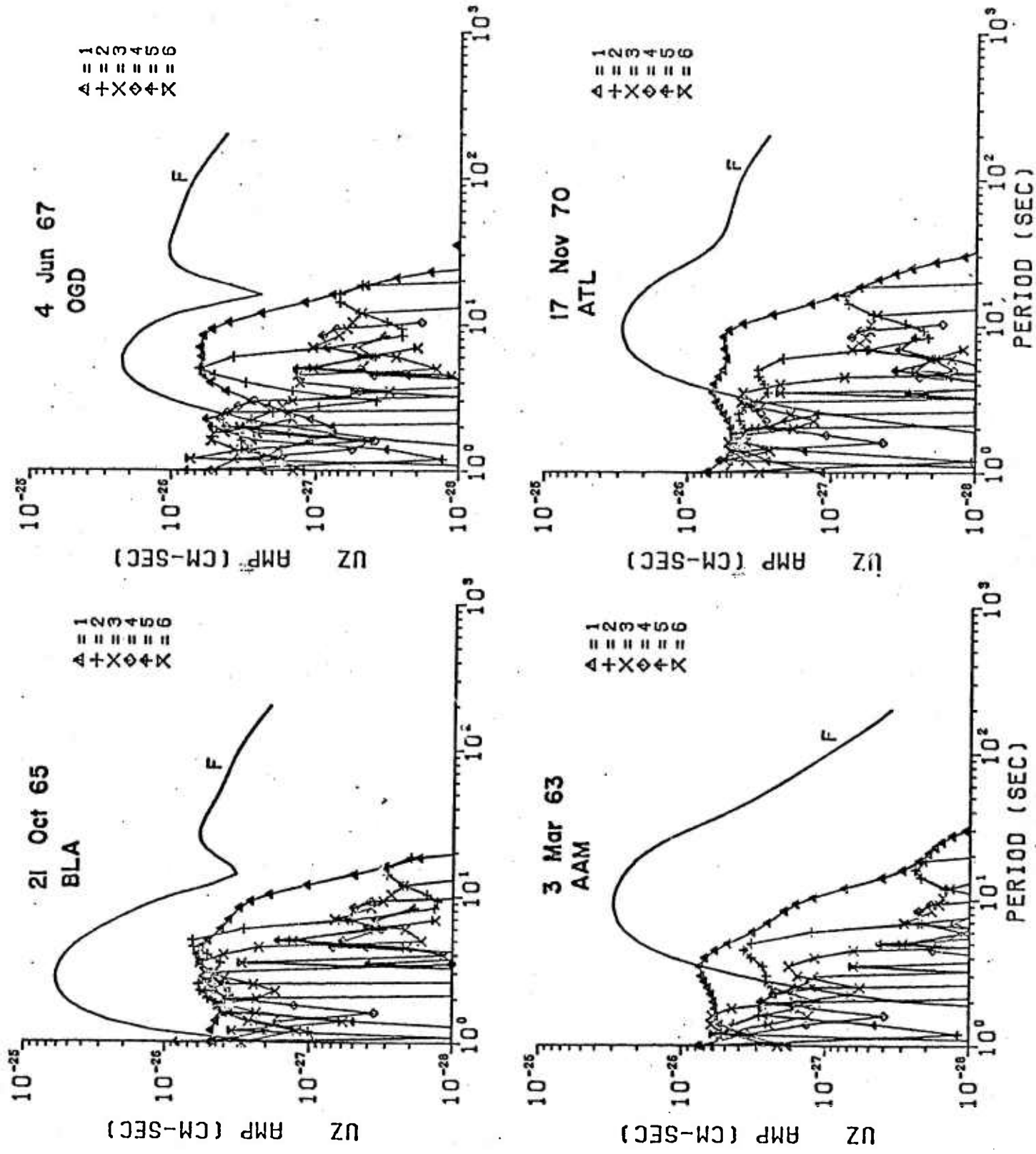
4 Jun 67
OGD
17 Nov 70
ATL
21 Oct 65
BLA
3 Mar 63
AAM
Δ = 1
+ = 2
X = 3
◇ = 4
✦ = 5
⋊ = 6
F
UZ AMP (CM-SEC)
PERIOD (SEC)

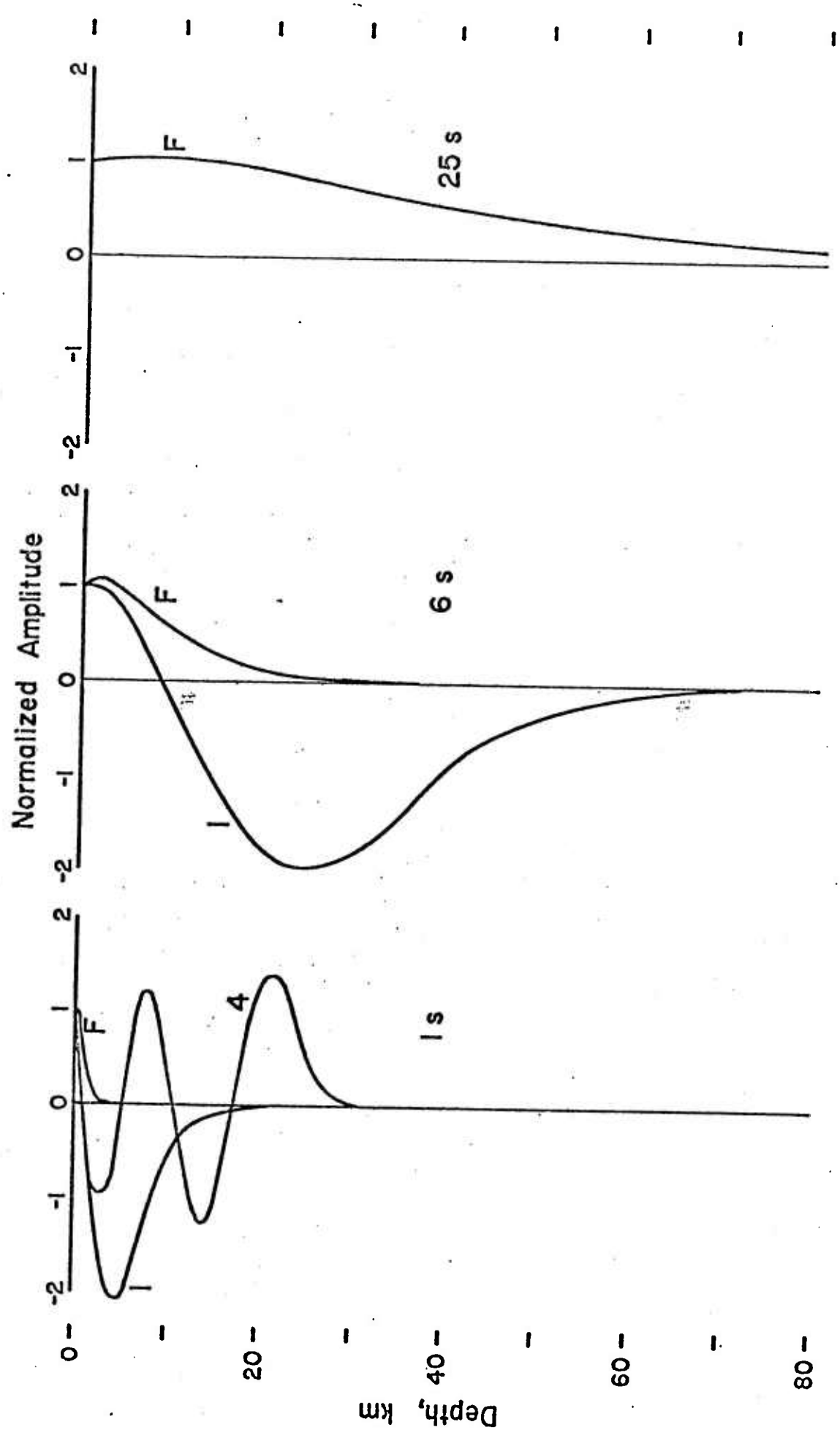
Normalized Amplitude
Depth, km
0
20
40
60
80
2
1
0
-1
-2
F
I
4
1 s
6 s
25 s

Figure 6

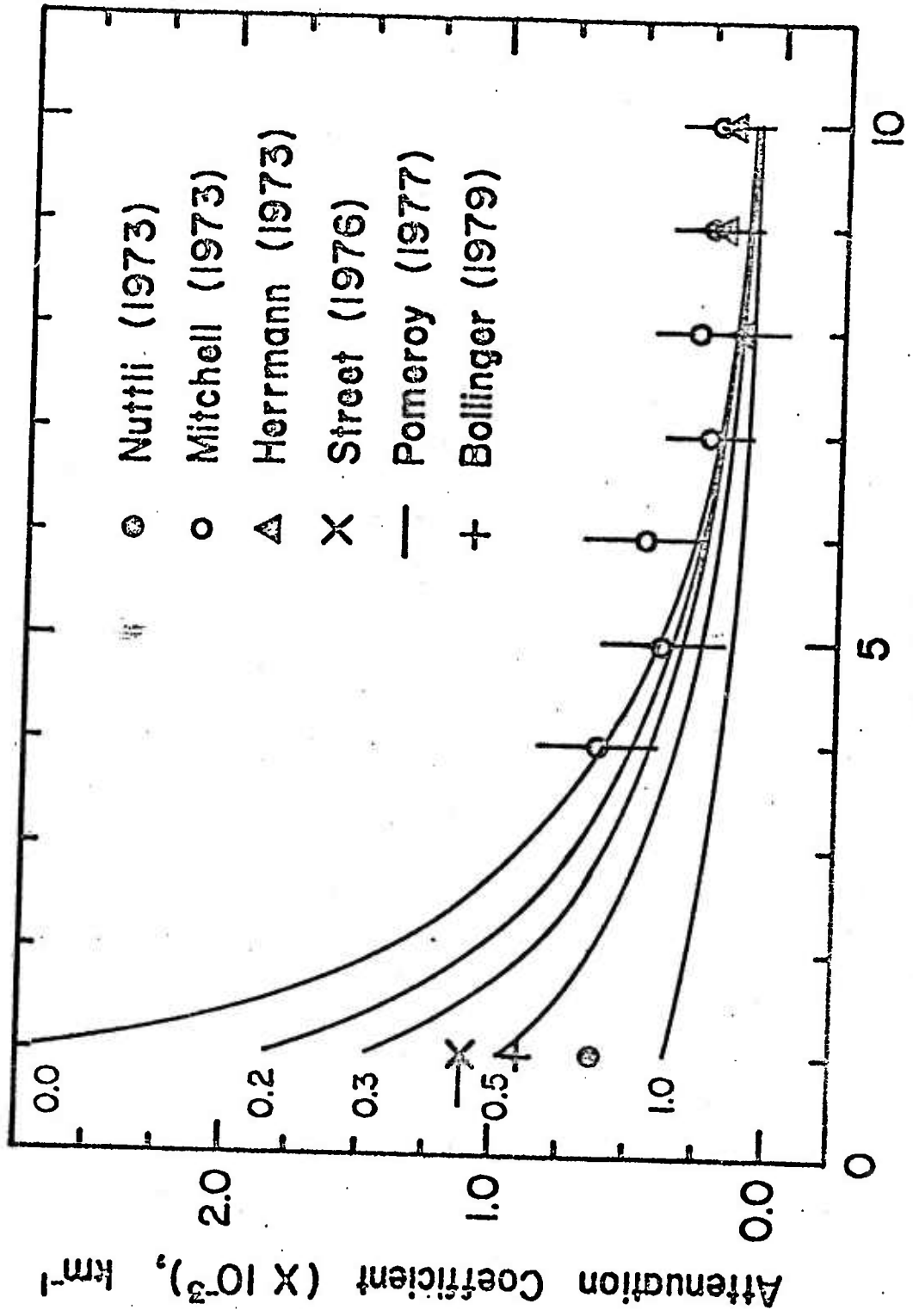
Attenuation Coefficient (X 10⁻³), km⁻¹
Period, sec
0.0
2.0
1.0
0.0
0
5
10
0.0
0.2
0.3
0.5
1.0
Nuttli (1973)
Mitchell (1973)
Herrmann (1973)
Street (1976)
Pomeroy (1977)
Bollinger (1979)

Figure 7

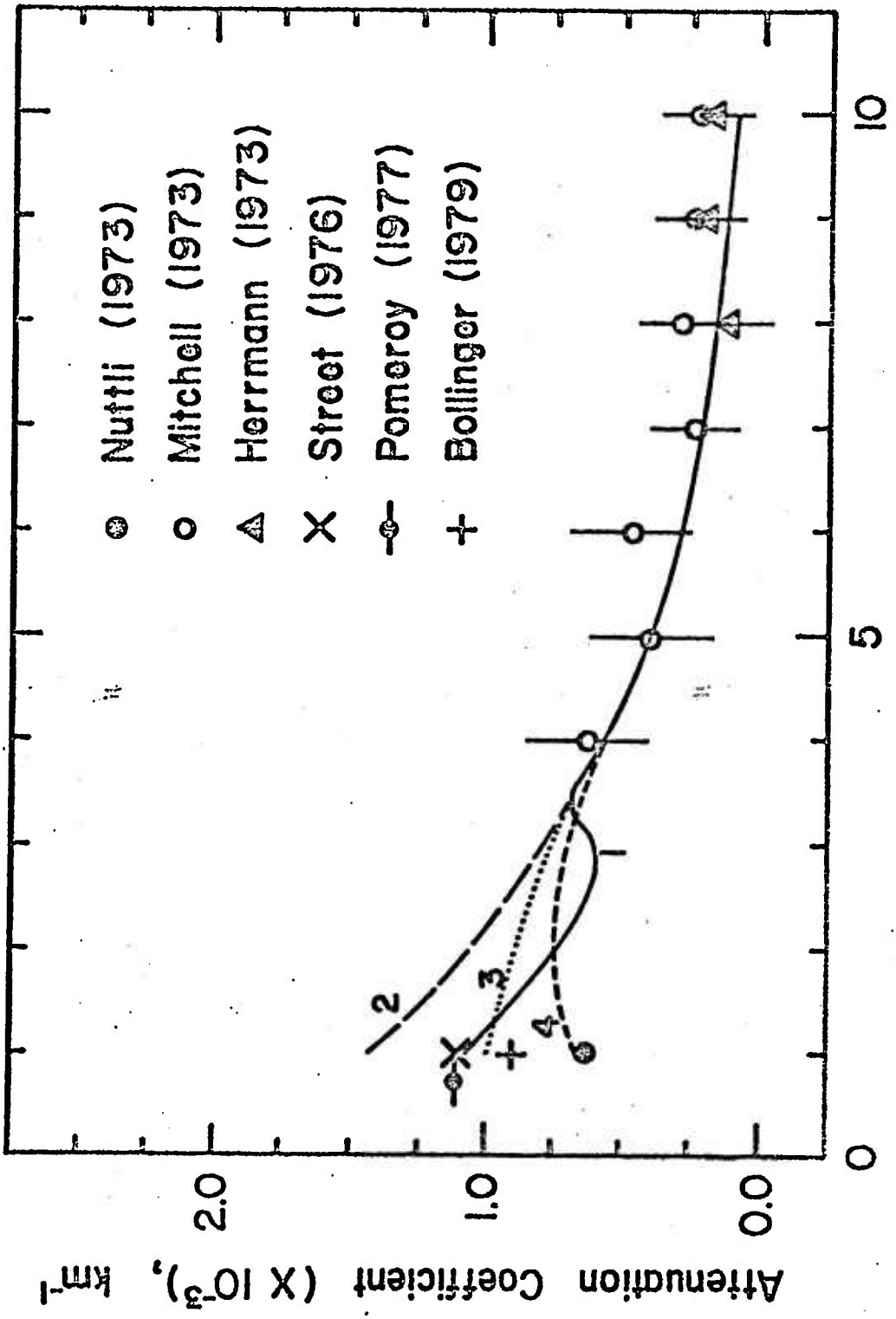
Attenuation Coefficient (X 10⁻³), km⁻¹
2.0
1.0
0.0
0
5
10
Period, sec
Nuttli (1973)
Mitchell (1973)
Herrmann (1973)
Street (1976)
Pomeroy (1977)
Bollinger (1979)
2
3
4

Figure 8

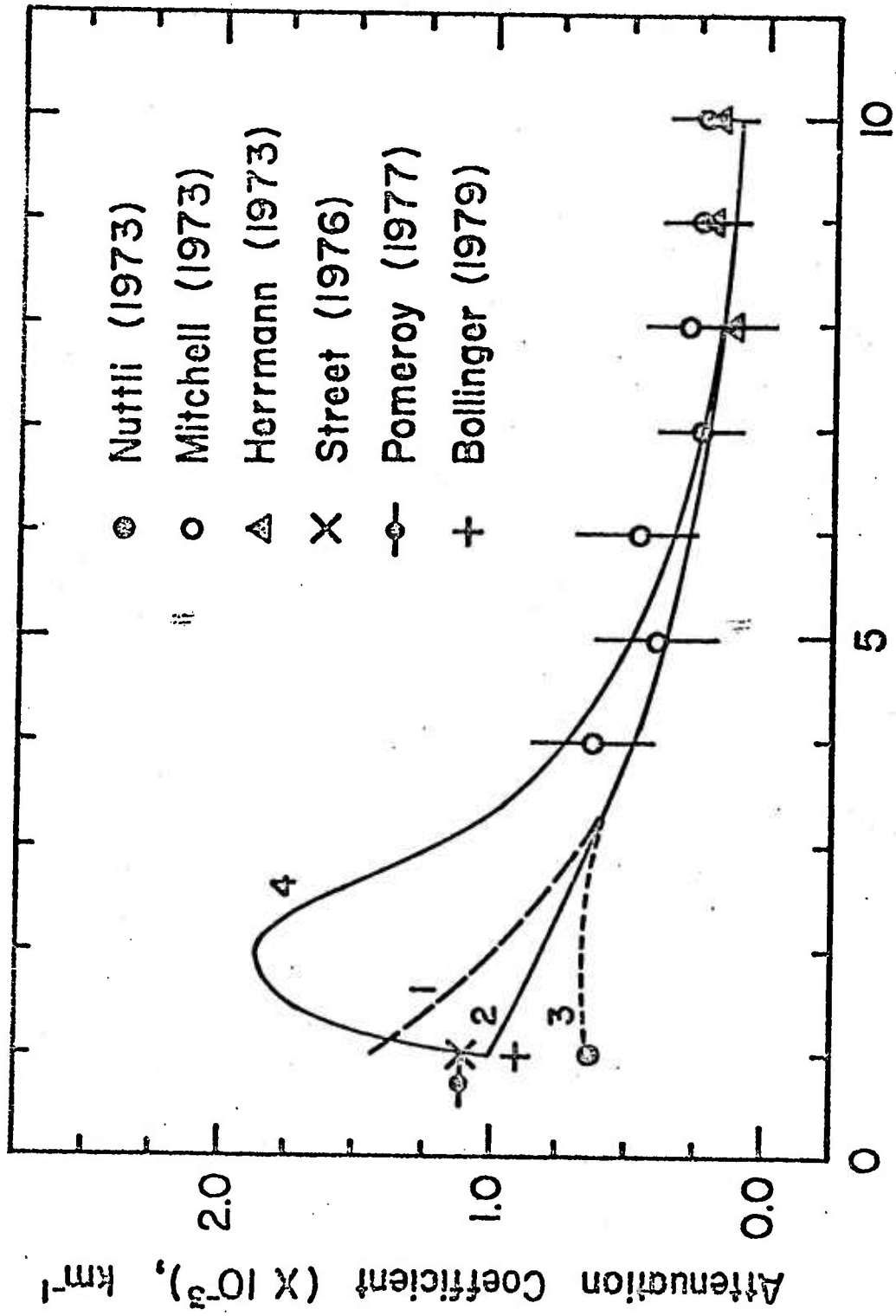
Attenuation Coefficient (X 10⁻³), km⁻¹
2.0
1.0
0.0
0
5
10
Period, sec
Nuttli (1973)
Mitchell (1973)
Herrmann (1973)
Street (1976)
Pomeroy (1977)
Bollinger (1979)
1
2
3
4

Figure 9

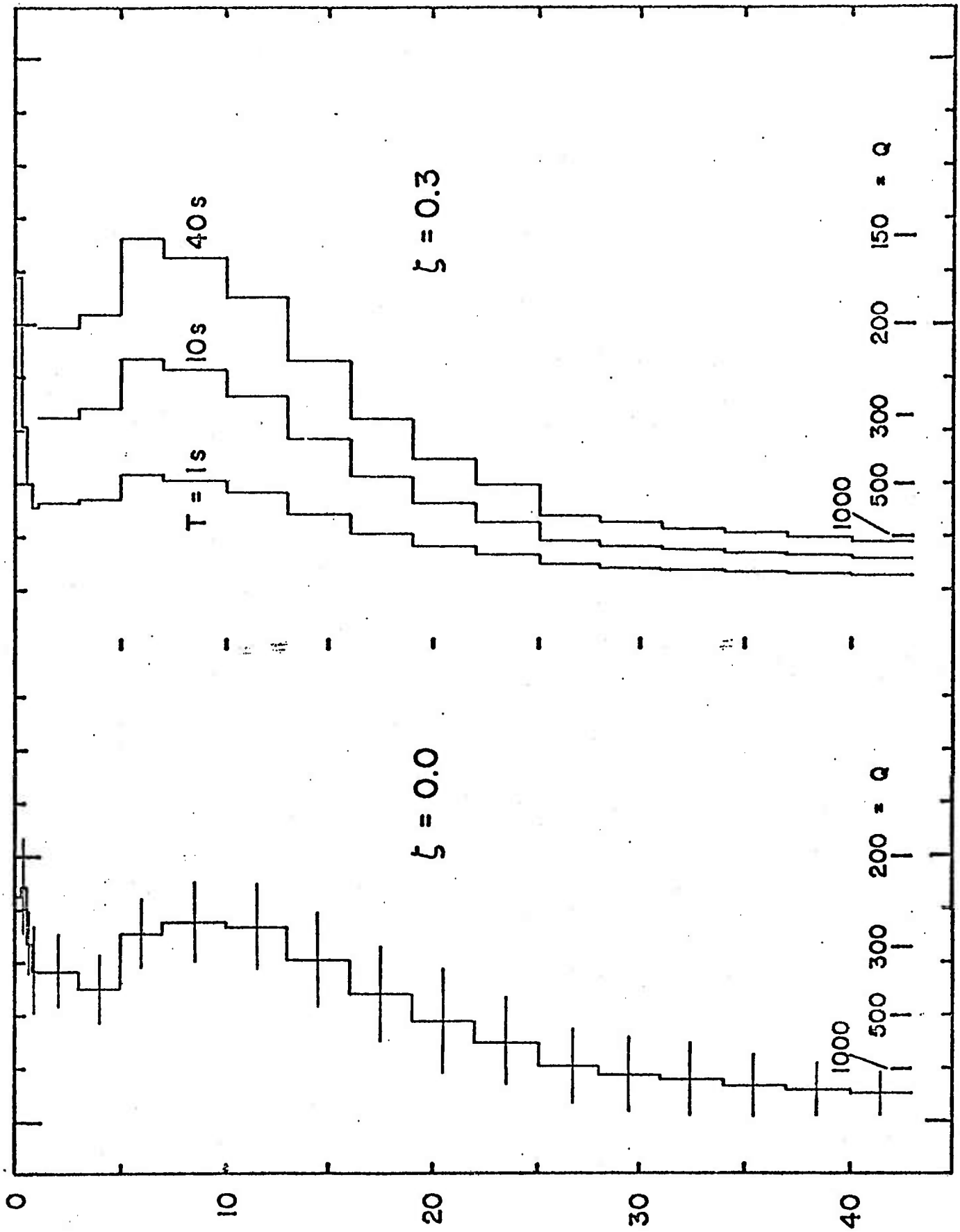
Depth, km
0
10
20
30
40
ζ = 0.0
ζ = 0.3
T = 1s
10s
40s
1000
500
300
200
150
Q
0
5
10
Q_β^{-1} (X 10^{-3})

Figure 10

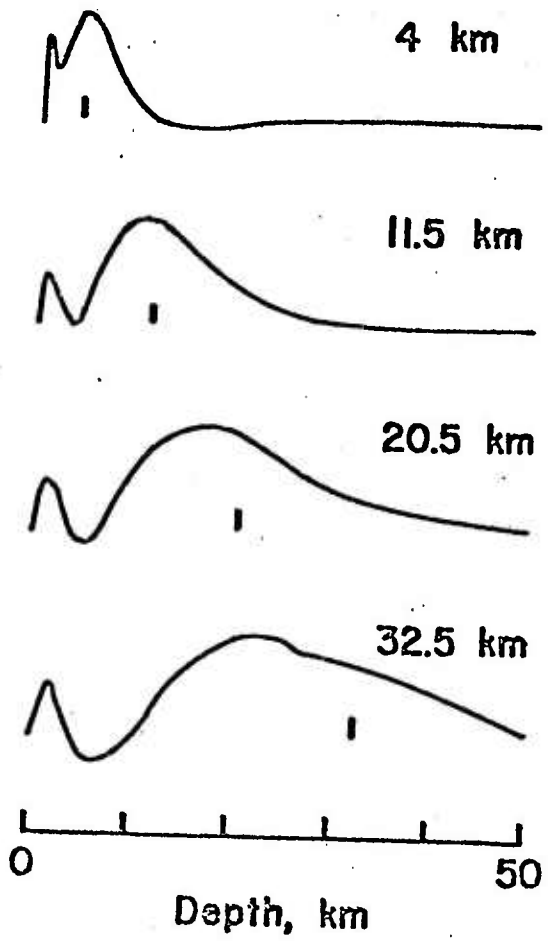

Figure 11

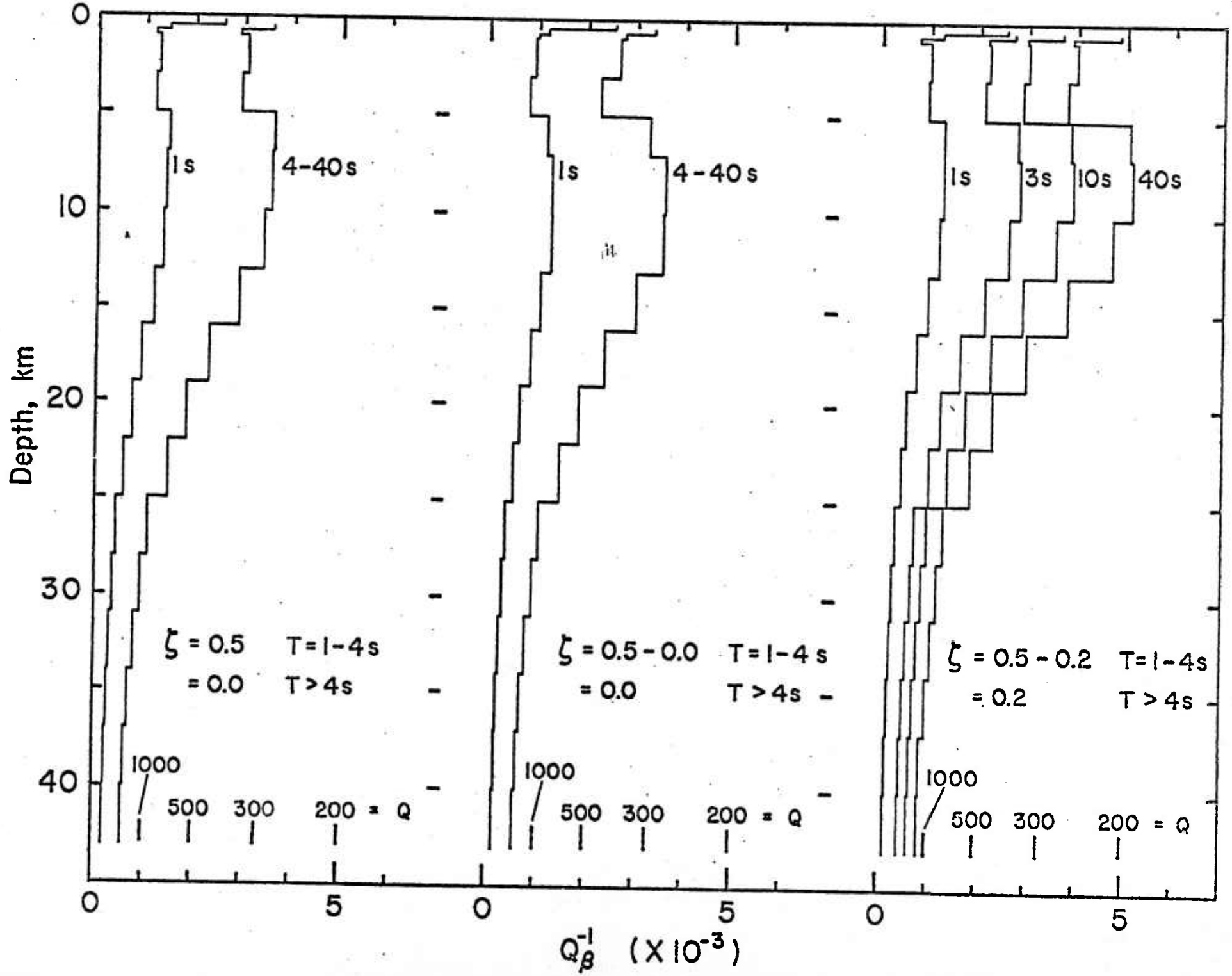
Depth, km
0
10
20
30
40
1s
4-40s
ζ = 0.5 T=1-4s
= 0.0 T>4s
1000
500
300
200 = Q
1s
4-40s
ζ = 0.5-0.0 T=1-4s
= 0.0 T>4s
1000
500
300
200 = Q
1s
3s
10s
40s
ζ = 0.5-0.2 T=1-4s
= 0.2 T>4s
1000
500
300
200 = Q
0
5
0
5
0
5
Q_β^{-1} (X 10^{-3})

Figure 12

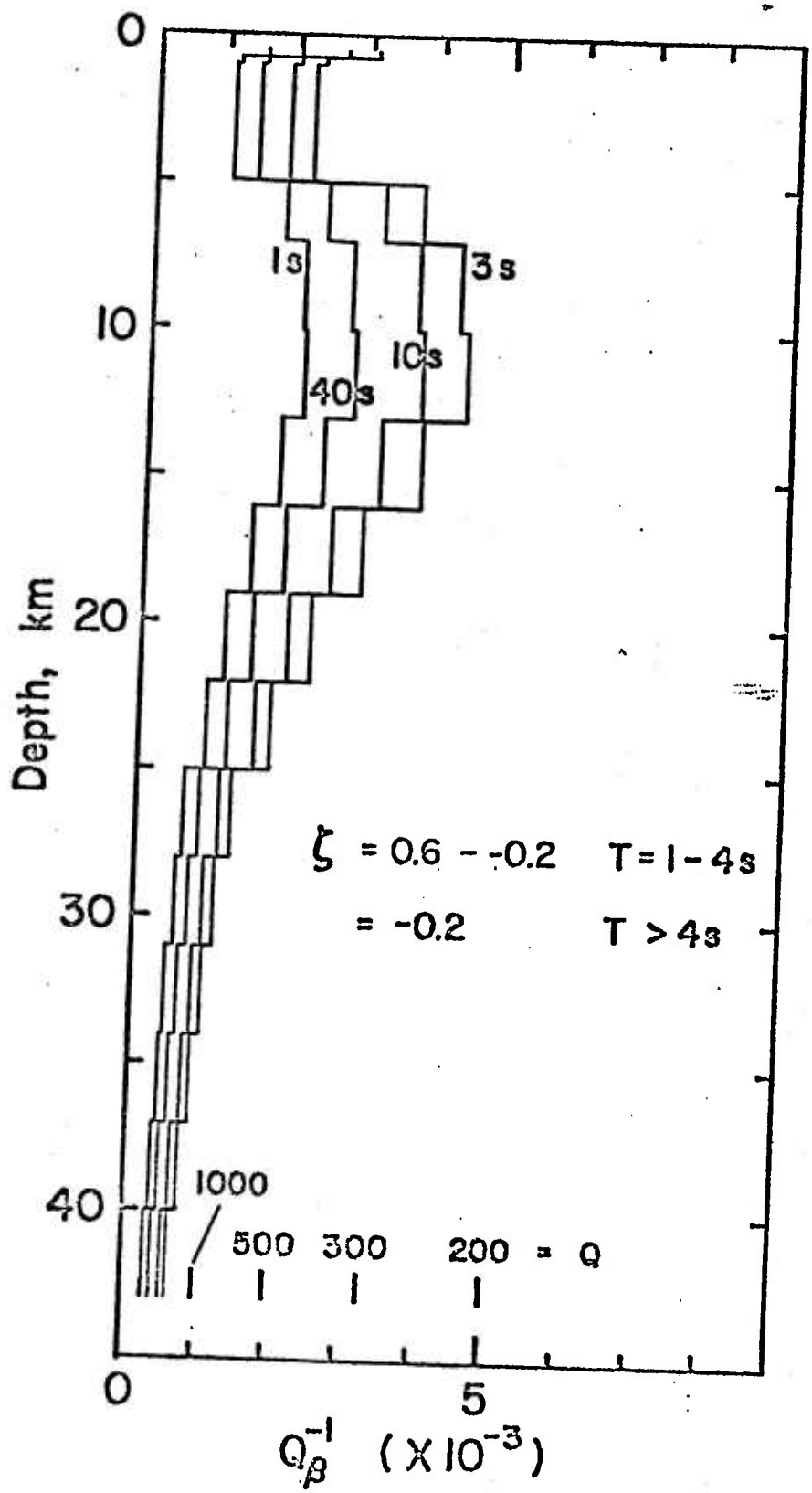
0
10
20
30
40
Depth, km
1s
3s
10s
40s
ζ = 0.6 - -0.2 T = 1-4s
= -0.2 T > 4s
1000
500 300 200 = Q
0
5
Q_β^{-1} (X 10^{-3})

Figure 13

REGIONALIZED CRUSTAL Q MODELS IN NORTH AMERICA FROM THE INVERSION OF RAYLEIGH WAVE SPECTRA

by

Chiung-Chuan Cheng

The importance of the method developed in our previous studies for determining crustal shear wave Q models lies in its ability to utilize relatively short paths between a single source and single receiver, both of which are preferably located within a single geologic province. The method was previously employed to analyze Rayleigh wave paths in the eastern United States, the Colorado Plateau, and the Basin and Range province through trial-and-error procedures. However, the method was extended by employing stochastic inversion techniques as stated in our last report. The inversion scheme has thus been applied to obtain Q models for these three regions.

DATA

Figure 1 is a map indicating the Rayleigh wave path used for determining a Q model in the eastern United States. Figure 2 shows the paths used for the Colorado Plateau and the Basin and Range province. The three earthquakes are listed in Table I. Table II gives for each wave path the epicentral distance, azimuth, and back azimuth.

Data were obtained from long period vertical component seismograms. The observed seismograms appear in Figure 3. Higher mode arrivals can be noticed with group velocity about 3.5 km/sec.

Spectral amplitudes at selected periods are obtained with the application of the band-pass filtering technique (Dziewonski et al., 1969; Herrmann, 1973a).

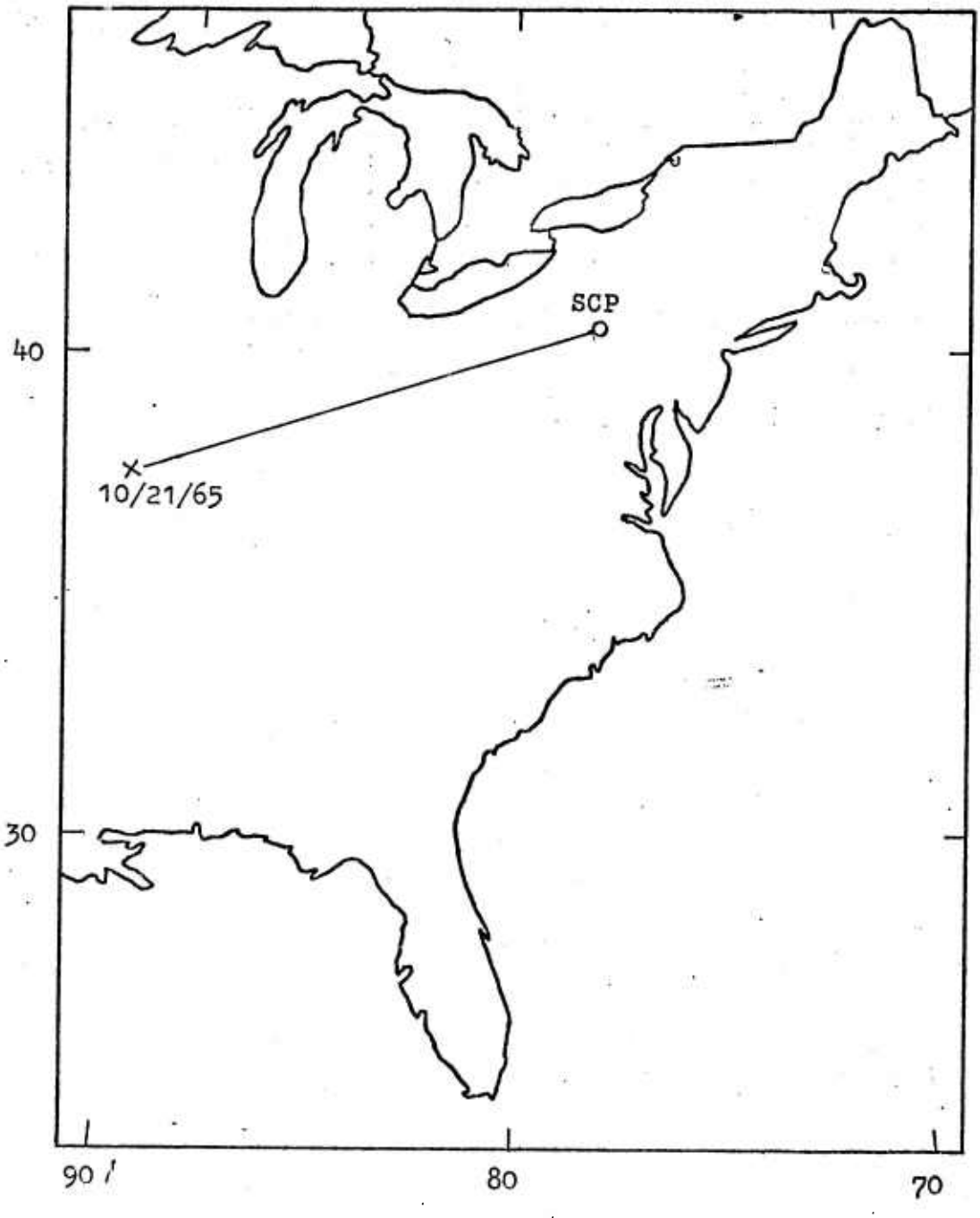

Figure 1. Rayleigh wave path analyzed for the eastern United States.

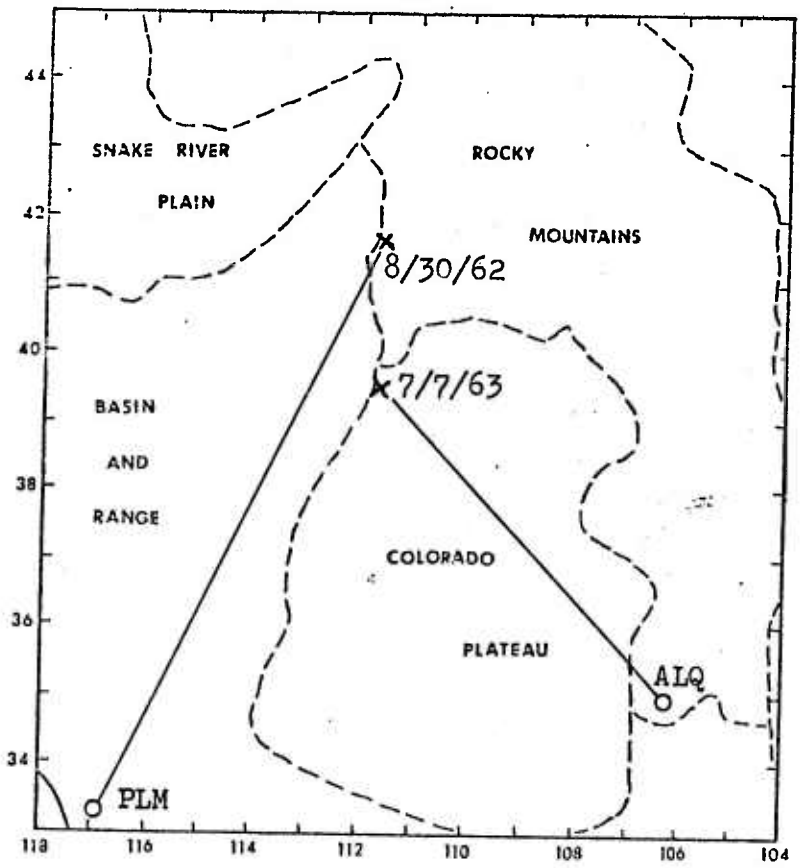

Figure 2. Rayleigh wave paths analyzed for the Colorado Plateau and the Basin and Range province.

Table 1

EVENT PARAMETERS

EVENT	DATE (m/d/yr)	ORIGIN TIME (h:m:s)	LATITUDE (°N)	LONGITUDE (°W)	DEPTH (km)	FOCAL MECHANISM STRIKE	DIP	SLIP
1	10/21/65	02:04:38.3	37.5	91.0	4.5	70.	50.	265.
2	07/07/63	19:20:42.4	39.6	111.9	10.0	350.	74.	235.
3	08/30/62	13:35:28.7	41.8	111.8	12.0	5.	32.	259.

Table 2

EVENT-STATION QUANTITIES

EVENT	STATION	EPICENTRAL DISTANCE (km)	AZIMUTH	BACK AZIMUTH
1	SCP	966.7	67.9	254.6
2	ALQ	707.0	135.3	318.6
3	PLM	1038.3	207.1	24.0

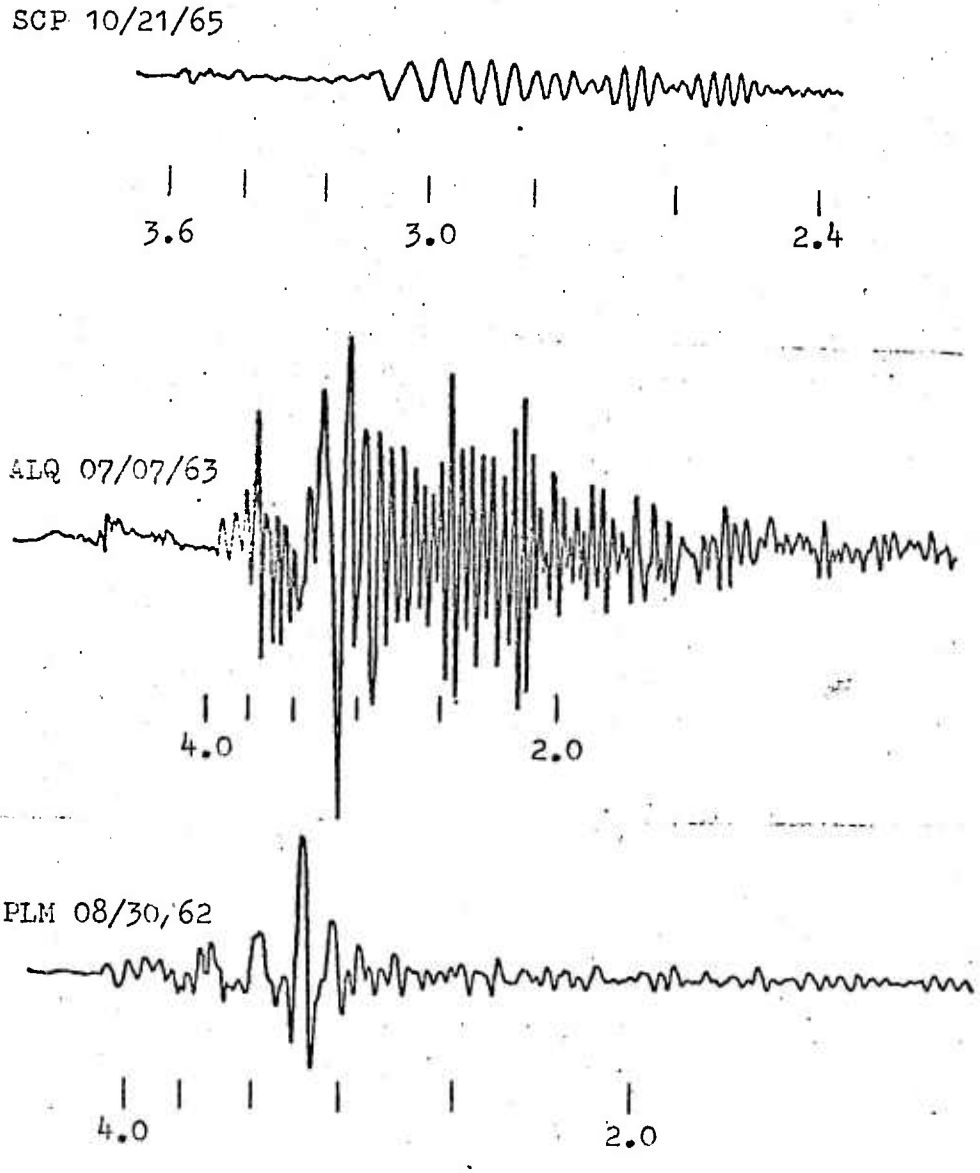

Figure 3. Seismograms analyzed for Rayleigh wave paths of Figures 1 and 2.

Q_β MODELS

The problem to fit the theoretical spectral amplitude y and the observed spectral amplitude z is of the form:

$$Ax = b,$$

where x is the vector to be solved,

$$x = (\Delta Q_{\beta 1}^{-1},\ \Delta Q_{\beta 2}^{-1},\ \Delta Q_{\beta 3}^{-1},\ \ldots\ ,\ \Delta Q_{\beta N}^{-1},\ C)^T,$$

b is the vector given as

$$b_i = \ln y_i - \ln z_i,$$

and A is a matrix having its elements given by

$$A_{ij} = \frac{R\pi}{T}\left[\tfrac{1}{2}\left(\frac{\alpha_\ell}{C^2}\frac{\partial C}{\partial \alpha_\ell}\right) + \left(\frac{\beta_\ell}{C^2}\frac{\partial C}{\partial \beta_\ell}\right)\right] \qquad \text{for } j = 1,\ 2,\ \ldots\ N$$

$$A_{i(N+1)} = R$$

with R being the epicentral distance, T the period.

The theoretical spectral amplitude y is initially computed with known fault plane solution, focal depth, and a presumed seismic moment, as well as presumed Q model.

The solution of x is obtained as:

$$x = (W^{\frac{1}{2}} A^T S^{-1} A + \delta^2 I)^{-1} W^{\frac{1}{2}} A^T S^{-1} b.$$

Thus, the Q model is modified by adding $\Delta Q_{\beta\ell}^{-1}$ to $Q_{\beta\ell}^{-1}$ in each layer, and the seismic moment is multiplied by exp(-RC).

The inversions of the three observed spectra are restricted to simple two- and three-layer models. In both cases, the lower crust is assumed to be characterized by high Q_β values and fixed at 2000. The

results of inversion yield the Q models shown in Figures 4 and 5 for the two-layer and three-layer models, respectively.

The two-layer models have amplitude residuals comparable to those of the three-layer models. Furthermore, these two-layer models are consistent with results of our previous study made with trial-and-error procedures. The eastern United States model is similar to that obtained by Herrmann and Mitchell (1975).

Rayleigh wave attenuation coefficients computed from the two-layer models for these three regions are shown in Figure 6 for the fundamental and first higher modes. Curves of the eastern United States model are compared to data of Herrmann and Mitchell (1975) for the fundamental mode and that of Mitchell (1973) and Herrmann (1973b) for the first higher mode, as shown in Figure 7. The model provides an adequate fit to these data.

DISCUSSION

The inversion scheme has shown to be effective in finding Q models which explain spectral data adequately. The Q models obtained from the inversions are consistent with results of spectral comparisons in previous studies. These results indicate that upper crustal Q_β values in the western United States are significantly lower than those for the upper crust of the eastern United States. In addition, distinct differences have been found between upper crustal Q_β values in the Basin and Range province and in the Colorado Plateau.

REFERENCES

Dziewonski, A.M., S. Bloch, and M. Landisman, A technique for the analysis of transient seismic signals, Bull. Seism. Soc. Am., 59, 427-444, 1969.

Herrmann, R.B., Some aspects of band-pass filtering of surface waves, Bull. Seism. Soc. Am., 63, 663-671, 1973a.

Herrmann, R.B., Surface wave generation by the south central Illinois earthquake of November 9, 1968, Bull. Seism. Soc. Am., 63, 2121-2134, 1973b.

Herrmann, R.B., and B.J. Mitchell, Statistical analysis and interpretation of surface wave anelastic attenuation data for the stable interior of North America, Bull. Seism. Soc. Am., 65, 1115-1128, 1975.

Mitchell, B.J., Radiation and attenuation of Rayleigh waves from the southeastern Missouri earthquake of 21 October 1965, J. Geophys. Res., 78, 886-899, 1973.

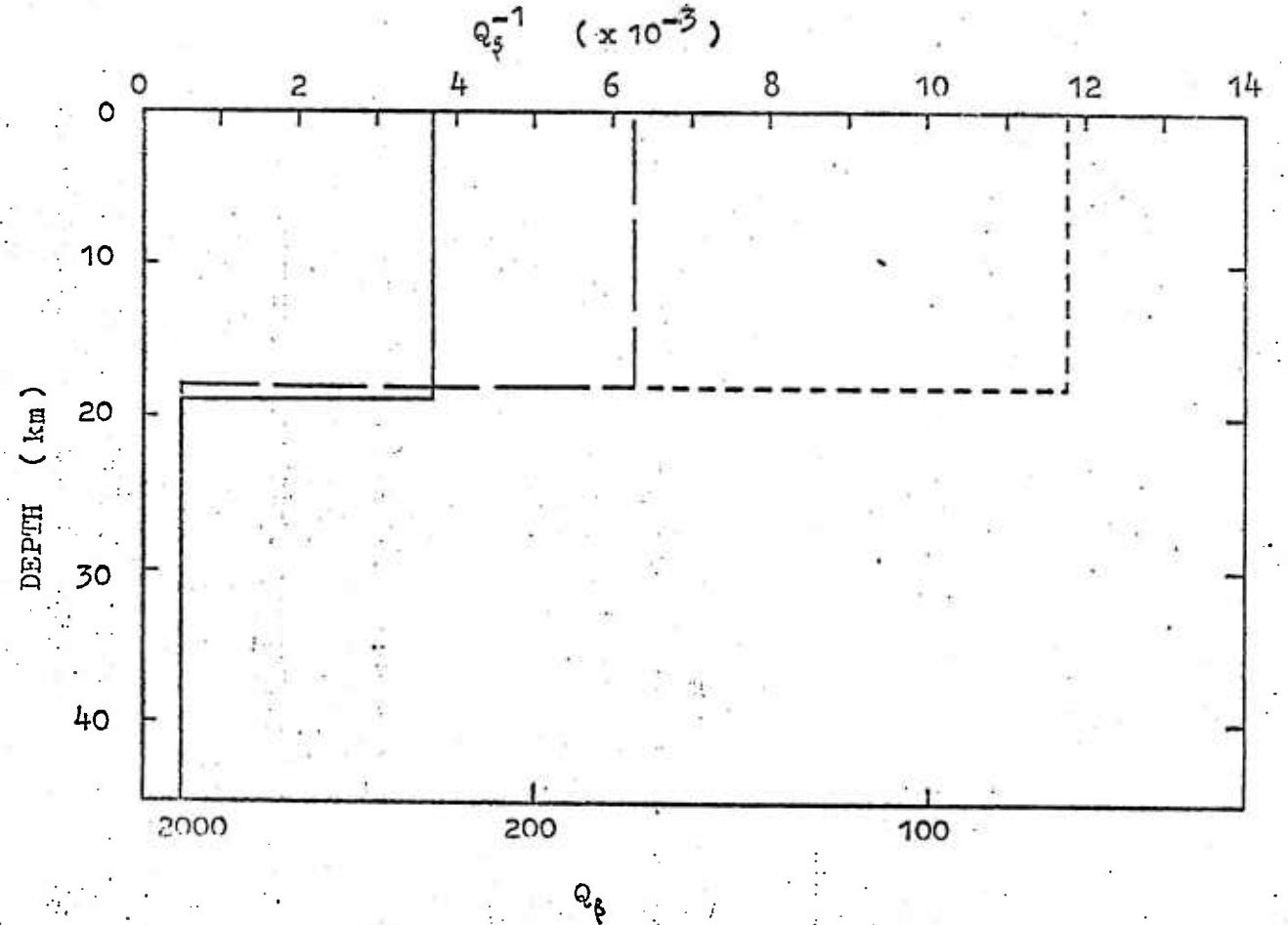

Figure 4. Two-layer Q models obtained for the eastern United States (solid), the Colorado Plateau (long dash), and the Basin and Range (short dash).

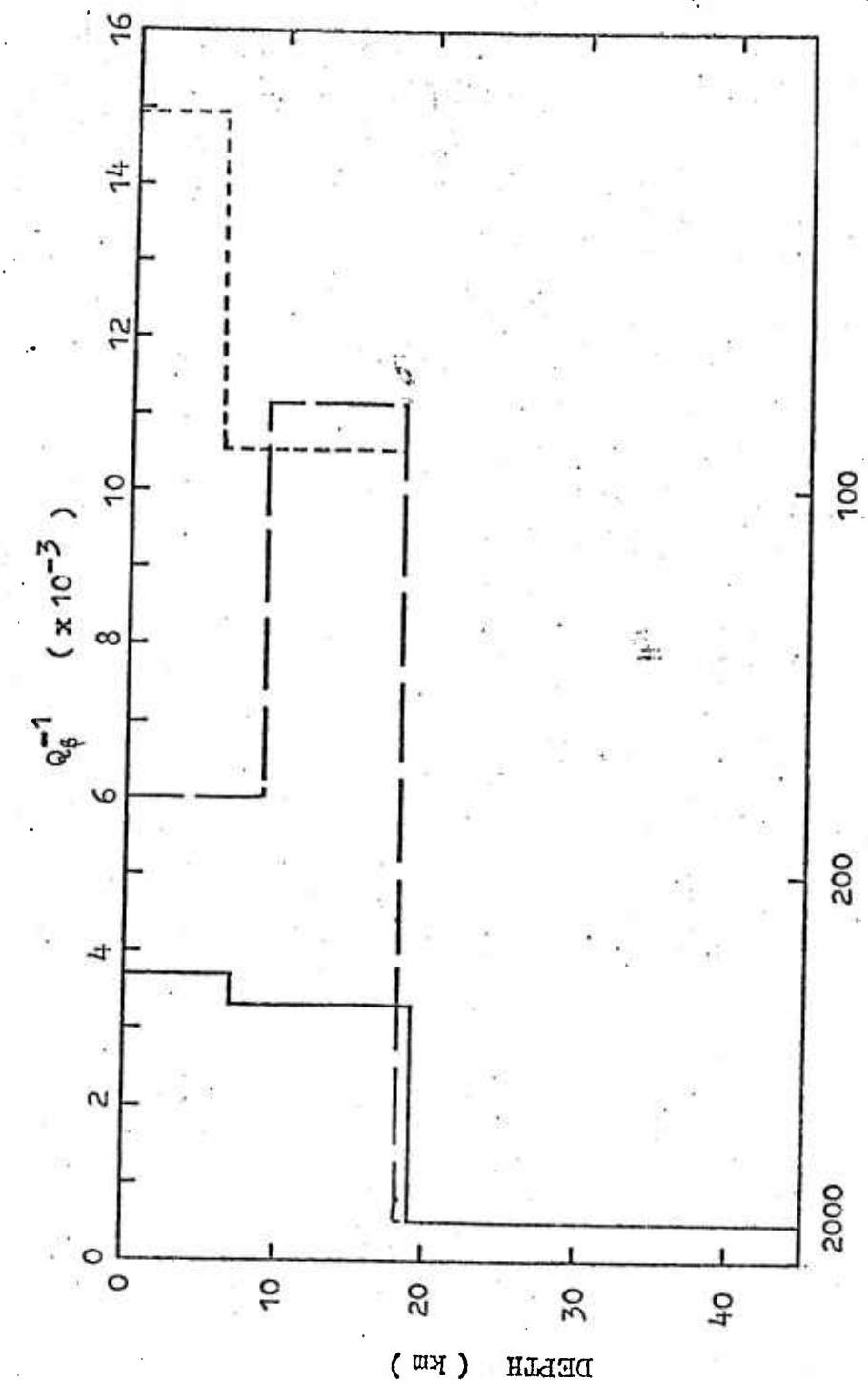

Figure 5. Three-layer Q models obtained for the eastern United States (solid), the Colorado Plateau (long dash), and the Basin and Range (short dash).

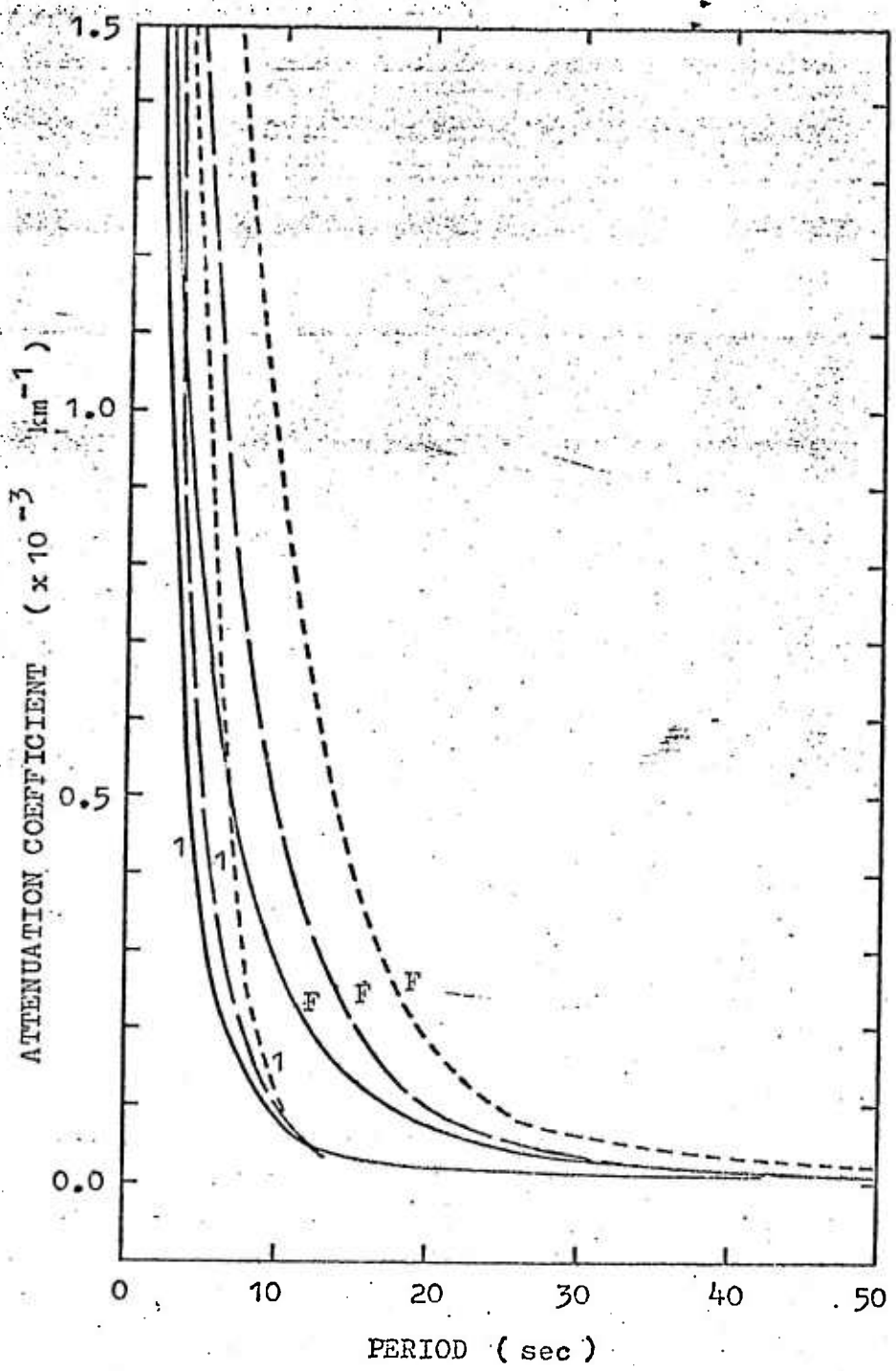

Figure 6. Rayleigh wave attenuation coefficients computed from Q models of Figure 4 for the fundamental and the first higher modes.

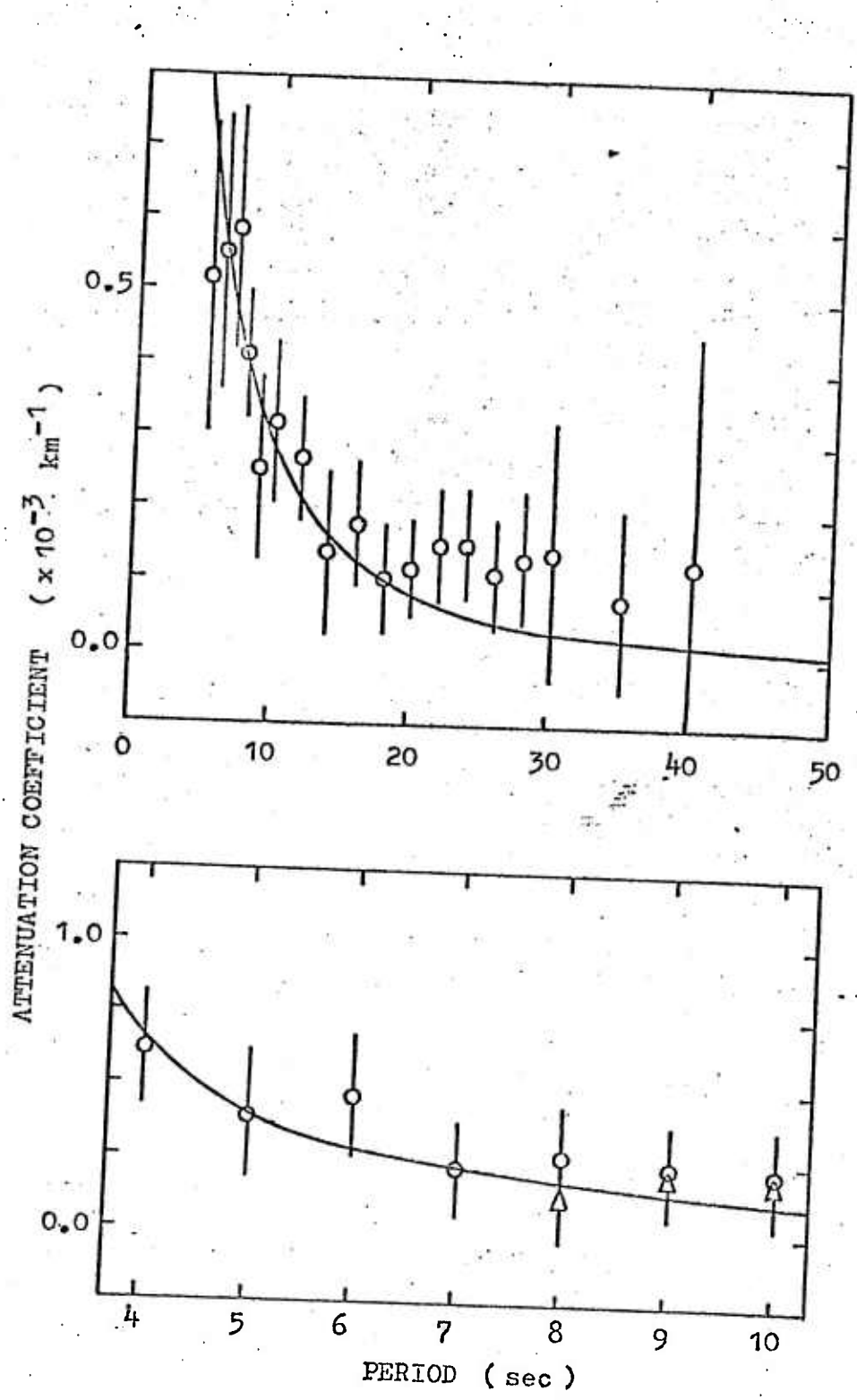

Figure 7. (top) Comparison of fundamental Rayleigh mode attenuation coefficient computed from two-layer model for the eastern United States with observed data of Herrmann and Mitchell (1975).
(bottom) Comparison of computed first higher mode Rayleigh wave attenuation coefficients with data of Mitchell (1973), circle, and Herrmann (1973b), triangle.

THE EXCITATION AND ATTENUATION OF SEISMIC CRUSTAL PHASES IN IRAN

Otto W. Nuttli

ABSTRACT

The most prominent crustal phases of Iranian earthquakes recorded by stations in Iran are the first P (Pn or refracted P), Pg, Sn and Lg. Pg, Sn and Lg appear as trains of waves whose attenuation behaves as that of dispersed surface waves. For 1-sec period Pg, Sn and Lg the coefficient of anelastic attenuation has an average value of 0.0045 km^{-1}, similar to that for California but much greater than that for eastern North America. For 3-sec period Lg waves the average value is 0.003 km^{-1}. The excitation of 1-sec Pg and Lg waves is approximately equal. The amplitude of their vertical components for an m_b = 5.0 earthquake at 10-km epicentral distance is 270 microns. The 10-km amplitude of vertical-component, 3-sec period Lg waves is 800 microns for an m_b = 5.0 earthquake. For all epicentral distances the resultant horizontal, 1-sec period Lg motion is twice that of the vertical component. The 10-km value of the resultant horizontal Sn motion for an m_b = 5.0 earthquake is 240 microns, slightly less than half that of Lg. The amplitude of the first P motion is in general one or more orders of magnitude smaller than that of the other crustal phases to distances of 500 km. However, at distances of 1000 to 1500 km the amplitude of first P is comparable to that of the other phases. Formulas are given to compute body-wave magnitude of Iranian earthquakes from the amplitudes of 1-sec period, vertical component Pg and Lg waves as well as amplitudes of the first arrival.

INTRODUCTION

In recent years a number of studies on the seismicity and seismotectonics of Iran have appeared (e.g. Nowroozi, 1971, 1976; McEvilly and Razani, 1973; Dewey and Grantz, 1973; Hedayati et al., 1976; Quittmeyer and Jacob, 1979). However, less is known and little has been published on the crustal structure of that country, or on the exictation and attenuation of crustal phases in it. The present paper is concerned with the latter problems, which are considered important because a knowledge of excitation and attenuation is needed for determining regional magnitude formulas and for determining the Q structure of the crust. Also attenuation and excitation are required sets of information, along with maximum magnitude and magnitude recurrence, for estimating the seismic hazard of the country.

Seismograms of the World-Wide Standard Seismograph Network (WWSSN) stations at Shiraz (SHI), Mashed (MSH) and Tabriz (TAB) provided the data for this study. With some few exceptions only the short-period seismograms were used. All of the earthquakes selected for study occurred within or on the boundaries of Iran. In the years 1972 through 1974, which were selected for study, 99 earthquakes provided usable seismograms. For these earthquakes the body-wave magnitude, m_b, varied from 3.7 to 6.0, with a median of 4.8, and the focal depth varied from 0 to 94 km, with a median of 43 km. Magnitudes, focal depths and epicentral coordinates were taken from the values published in the Bulletin of the International Seismological Centre.

The crustal phases selected for analysis were P, Pg, Sn and Lg. The P phase is the first-arriving phase, which at distances of 200 km and greater corresponds to Pn or to a wave refracted into the upper mantle. The Pg phase is a group of waves whose onset has a group velocity of 5.4 ± 0.2 km/sec. The phase Sn also corresponds to a

group of waves, rather than a single phase, whose onset has a velocity of 4.5 $\pm$ 0.2 km/sec. The dominant period of Pg and Sn as seen on the short-period WWSSN seismograms is about 1 sec. Lg is observed to have periods of approximately 1 to 3 sec, with the 1-sec period waves having a gorup velocity of 3.45 $\pm$ 0.2 km/sec and the 3-sec period waves a group velocity of 3.2 $\pm$ 0.2 km/sec. For some earthquakes large-amplitude arrivals corresponding to P* and S* could be observed, but in general these phases could not be followed over an appreciable range of epicentral distance. In this study the amplitudes of P and Pg were determined solely from the vertical-component seismograms. For the phase Sn only horizontal-component seismograms were used, although it is oftem prominant on the vertical-component as well. For Lg both vertical and horizontal seismograms were read. The amplitudes of phases from horizontal-component seismograms were taken to be the resultant of the maxima on the N-S and E-W components. Figure 1 shows an example of a short-period vertical seismogram recorded at SHI, at an epicentral distance of 545 km. The phases P, P*, Pg, Sn and Lg have been marked. The two sharp onsets beginning 4 and 6 sec after the first P wave may be pP and sP.

All the amplitude data were equalized to those of an m_b = 5.0 earthquake, assuming that $\Delta(\log A) = \Delta m_b$, where Δm_b is m_b minus 5. The m_b values employed for this equalization are those given in the Bulletin of the International Seismological Centre. As most of the m_b values of the studied earthquakes did not depart by more than 0.5 units from 5.0 (the median was 4.8), errors introduced by equalization are not expected to be large.

Lg WAVE

Three separate sets of Lg data were obtained from the seismograms. The first consists of amplitude and epicentral-distance values for the sustained maximum of the vertical-component, 1-sec period motion in the Lg wave train. Sustained maximum motion is used in the sense originally defined by Nuttli (1973), namely the amplitude equaled or exceeded by the three largest-amplitude waves in the train. The second set consists of similar data for the vertical-component, 3-sec period motion in the Lg-wave train. The third set contains the horizontal-component, 1-sec period motion. The amplitude of the horizontal-component motion is taken as the vector resultant of the sustained maxima on the N-S and E-W components.

The 1-sec period, vertical-component data are plotted in Figure 2. Two theoretical curves, whose equations are given by Ewing et al. (1957) as

$$A \sim (\sin \Delta)^{-1/2} \Delta^{-1/3} \exp(-\gamma \Delta) \qquad (1)$$

are plotted in the figure for values of the coefficient of anelastic attenuation, γ, equal to 0.004 and 0.005 km^{-1}. The curves are simply fitted by eye. Attempts at least-square curve fitting were unsuccessful owing to the small amplitudes for 15 points in the distance range of 135 to 500 km from SHI. In general, the same problem was encountered for all the waves studied. An explanation of the observed low amplitudes will be offered later in this section. From Figure 2 the γ value of 1-sec Lg waves appears to lie between 0.004 and 0.005 km^{-1}. An extrapolation of the theoretical curve back to 10-km epicentral distance (this

assumes a point, rather than an extended, source of waves) gives a value of 270 microns.

An alternate way of presenting the amplitude-distance data is to rewrite equation (1) as

$$56.306\ A\ (\sin \Delta)^{1/2}\ \Delta^{1/3} \sim \exp(-\gamma\ \Delta) \qquad (2)$$

where the number 56.306 is a normalization factor to make the product

$$56.306\ (\sin \Delta)^{1/2}\ \Delta^{1/3}$$

equal to unity at 10 km (0.009 deg) when Δ is expressed in degrees. In the future the product of this term and A will be called A*. On semi-logarithmic paper equation (2) plots as straight-line curves for constant values of γ. A plot of this type is given as Figure 3. An advantage of this method of presentation over that of Figure 2 is that the data are more spread out, so that the average value of γ, and the possible range of values of it, can be better estimated. As for Figure 2, the large number of low-amplitude values at distances to 500 km preclude the use of least squares to obtain an average value of γ and its confidence limits. However, from the figure it can be seen that with the exception of the anomalous values most of the points lie between the curves $\gamma = 0.006$ km^{-1} and $\gamma = 0.003$ km^{-1}, the average value of γ being approximately 0.0045 km^{-1}. The 10-km intercept is 270 microns, similar to that found in Figure 2.

There are a number of possible explanations for the scatter of the data of Figures 2 and 3. They include variation of excitation with focal depth, azimuthal variation in the radiation of Lg owing to source mechanism, incorrect estimate of m_b and variation in the absorption

coefficient over the area of Iran. To investigate the causes of the data scatter, maps are constructed showing the coefficient of absorption for each path from epicenter to seismograph station. In constructing these maps the assumption is made that the source excitation of Lg for each earthquake, when equalized to an $m_b = 5.0$ event, has the same value. This assumption will be violated if incorrect m_b values are assigned to any of the earthquakes or if there is a variation of Lg excitation with focal depth over the range of focal depths (0 to 94 km) encountered. Figures 4, 5 and 6 present the results. For the station SHI (Figure 4) the γ values for all sources except those to the west and south are close to 0.005 km^{-1}. Larger γ values, corresponding to large apparent values of anelastic attenuation, are seen for the southern and western paths. The fact that these anomalous values occur for a well-defined range of azimuths makes it unlikely that they result from an overestimate of the magnitudes of the earthquakes. The reported depth of the earthquake to the south of SHI with a $\gamma = 0.009$ km^{-1} is 43 km. Proceeding in a clockwise manner, the depths of the other most anomalous earthquakes are 20 km, 84 km, 24 km and 57 km. Thus there does not appear to be any strong relation between high γ values and greater focal depth, except possible for the earthquake with a depth of 84 km and a γ value of 0.018 km^{-1}. It would appear more likely, although it is by no means proved, that the high values of γ are associated with low Q values for the crust south and west of SHI. An inspection of Figure 5 reveals that short-distance paths to MSH have average or low γ values, as contrasted to the high values for earthquakes near SHI as seen in Figure 4. This rules out the possibility that the fit of theoretical curves to the

amplitude data of Figures 2 and 3 was incorrect, and that a curve with a smaller intercept and a smaller γ value should have been selected.

Comparison of Figures 4 and 5 shows that common paths for earthquakes in northeast Iran recorded at SHI and in south central Iran recorded at MSH have similar γ values. This suggest that the average γ value for such paths is little affected by the possible sources of error mentioned previously, and that it is representative of the Q crustal structure between SHI and MSH. Comparison of Figures 4 and 6 allows a similar statement to be made for the path between SHI and TAB, and of Figures 5 and 6 for the path between MSH and TAB.

In Figure 2 a curve with $\gamma = 0.0045$ km^{-1} can be approximated by a series of straight-line segments, and these in turn can be used in the derivation of formulas relating the amplitude of vertical-component, 1-sec period Lg waves to m_b. The resulting formulas are

$$m_b = \log A + 3.62 \log \Delta - 4.80 \qquad \text{for } 400 \leq \Delta \leq 1000 \tag{3}$$

$$m_b = \log A + 6.40 \log \Delta - 13.15 \qquad \text{for } 1000 \leq \Delta \leq 1500 \tag{4}$$

where A is the zero-to-peak sustained maximum amplitude of 1-sec period waves in microns, and Δ is epicentral distance in kilometers. No formula is given for Δ less than 400 km because of the large scatter of amplitudes observed in Iran at such near distances.

Figure 7 gives the A* values for the resultant horizontal, 1-sec period Lg motion equalized to $m_b = 5.0$. For Δ greater than 500 km, most of the points lie between the curves for which $\gamma = 0.003$ and 0.006 km^{-1}, indicating an average value of 0.0045 km^{-1}. This is the same value

which was obtained from the vertical-component data. However, the intercept is 540 microns, exactly twice that found for the vertical component. Ratios of Lg_h to Lg_z were determined for each earthquake and each recording station. For 40 such observations the average ratio is 2.08 ± 1.02, where the latter number is the standard deviation.

On the short-period seismograms the predominant period of Lg is close to 1 sec at the beginning of the wave train and lengthens to about 3 sec at later times. The seismograph response at periods greater than 3 sec is too low to enable such waves to be seen. At small epicentral distances ($\leq$ 400 km) the difference in group velocities is inadequate to separate the 1- and 3-sec period waves by arrival time. Thus the 1-sec period motion predominates, because the peak seismograph magnification occurs near 1 sec. However, the long-period seismograms can be used to obtain Lg amplitudes at these distances. Figure 8 shows the 3-sec period, higher-mode Lg waves arriving ahead of the fundamental-mode waves.

Figure 9 is a plot of the vertical-component, 3-sec period Lg amplitudes. A curve with $\gamma = 0.003$ km^{-1} passes through the distribution of most of the data points, although it tends to overestimate amplitudes beyond 1000 km. The 10-km intercept is 800 microns. When compared with a value of 270 microns for 1-sec period waves it follows that the 10-km amplitudes are falling off as the first power of the period for periods between 3 and 1 sec. Figure 10 presents the A* values, most of which lie between the curves $\gamma = 0.001$ and $\gamma = 0.005$ km^{-1}. The 10-km intercept obtained from this figure is 780 microns, slightly less than that obtained from Figure 9.

Pg WAVE

The amplitudes of vertical-component, 1-sec period Pg waves are given in Figure 11. At small distances the short-period seismogram traces frequently either go off scale or are whited out. Thus the long-period seismograms were used to supplement the data set at these distances. As in Figure 2 there are a number of amplitudes at SHI at distances less than 400 km which are anomalously small. Their probable cause is large absorption or low Q values for paths to the south and west of SHI.

In order to select a theoretical attenuation curve to fit the data, the dependence of the non-absorptive attenuation on distance must be known. This can best be determined from data at small epicentral distances, at which anelastic attenuation is of lesser significance. Unfortunately the scatter in the data of Figure 11 at distances less than 200 km is large. Excluding the low-amplitude point at Δ = 50 km, the slope of a straight line through the data out to 200 km is approximately -5/6, which at these small distances is equivalent to the $(\sin \Delta)^{-1/2} \Delta^{-1/3}$ dependence that applies for dispersed, Airy-type surface waves. Thus the data of Figure 11 suggest that Pg behaves as a dispersed surface wave, which is in harmony with its observed character of being a train of waves rather than a single phase.

Assuming that Pg attenuates as a dispersed surface wave, the γ value corresponding to the solid-line curve shown in Figure 11 is 0.0045 km^{-1}. This is the same value as obtained for 1-sec period Lg waves. The 10-km intercept is 230 microns, only slightly less than that of 1-sec period Lg. Equal values of γ for Pg and Lg lead to the surprising conclusions that Q for Pg is less than Q for Lg by the ratio of their group velocities, about 3.4/5.4 or 0.63.

Figure 12 presents the A* values of Pg. Excluding values at distances less than 500 km, most of the data points fall between the curves $\gamma = 0.003$ and $0.008\ km^{-1}$. The value $\gamma = 0.0045\ km^{-1}$, which was obtained from Figure 11, can be taken as an approximation for the average curve. The 10-km intercept is 280 microns, similar to the Lg intercept and slightly larger than the Pg intercept obtained from Figure 11. Considering the scatter of the observational data, Pg and Lg can be said to have the same 10-km intercepts for Iranian earthquakes.

Magnitude formulas can be derived by fitting the curve of Figure 11 by straight-line segments. The resulting equations are identical to equations (3) and (4) because the attenuation and excitation of 1-sec Pg and Lg waves are the same.

Sn WAVE

Resultant amplitudes of horizontal-component, 1-sec period Sn waves are plotted in Figure 13. As for Pg, scatter in the amplitude values at near distances makes it difficult to determine the exact nature of the non-absorptive attenuation term. From a trial-and-error procedure the data appear to be in accord with Sn being a dispersed surface wave. As Sn appears on the seismograms as a train of waves, rather than a pulse-like phase, it seems reasonable to consider it as a guided wave. Assuming such a relation, the data of Figure 13 are approximately satisfied by a curve with $\gamma = 0.0045$ km^{-1}. Its 10-km intercept is 240 microns, compared to 540 microns for resultant horizontal, 1-sec period Lg waves. Figure 14, which presents the A* values, suggests a slightly larger intercept of 270 microns, and a γ value lying between 0.003 and 0.006 km^{-1}.

P WAVE

The largest zero-to-peak amplitude in the first 3 sec of the P-wave motion is taken as the amplitude of P. The data of vertical-component, 1-sec period P waves are plotted in Figure 15. A noteworthy feature of the figure is the large scatter in the data, at least an order of magnitude over the entire distance range of 150 to 1400 km. The most likely cause of data scatter is that the data have not been corrected for focal mechanism, although other explanations can be offered.

In the figure the horizontal solid lines are the logarithmic average values over 100-km distance intervals, and the dashed lines indicate the average values plus or minus one standard deviation. A smooth curve has been somewhat arbitrarily drawn through the average values. The differences, $5.0 - \log A(\Delta)$, can be taken as the magnitude-calibration function $\beta(\Delta)$. The appropriate magnitude formula is

$$m_b = \log A + \beta(\Delta). \qquad (5)$$

CONCLUSIONS

The attenuation of 1-sec period crustal phases in Iran is relatively high. A γ-value of 0.0045 km^{-1} corresponds to an apparent Q of 200 for Lg, 150 for Sn and 125 for Pg. By way of comparison, Nuttli (1973) found an apparent Q of 1500 for 1-sec Lg waves in eastern North America and Herrmann (1979) found $\gamma = 0.0048$ km^{-1} and apparent Q = 229 for the coda of 1-sec Lg waves recorded at Berkeley, California. The results of the present study agree with the conclusions of Chandra et al. (1979) who found that the attenuation of seismic intensity in Iran is slightly greater than in the San Andreas province of California.

The 10-km intercept for vertical-component, 1-sec Lg waves in Iran is 270 microns. For eastern North America, using the data in Nuttli (1973), the intercept can be shown to be 150 microns. The difference in excitation levels for these two regions is equivalent to 0.25 m_b units, which is approaching the uncertainty in body-wave magnitude estimates. Thus the excitation levels of 1-sec period Lg waves for $m_b = 5.0$ earthquakes are not significantly different in eastern North America and Iran. This is not unexpected, for m_b is a measure of 1-sec period P-wave excitation, and it appears reasonable to expect a correspondence between 1-sec period P-wave and 1-sec period Lg-wave excitations.

The formulas presented in this paper indicate that earthquakes in Iran with m_b values as small as 4.3 can be detected by a short-period vertical seismograph, such as at SHI, with a 1-sec magnification of 50,000 at a distance of 1000 km. This assumes that a 1-mm trace amplitude for

Pg and Lg is the lower threshold of detection. For a 1-mm trace amplitude for the first P-wave arrival, the corresponding threshold m_b is 4.5. At 500-km distance the m_b values are 3.2, using Pg and Lg, and 4.1, using first P. Because the onsets of Pg and Lg generally are not sharp, the first P wave must be used for detection purposes. Thus if earthquakes down to $m_b = 3.0$ are to be detected and located in Iran, it will be necessary to operate seismographs at substantially higher gain than 50,000 at 1-sec period and to have a station density of less than 500-km separation between stations. Such a network of stations could provide the information required to determine the magnitude-recurrence relation for the seismic source regions and to model the crustal structure of Iran.

ACKNOWLEDGMENT

This research was supported by the Defense Advanced Research Projects Agency and was monitored by the Air Force Office of Scientific Research under Contract No. F49620-79-C-0025.

REFERENCES

Chandra, U., J.G. McWhorter, and A.A. Nowroozi (1979). Attenuation of intensities in Iran, Bull. Seism. Soc. Am., 69, 237-250.

Dewey, J.W. and A. Grantz (1973). The Ghir earthquake of April 10, 1972 in the Zagros Mountains of Southern Iran: Seismotectonic aspects and some results of a field reconnaissance, Bull. Seism. Soc. Am., 63, 2071-2090.

Ewing, M., J.M. Jardetzky, and F. Press (1957). Elastic Waves in Layered Media, p. 358, McGraw-Hill, New York.

Hedayati, A., J.C. Brander, and M. Berberian (1976). Microearthquake study of Tehran region, Iran, Bull. Seism. Soc. Am., 66, 1713-1725.

Herrmann, R.B. (1979). Q estimates using the coda of local earthquakes, submitted to Bull. Seism. Soc. Am.

McEvilly, T.V. and R. Razani (1973). A preliminary report: The Qir, Iran earthquake of April 10, 1972, Bull. Seism. Soc. Am., 63, 339-354.

Nowroozi, A.A. (1971). Seismotectonics of the Persian Plateau, eastern Turkey, Caucasus, and Hindu-Kush regions, Bull. Seism. Soc. Am., 61, 317-341.

Nowroozi, A.A. (1976). Seismotectonic provinces of Iran, Bull. Seism. Soc. Am., 66, 1249-1276.

Nuttli, O.W. (1973). Seismic wave attenuation and magnitude relations for eastern North America, J. Geophys. Res., 78, 876-885.

Quittmeyer, R.C. and K.H. Jacob (1979). Historical and modern seismicity of Pakistan, Afghanistan, northwestern India, and southeastern Iran, Bull. Seism. Soc. Am., 69, 773-823.

DEPARTMENT OF EARTH AND ATMOSPHERIC SCIENCES
SAINT LOUIS UNIVERSITY
ST LOUIS, MO 63103

FIGURE CAPTIONS

Fig. 1. SHI seismogram (SPZ component) of the earthquake of May 24, 1973. Epicentral distance is 545 km. The origin time is $23^h\ 14^m\ 36^s$, the focal depth 50 km, the body-wave magnitude 4.4, and the epicentral coordinates 28.10°N, 57.82°E. The instrument magnification is 50,000 at 1-sec period.

Fig. 2. Lg amplitudes (vertical-component, 1-sec period) equalized to $m_b = 5.0$. The average value of γ is taken to be 0.0045 km^{-1}.

Fig. 3. Lg amplitudes (vertical-component, 1-sec period) equalized to $m_b = 5.0$ and with the effects of geometric spreading and dispersion removed. The dashed lines are theoretical curves of constant γ value. The average value is taken to be 0.0045 km^{-1}.

Fig. 4. γ values of 1-sec period Lg waves for individual earthquakes recorded at SHI. The dots indicate the location of the epicenters.

Fig. 5. γ values of 1-sec period Lg waves for individual earthquakes recorded at MSH. The dots indicate the location of the epicenters.

Fig. 6. γ values of 1-sec period Lg waves for individual earthquakes recorded at TAB. The dots indicate the location of the epicenters.

Fig. 7. Lg amplitudes (horizontal-component, 1-sec period) equalized to $m_b = 5.0$ and with the effects of geometric spreading and dispersion removed.

Fig. 8. MSH seismogram (LPZ component) of the earthquake of May 24, 1973. Epicentral distance is 925 km. The instrument magnification is 1,500 at 20-sec period. See the caption of Fig. 1 for the hypocentral coordinates.

Fig. 9. Lg amplitudes (vertical-component, 3-sec period) equalized to $m_b = 5.0$.

Fig. 10. Lg amplitudes (vertical-component, 3-sec period) equalized to $m_b = 5.0$ and with the effects of geometric spreading and dispersion removed.

Fig. 11. Pg amplitudes (vertical-component, 1-sec period) equalized to $m_b = 5.0$.

Fig. 12. Pg amplitudes (vertical-component, 1-sec period) equalized to $m_b = 5.0$ and with the effects of geometric spreading and dispersion removed.

Fig. 13. Sn amplitudes (horizontal-component, 1-sec period) equalized to $m_b = 5.0$.

Fig. 14. Sn amplitudes (horizontal-component, 1-sec period) equalized to m_b = 5.0 and with the effects of geometric spreading and dispersion removed.

Fig. 15. Amplitudes of first P-wave arrivals (vertical-component, 1-sec period) equalized to m_b = 5.0. The solid horizontal lines are the average of the logarithms of the amplitudes, and the dashed lines the average plus and minus one standard deviation. The solid-line curve is a smooth curve drawn through the average values.

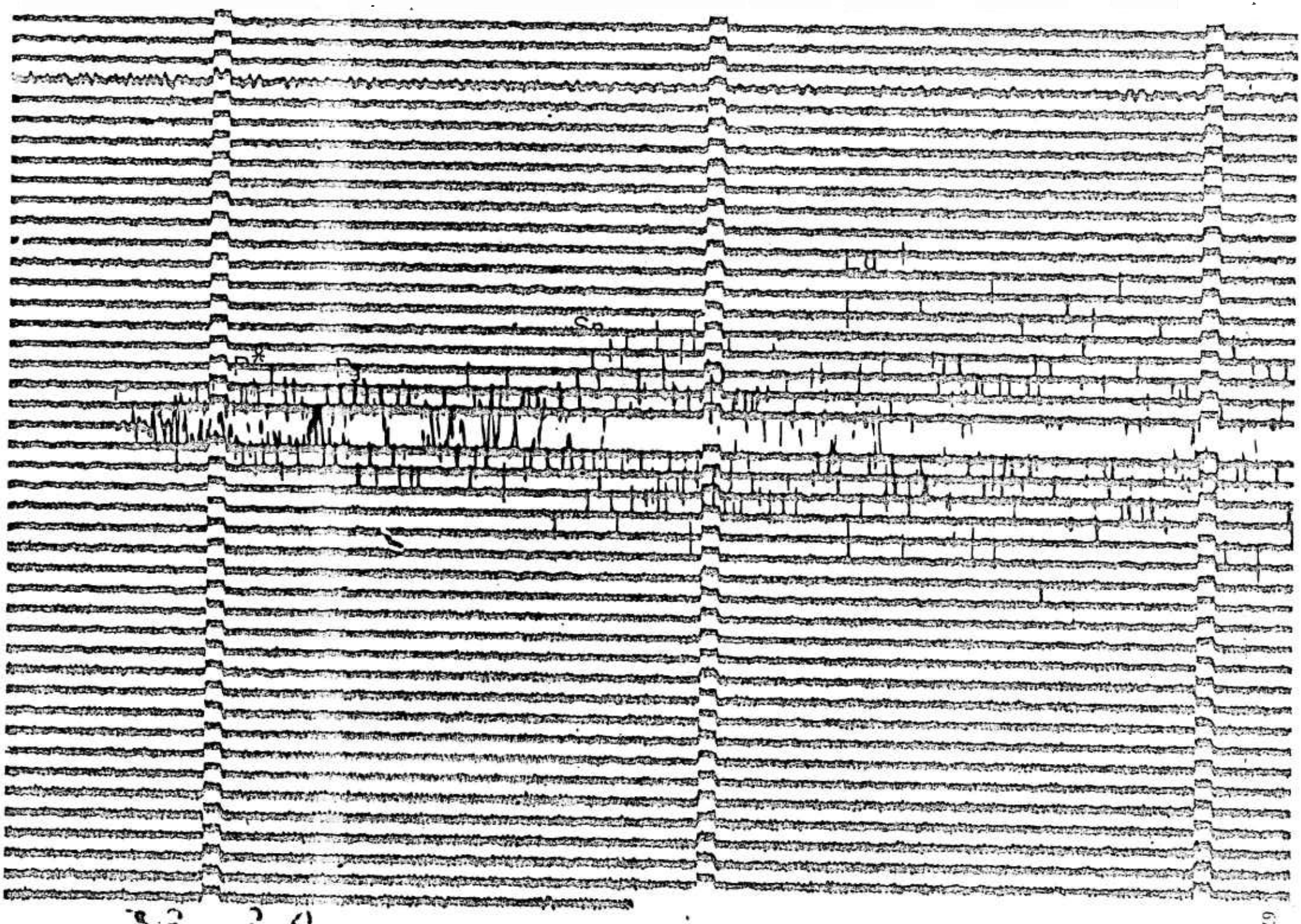

Figure 1.

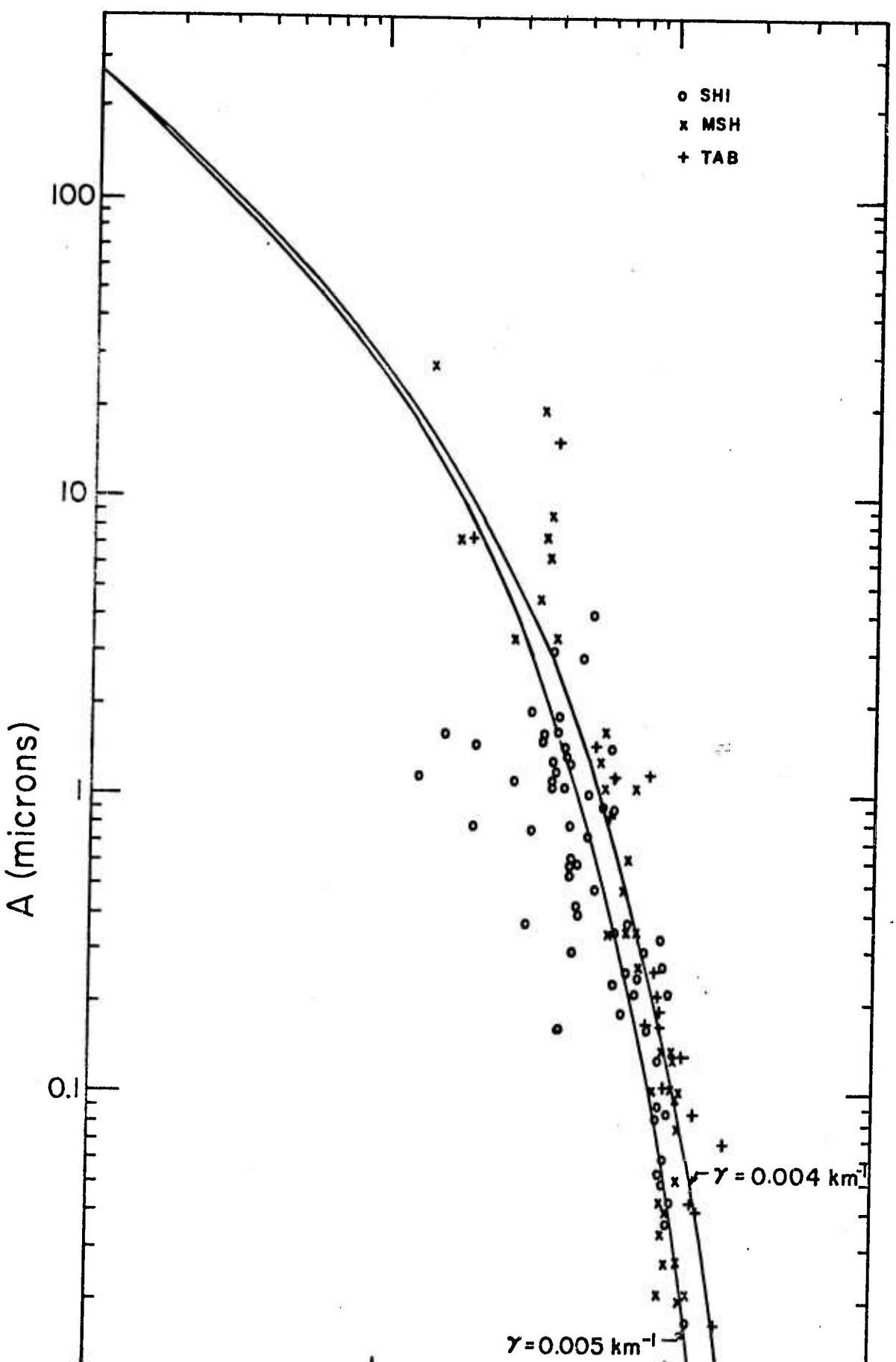
o SHI
x MSH
+ TAB
100
10
1
0.1
0.01
A (microns)
10
100
1000
Δ (km)
γ = 0.004 km⁻¹
γ = 0.005 km⁻¹

Figure 2.

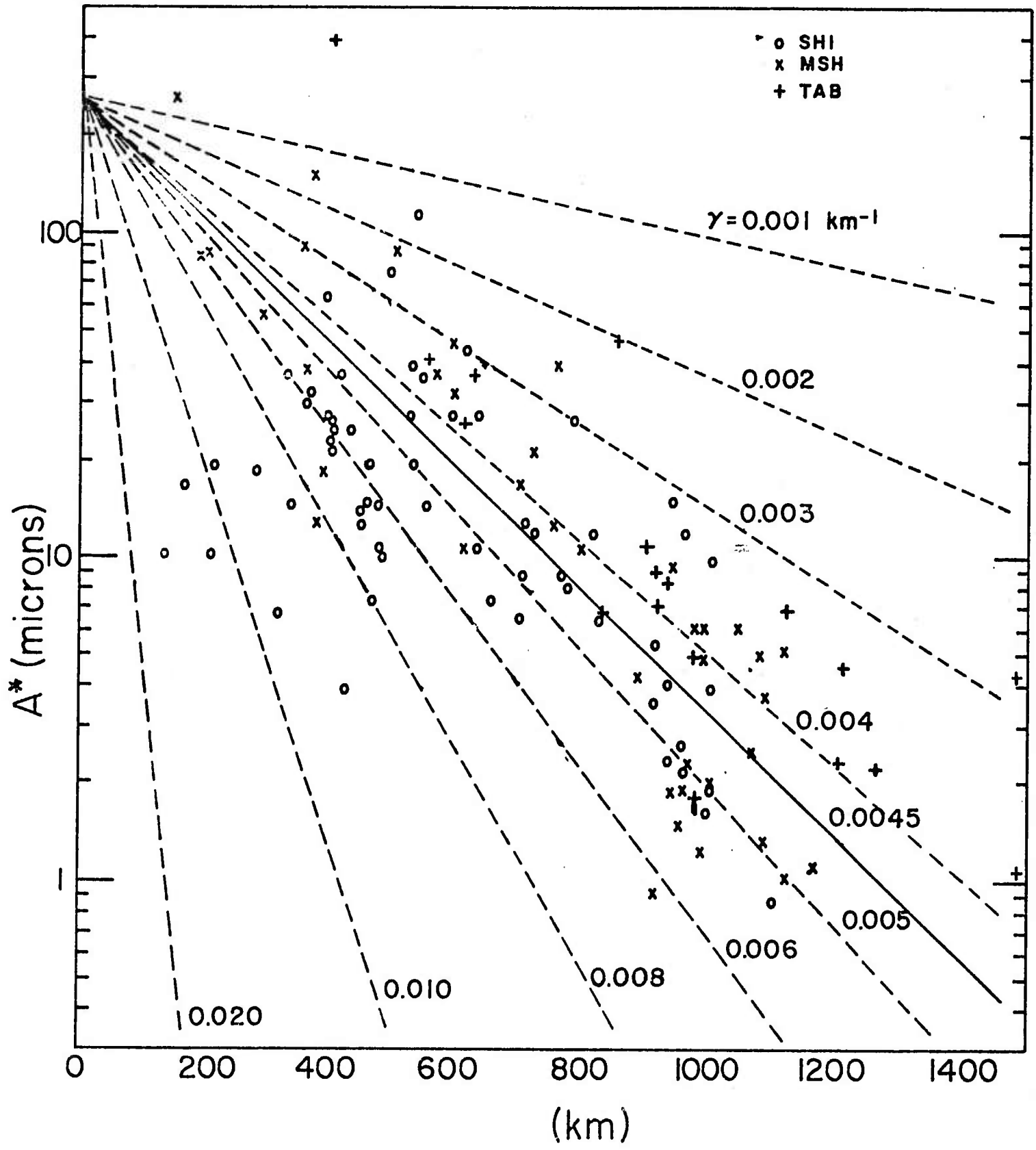
o SHI
x MSH
+ TAB
γ = 0.001 km⁻¹
0.002
0.003
0.004
0.0045
0.005
0.006
0.008
0.010
0.020
100
10
1
A* (microns)
0
200
400
600
800
1000
1200
1400
(km)

Figure 3.

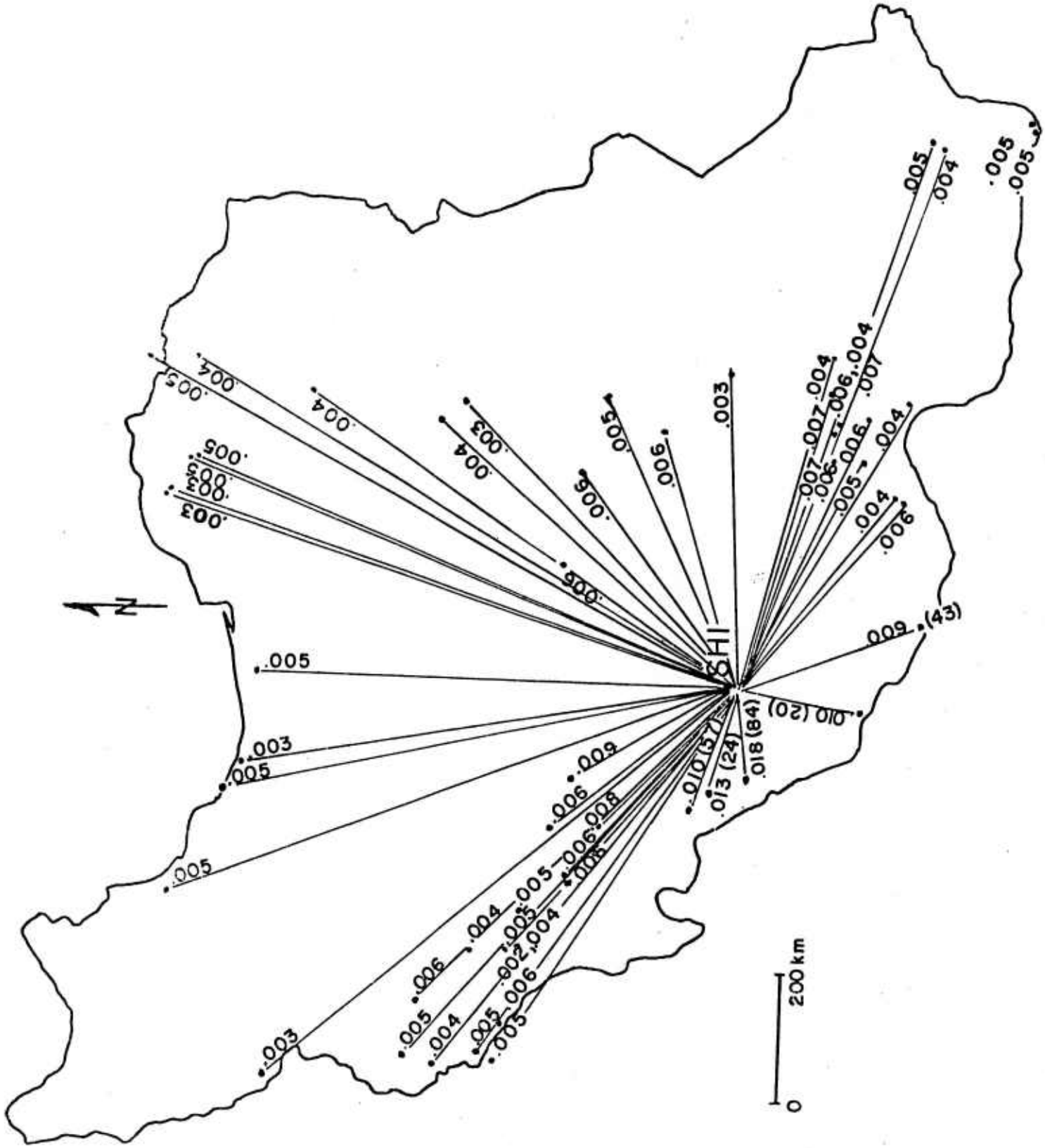
N
OHI
200 km
0
.005
.004
.003
.006
.007
.009
.010 (20)
.018 (84)
.013 (24)
.010 (57)
(43)

Figure 4.

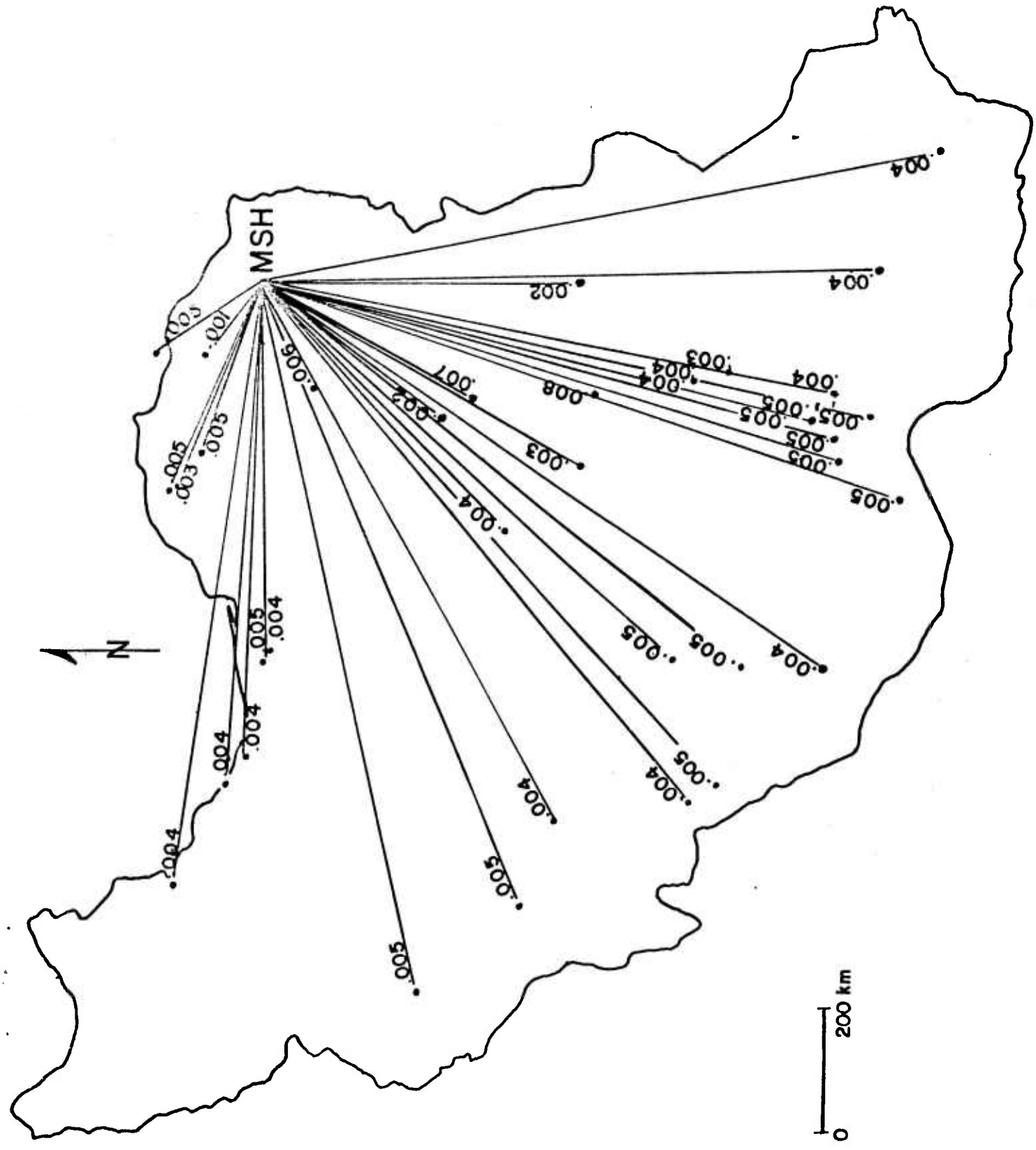

Figure 5.

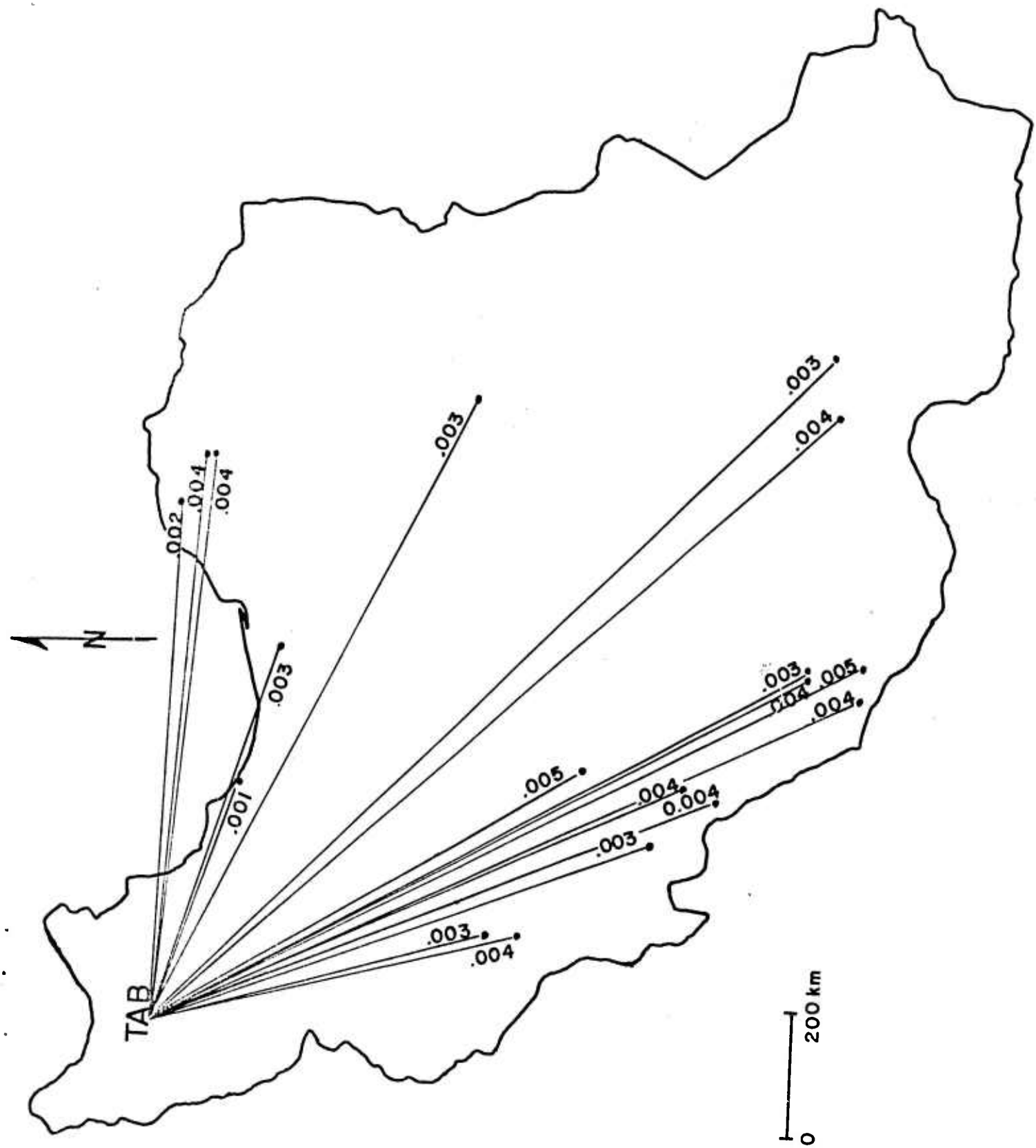
.003
.004
.002
.004
.004
.003
.003
.004
.005
.004
.004
.005
.004
0.004
.003
.003
.004
.001
.003
TAB
N
200 km
0

Figure 6.

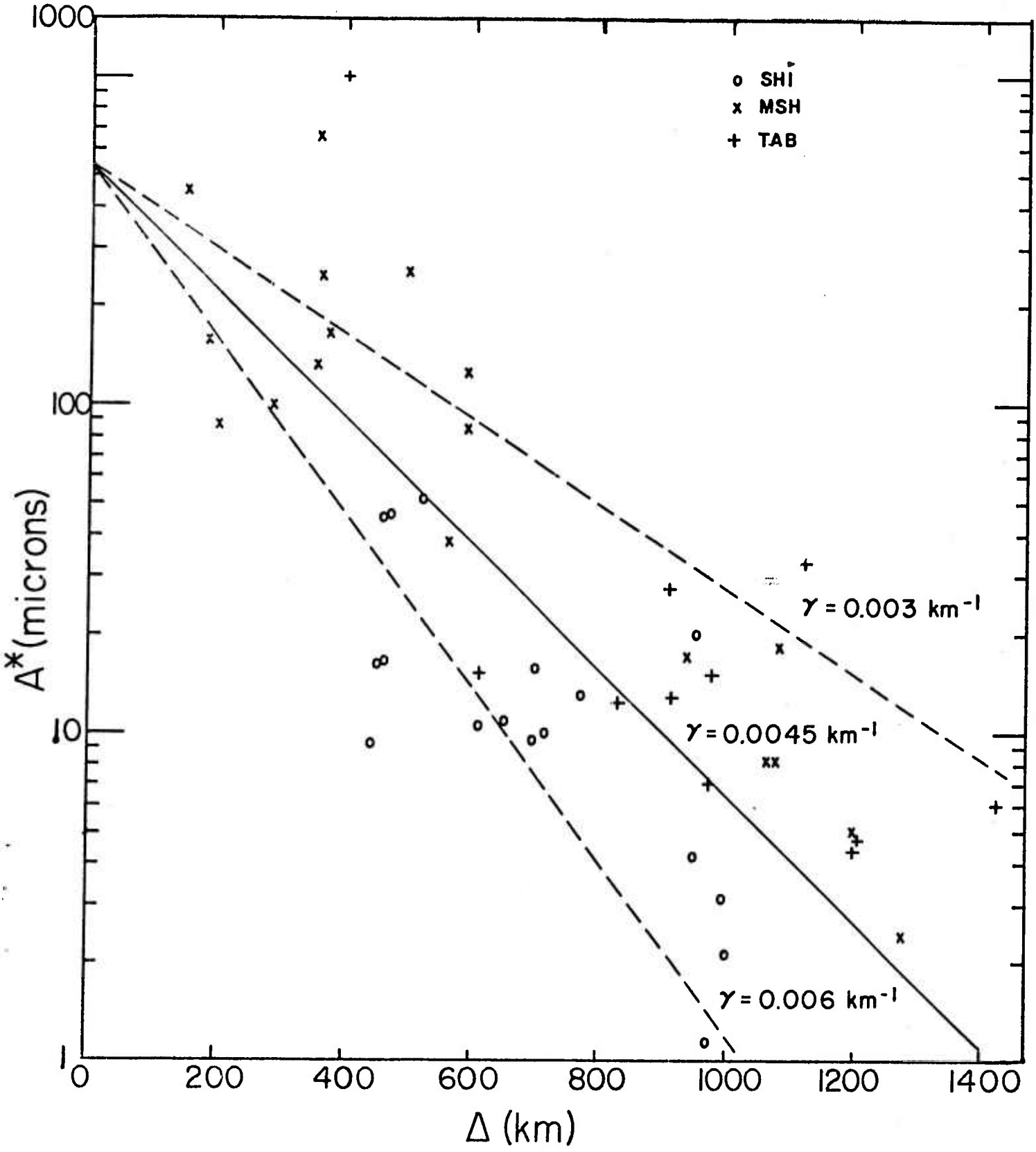
1000
100
10
1
A*(microns)
o SHI
x MSH
+ TAB
γ = 0.003 km⁻¹
γ = 0.0045 km⁻¹
γ = 0.006 km⁻¹
0
200
400
600
800
1000
1200
1400
Δ (km)

Figure 7.

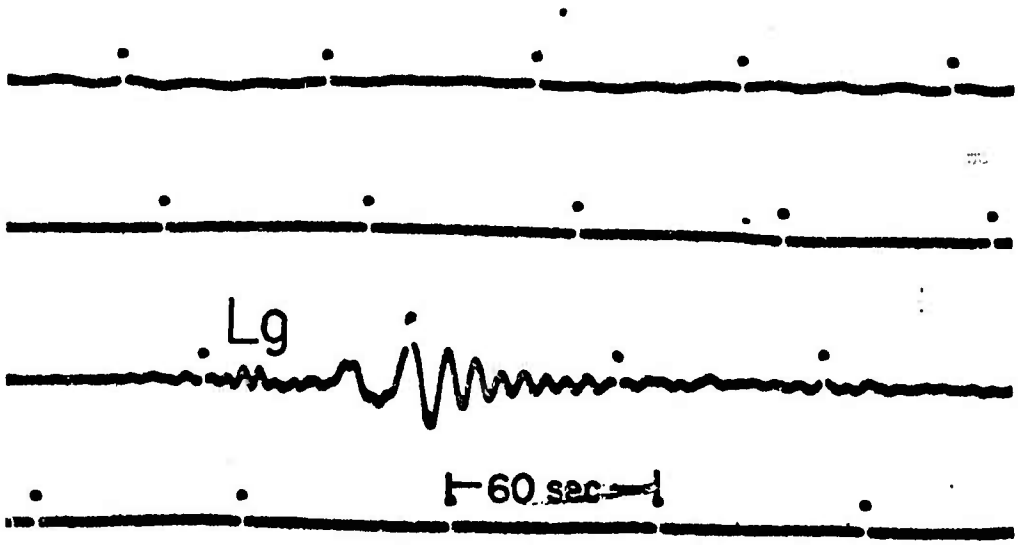

Figure 8.

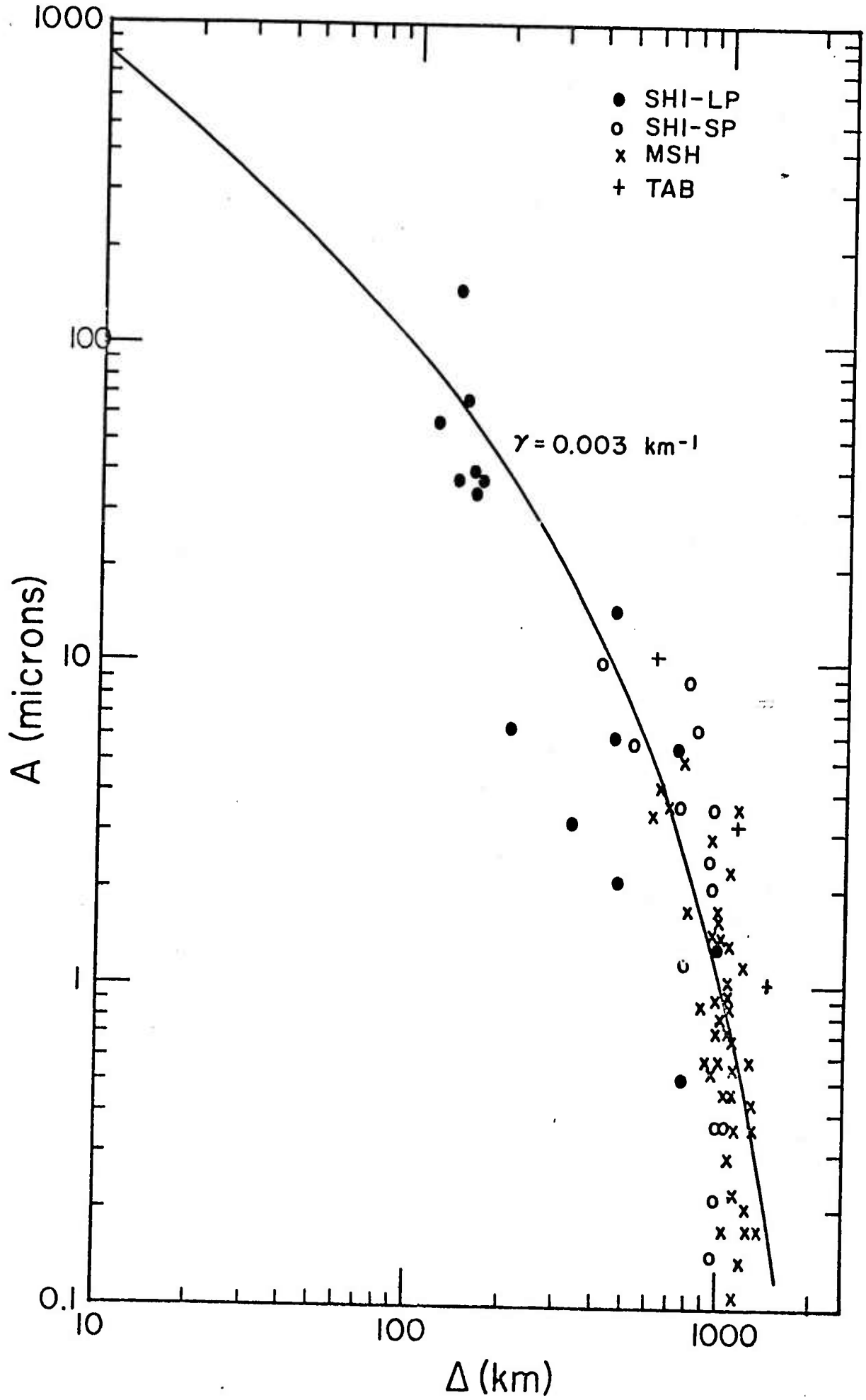
1000
100
10
1
0.1
10
100
1000
A (microns)
Δ (km)
SHI-LP
SHI-SP
MSH
TAB
γ = 0.003 km⁻¹

Figure 9.

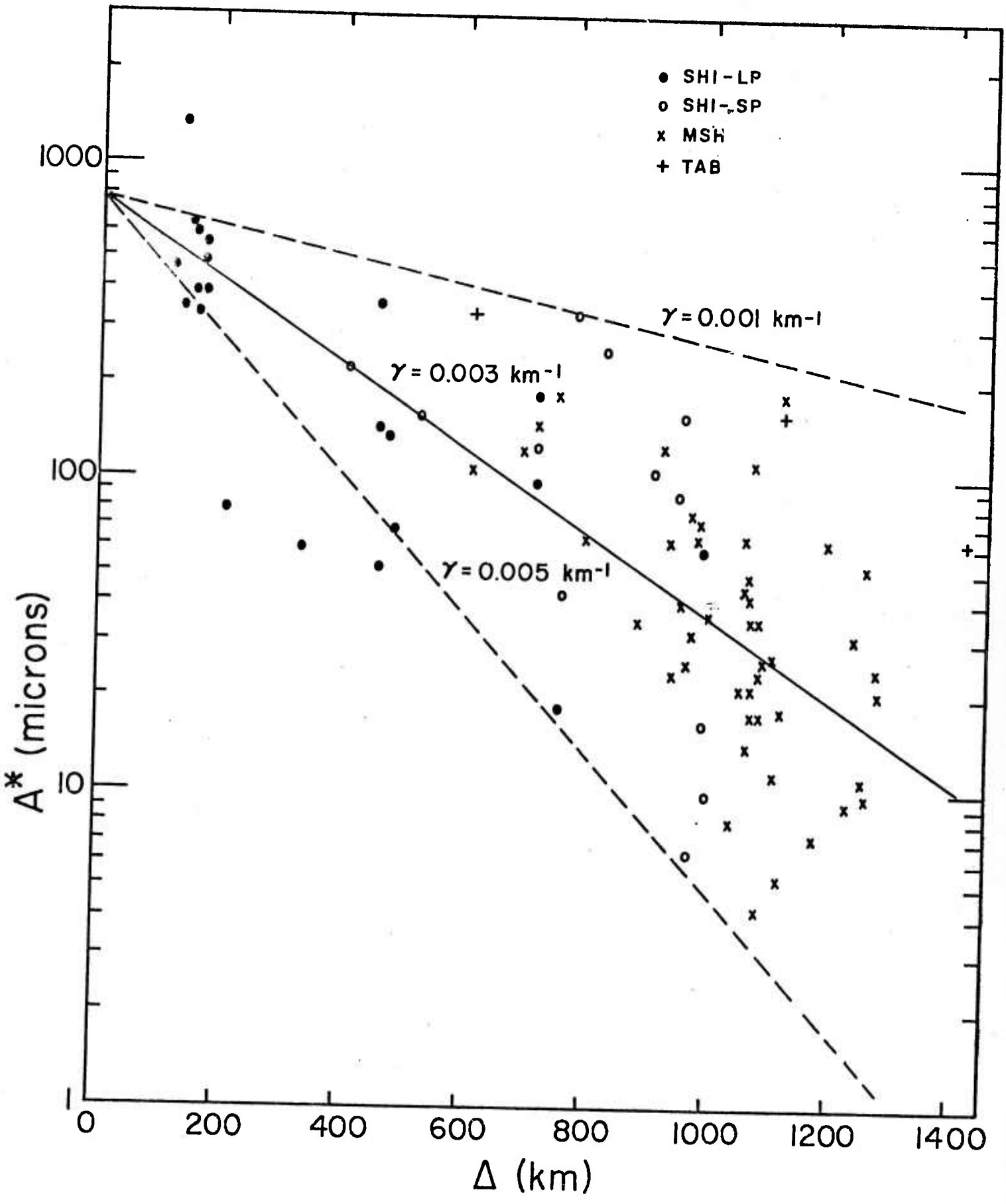
SHI-LP
SHI-SP
MSH
TAB
γ = 0.001 km-1
γ = 0.003 km-1
γ = 0.005 km-1
A* (microns)
Δ (km)
1000
100
10
1
0
200
400
600
800
1000
1200
1400

Figure 10.

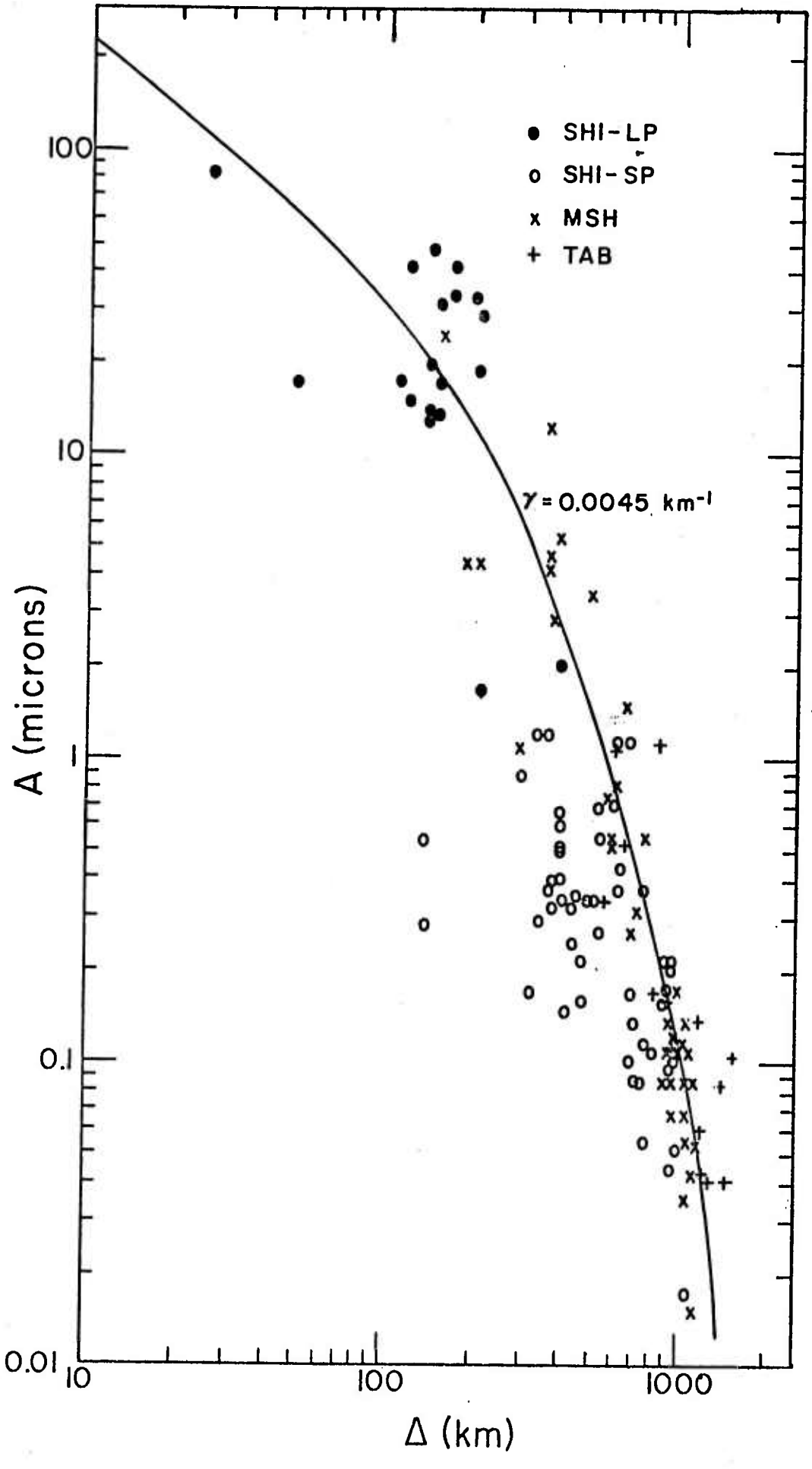
SHI-LP
SHI-SP
MSH
TAB
γ = 0.0045 km⁻¹
A (microns)
100
10
1
0.1
0.01
10
100
1000
Δ (km)

Figure 11.

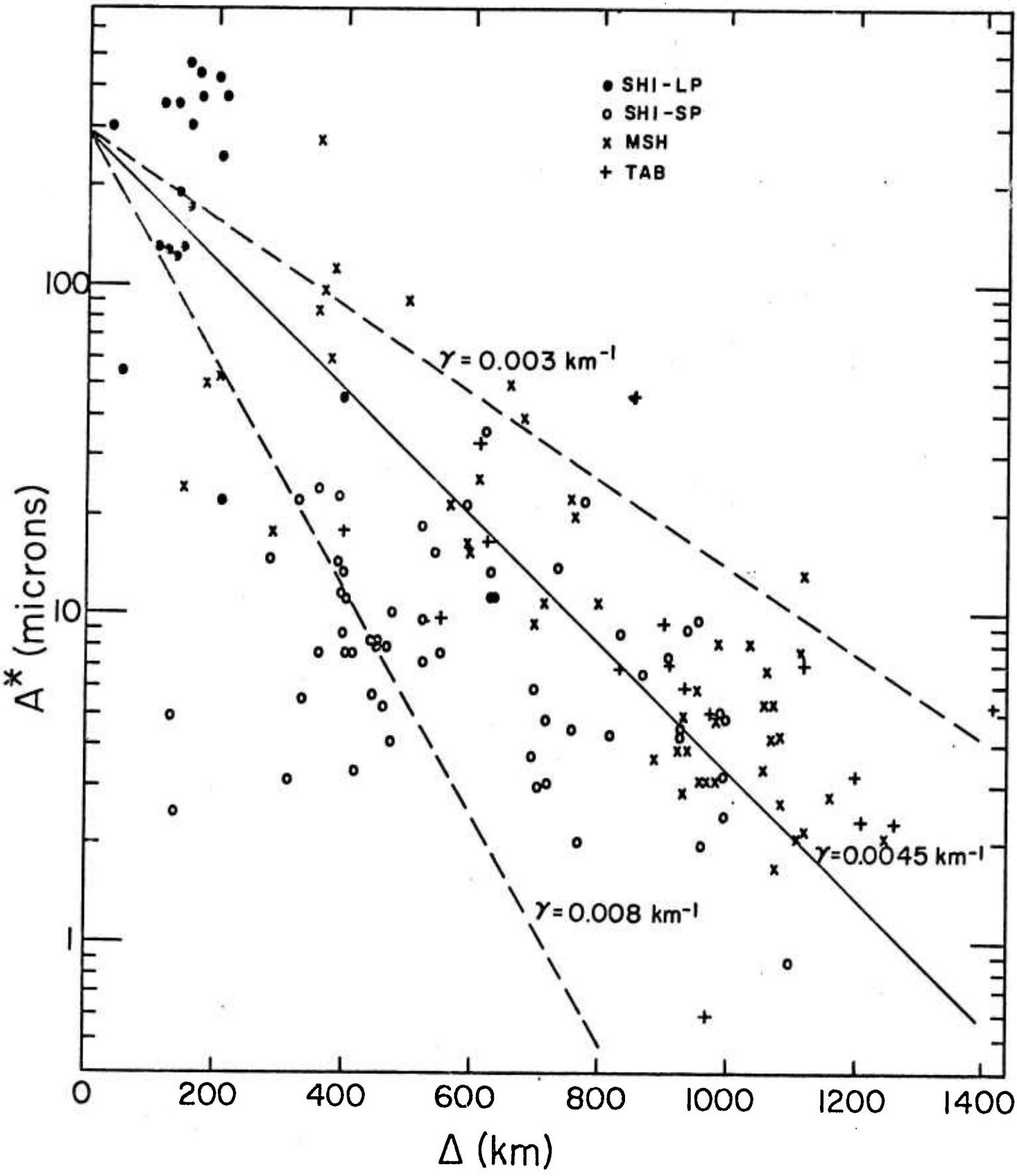
● SHI-LP
o SHI-SP
x MSH
+ TAB
γ = 0.003 km⁻¹
γ = 0.0045 km⁻¹
γ = 0.008 km⁻¹
A* (microns)
100
10
1
0
200
400
600
800
1000
1200
1400
Δ (km)

Figure 12.

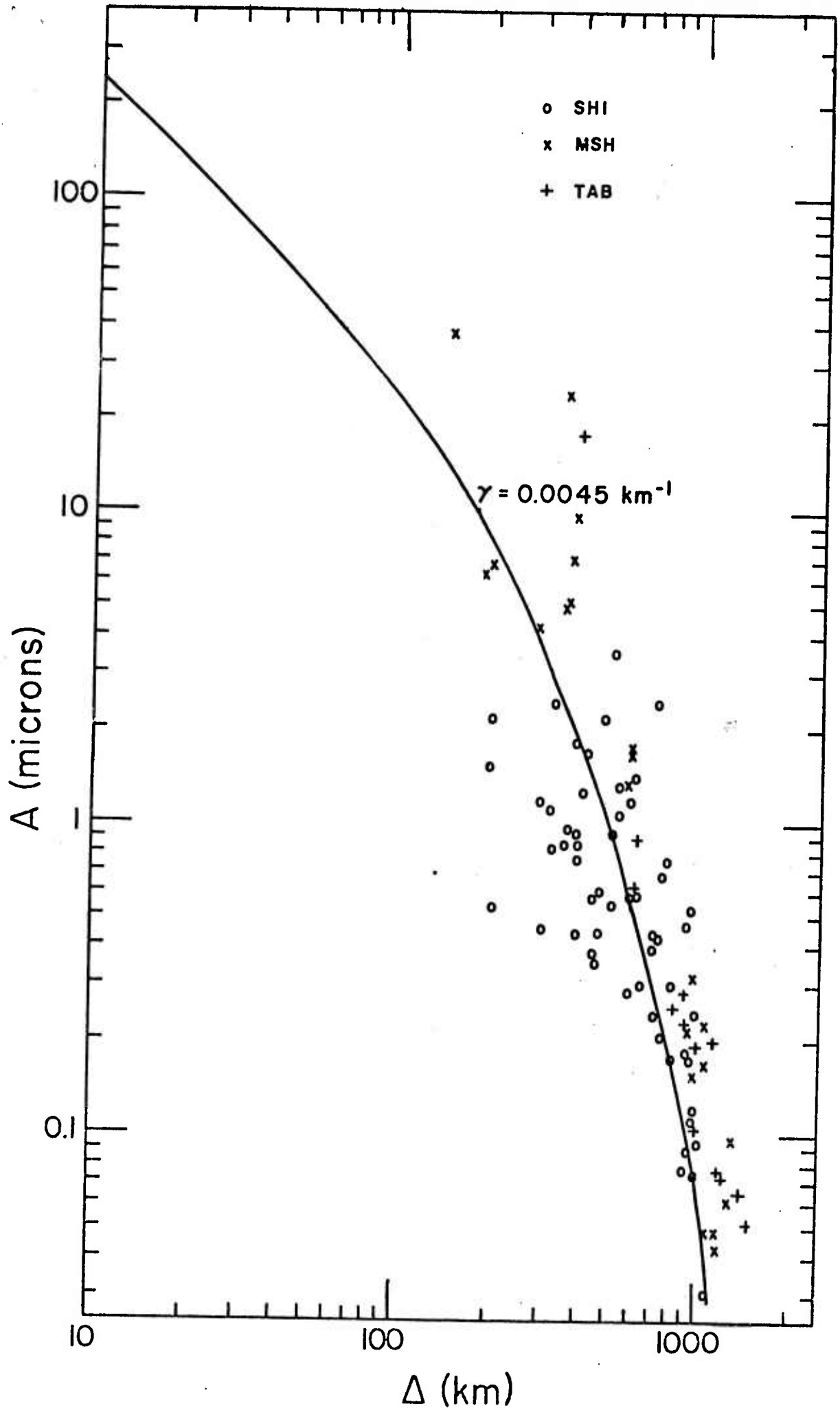

Figure 13.

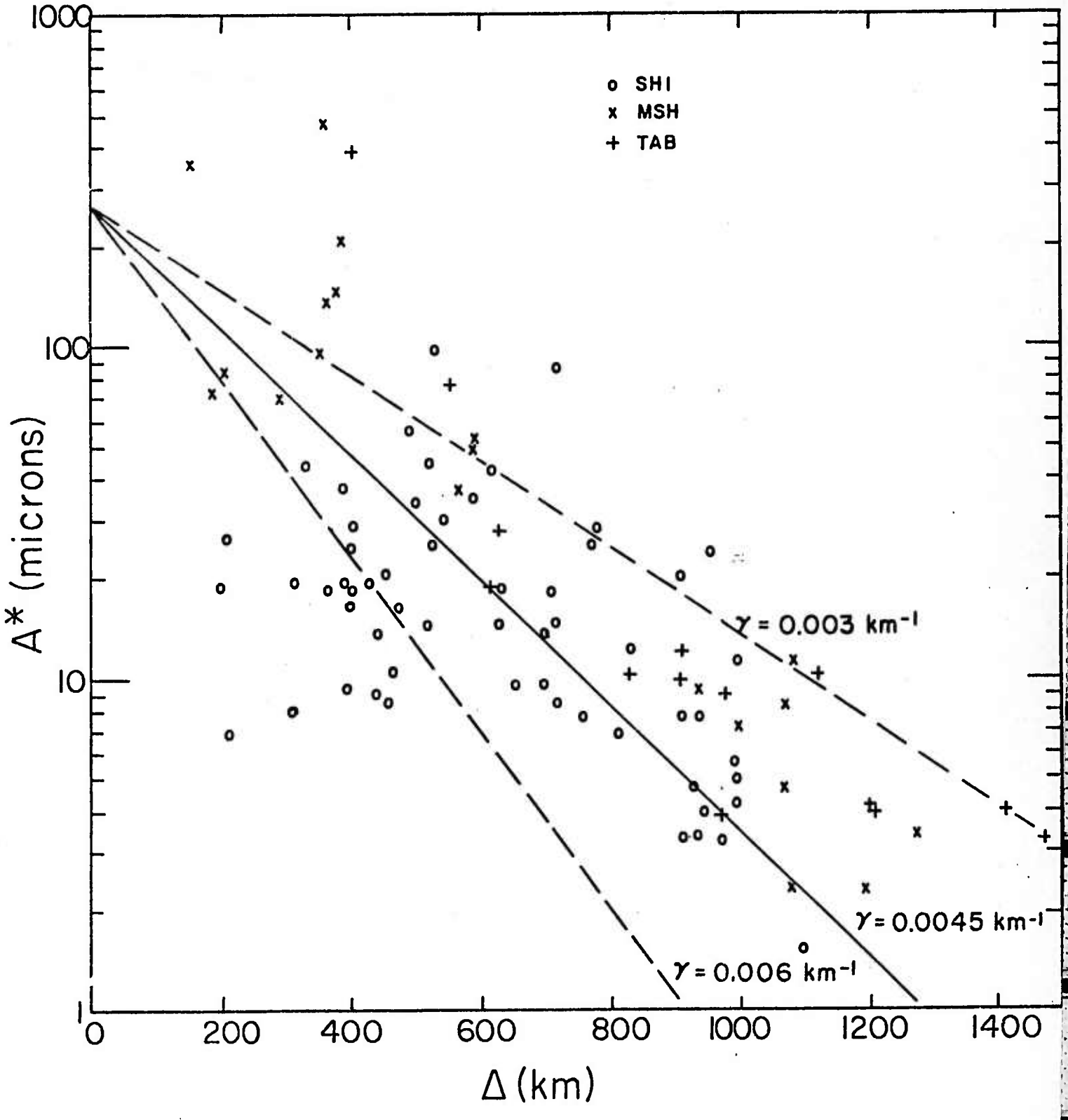
1000
100
10
1
A* (microns)
o SHI
x MSH
+ TAB
γ = 0.003 km⁻¹
γ = 0.0045 km⁻¹
γ = 0.006 km⁻¹
0
200
400
600
800
1000
1200
1400
Δ (km)

Figure 14.

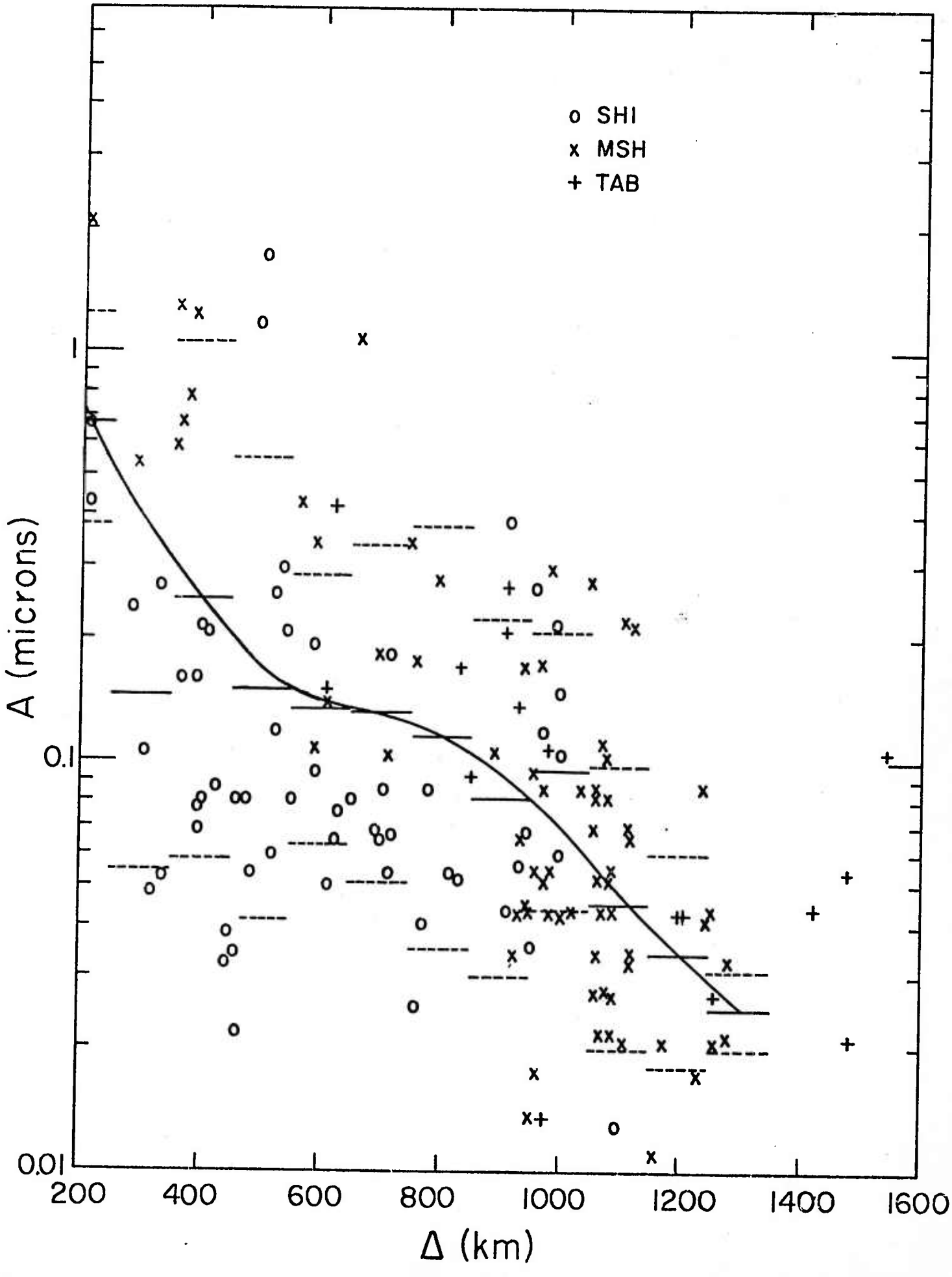
o SHI
x MSH
+ TAB
A (microns)
1
0.1
0.01
200
400
600
800
1000
1200
1400
1600
Δ (km)

Figure 15.

INVERSION OF RAYLEIGH-WAVE GROUP VELOCITY AND ATTENUATION DATA FOR THE TIBETAN PLATEAU

by

Huei-Yuin Wen Wang

The Tibetan seismic velocity model and attenuation data have been recalculated and improved by using an inversion technique instead of trial and error method. A general inversion method for determining an earth model has been developed by Backus and Gilbert (1970). Their method is based on the fact that a general inversion problem is assumed to be linear or to have been linearized. The linear approximation reduced the problem to the solution of an under-determined set of linear equations for the first-order corrections to the starting model. The exact velocities are computed for the corrected model, which is then used as a new starting model. The theoretical group and phase velocities are calculated by the Haskell method (Haskell, 1953) as modified by Harkrider (1964, 1970). In this study, for the Tibetan plateau, Chun and Yoshii's (1977) TP-4 model was used as the starting model. The computer program for the iterative stochastic inversion of surface wave dispersion data, written by Rodi (1977), was used to derive the earth model. The derived model is accepted if the RMS error between the observed and theoretical group velocities is satisfactorily small. An attempt to invert Rayleigh wave velocities for compressional velocity, shear velocity, and density simultaneously has been made.

We attempted to obtain a model which might fit all of the observed group velocities for Rayleigh waves. The final model is shown in Figure 1. The fit to the observed data is quite good for all the

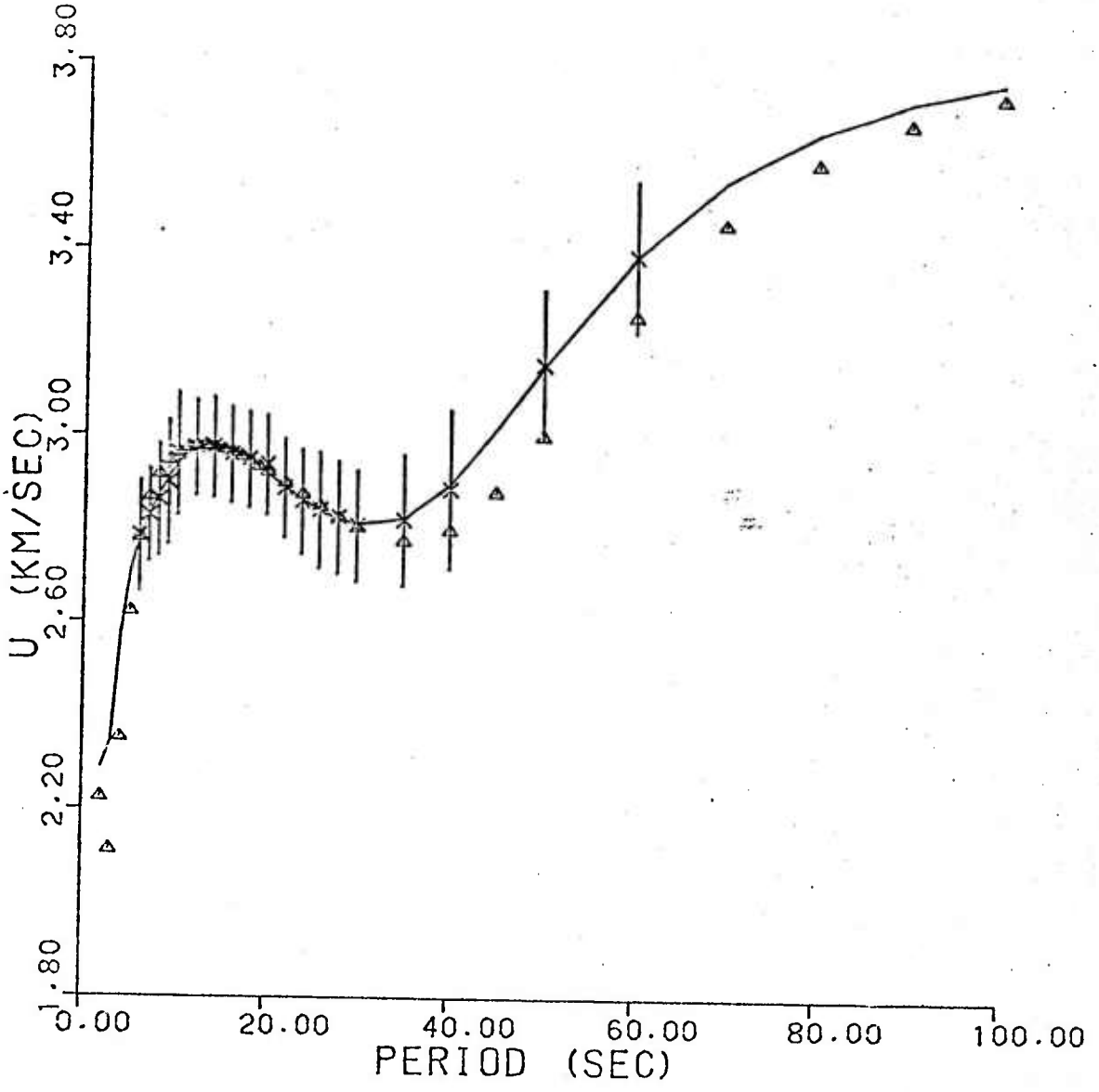

Figure 1. Rayleigh-wave group velocities for Tibetan plateau. Triangles represent group velocities for model TP-4. The solid line gives velocity obtained from the inversion method. Crosses and vertical bars indicate observed data and their standard deviation (see Figure 1 of previous semi-annual report)

periods considered. By comparing Figure 1 with Figure 1 of the previous semi-annual report, it is clear that the fit has been improved by the inversion method, especially at short periods.

Table 1 displays the parameters of the final model with standard deviations of the shear velocities. The standard deviations (S.D.) are generally quite large, as great as 0.768 km/sec. There seems to be no way to reduce S.D. values of the deeper layers.

Figure 2 shows the starting model and the final model obtained by the inversion method. Some features of the final model present in this figure: a lower velocity in the upper crust is required to fit the short-period observed group velocities, and a higher velocity in the upper mantle is required to match the observed long-period group velocities.

Figure 3 shows the resolving kernel versus depth at a few different depths. The resolution is reasonably good.

The inversion theory has also been applied to the attenuation data obtained by Yacoub and Mitchell (1977) (see Table 3 and Figure 4) for the Tibetan plateau to obtain average Q_β^{-1} models. We use the formulation of Anderson et al. (1965), assuming that the internal friction of the shear and compressional waves (Q_β^{-1} and Q_α^{-1}) is independent of frequency and that $Q_\beta^{-1} = 2Q_\alpha^{-1}$.

We have plotted the theoretical attenuation coefficients of fundamental-mode Rayleigh waves in Figure 5, and the corresponding final Q_β^{-1} models in Figure 6 as a function of depth beneath the Tibetan region. The theoretical γ values of Figure 5 seem too low at long periods as compared with observed data. But if we increase the γ

Table 1

Final Model Parameters for the Tibetan Plateau,
Obtained by Inverting Rayleigh Wave Data

LAYER	THICKNESS (km)	DEPTH (km)	P VELOCITY (km/sec)	S VELOCITY (km/sec)	DENSITY (g/cm^3)
1	0.70	0.35	4.549	2.655 ± 0.061	2.248
2	0.70	1.05	4.534	2.669 ± 0.167	2.262
3	0.70	1.75	4.528	2.734 ± 0.506	2.315
4	0.70	2.45	4.527	2.772 ± 0.713	2.363
5	0.70	3.15	4.530	2.759 ± 0.643	2.388
6	1.70	4.35	6.025	3.517 ± 0.243	2.782
7	1.70	6.05	6.026	3.362 ± 0.321	2.694
8	1.70	7.75	6.022	3.311 ± 0.441	2.644
9	1.70	9.45	6.018	3.377 ± 0.260	2.660
10	1.70	11.15	6.014	3.472 ± 0.261	2.702
11	3.20	13.60	6.010	3.520 ± 0.324	2.746
12	3.20	16.80	6.008	3.508 ± 0.232	2.756
13	3.20	20.00	6.006	3.448 ± 0.284	2.739
14	3.20	23.20	6.004	3.404 ± 0.354	2.726
15	3.20	26.40	6.002	3.391 ± 0.306	2.724
16	5.00	30.50	5.823	3.359 ± 0.219	2.691
17	5.00	35.50	5.822	3.399 ± 0.236	2.719
18	6.00	41.00	6.310	3.704 ± 0.261	2.886
19	6.00	47.00	6.307	3.756 ± 0.262	2.925
20	6.00	53.00	6.306	3.794 ± 0.260	2.959
21	6.00	59.00	6.306	3.813 ± 0.340	2.983
22	6.00	65.00	6.307	3.813 ± 0.768	2.998
23			7.70	4.45	3.300

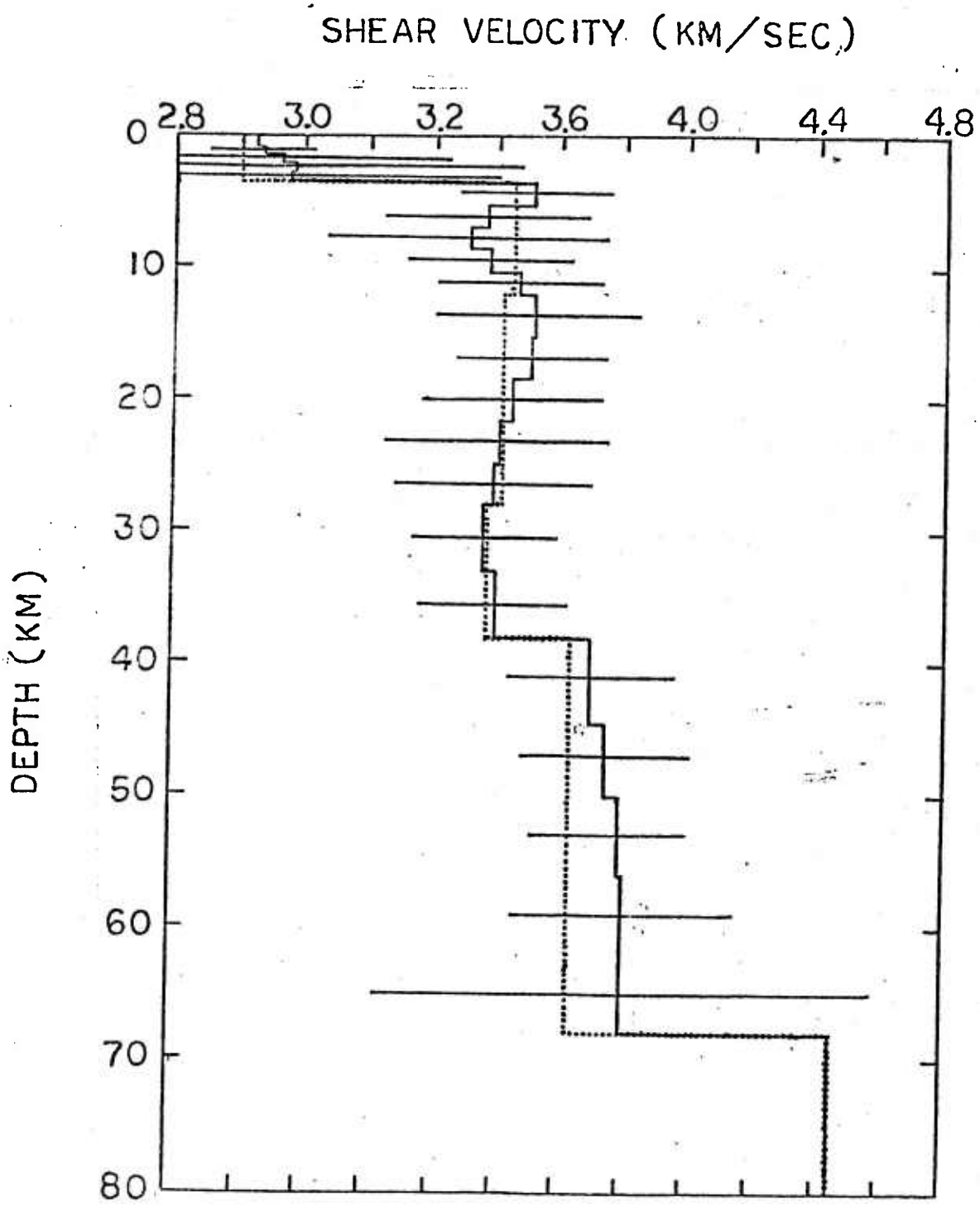

Figure 2. Shear velocity model and standard deviations for Tibetan plateau derived from the inversion of Rayleigh-wave group velocities. The dotted line indicates the starting model (TP-4) for the inversions

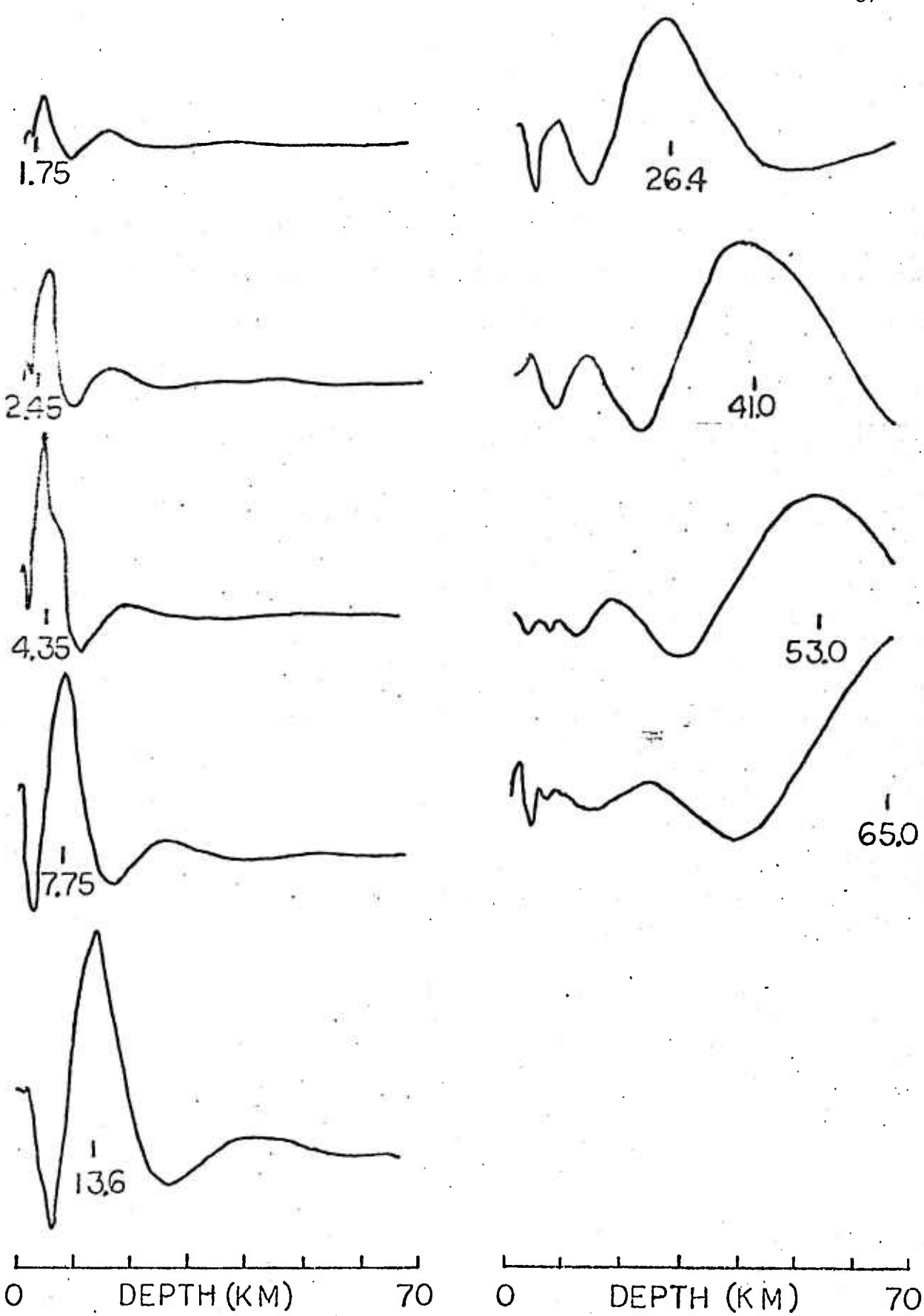

Figure 3. Averaging kernels for shear velocity perturbations in Tibetan plateau at various depths.

Table 2

Q_β^{-1} Model for Tibetan Plateau

LAYER	THICKNESS (km)	DEPTH (km)	Q_β^{-1} ($\times 10^{-3}$)
1	0.70	0.35	4.697
2	0.70	1.05	3.681
3	0.70	1.75	2.083
4	0.70	2.45	0.780
5	0.70	3.15	0.071
6	1.70	4.35	1.656
7	1.70	6.05	2.747
8	1.70	7.75	4.773
9	1.70	9.45	5.788
10	1.70	11.15	5.923
11	3.20	13.60	5.588
12	3.20	16.80	4.893
13	3.20	20.00	4.198
14	3.20	23.20	3.545
15	3.20	26.40	2.967
16	5.00	30.50	2.416
17	5.00	35.50	1.805
18	6.00	41.00	1.180
19	6.00	47.00	0.884
20	6.00	53.00	0.676
21	6.00	59.00	0.528
22	6.00	65.00	0.421
23	--	--	0.088

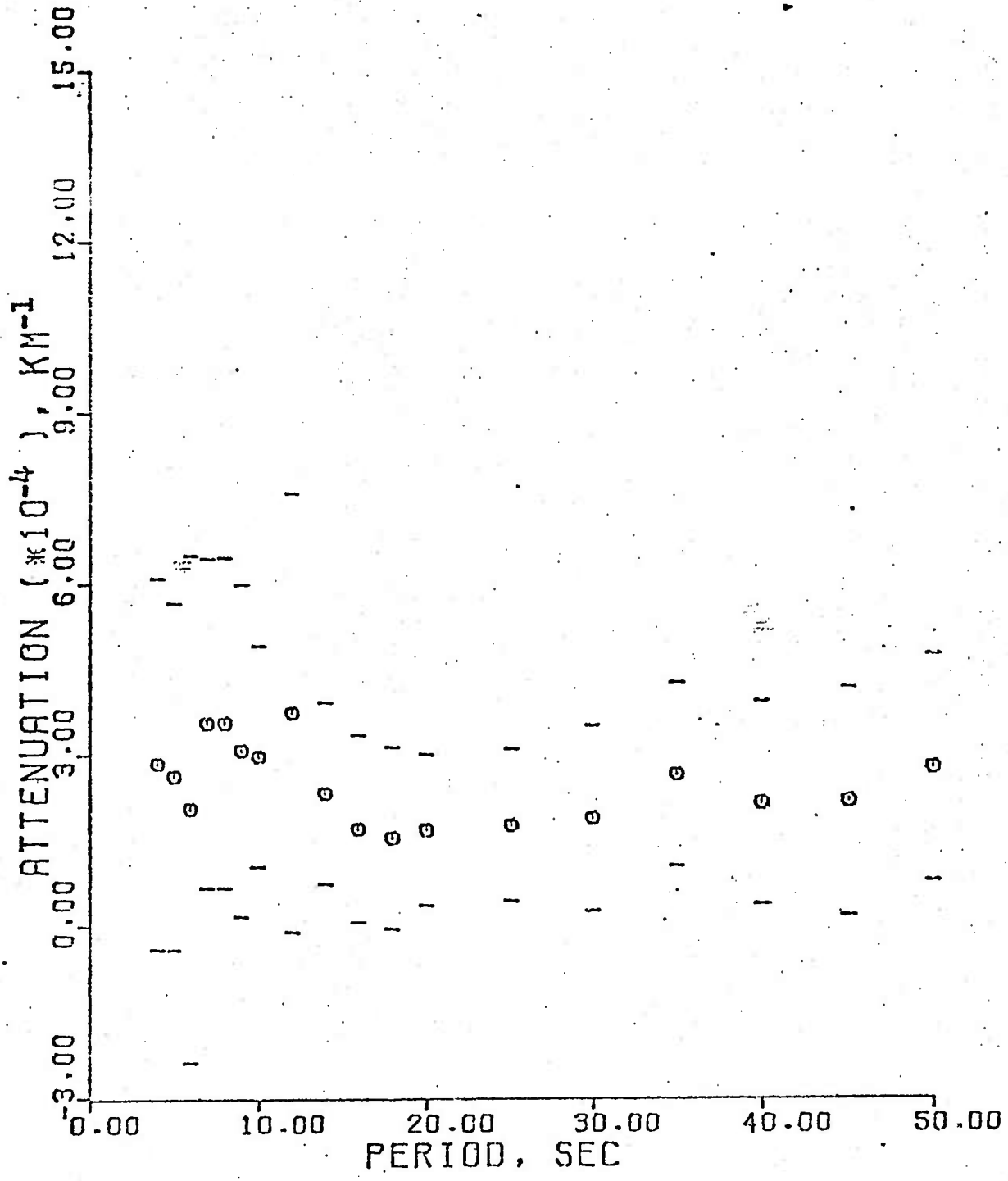

Figure 4. Rayleigh-wave attenuation coefficients for Tibetan region (after Yacoub and Mitchell, 1977)

Table 3

Rayleigh Wave Attenuation Coefficients for
Tibetan Region (after Yacoub and Mitchell, 1977)

PERIOD (sec)	$\gamma \times 10^{-4}$ (km^{-1})		S.D. $\times 10^{-4}$ (km^{-1})
4.0	5.737	$\pm$	3.655
5.0	6.422		3.318
6.0	6.284		4.733
7.0	7.501		3.407
8.0	7.451		3.353
9.0	7.172		3.238
10.0	6.783		2.560
12.0	6.946		4.831
14.0	4.365		2.184
16.0	3.193		1.737
18.0	3.397		1.498
20.0	3.138		1.517
26.0	2.481		1.810
30.0	2.156		2.176
35.0	3.240		2.159
40.0	3.378		2.246
45.0	3.201		2.735
50.0	3.159		2.742

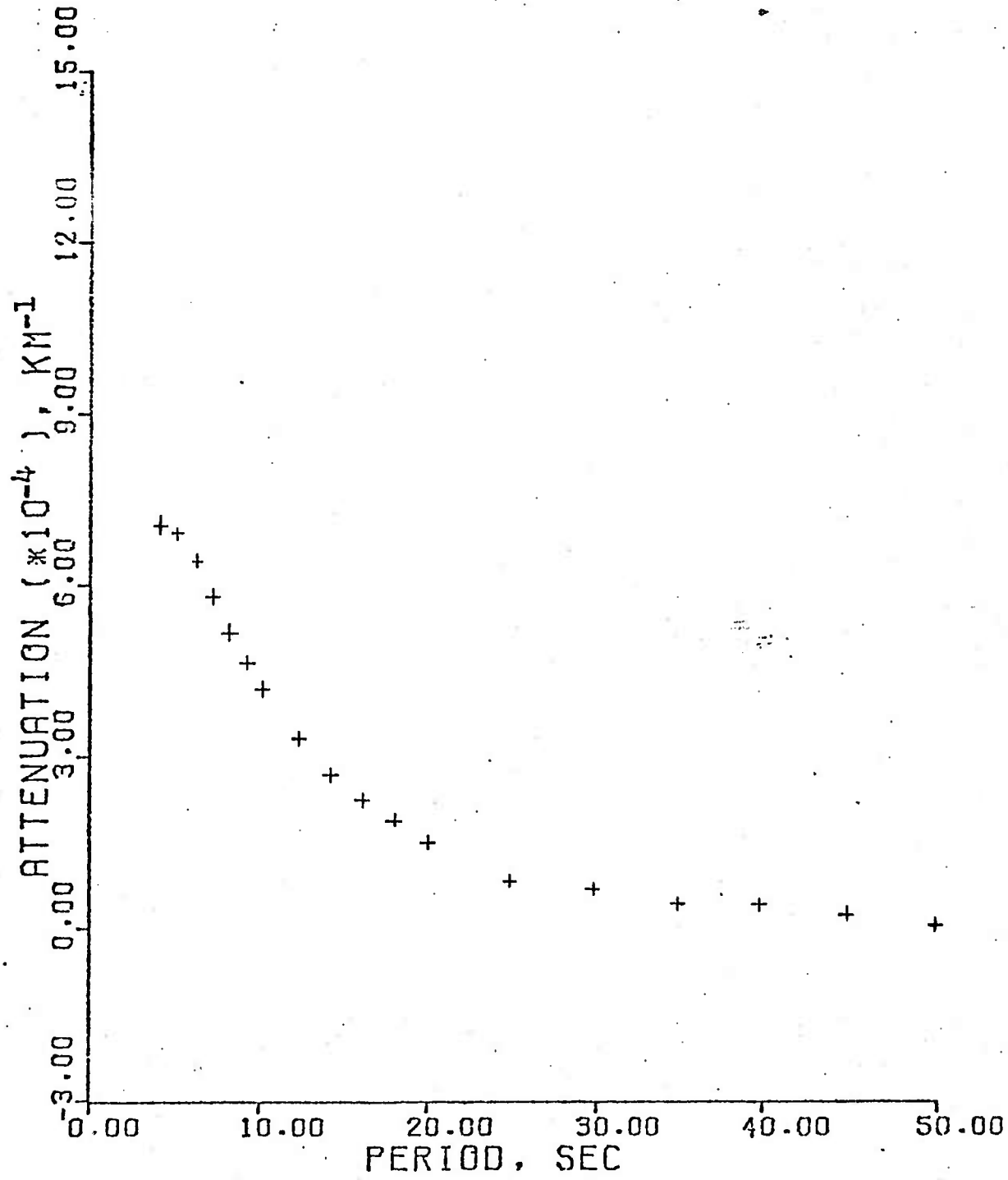

Figure 5. Theoretical attenuation coefficients for the fundamental-mode Rayleigh wave for the Tibetan region

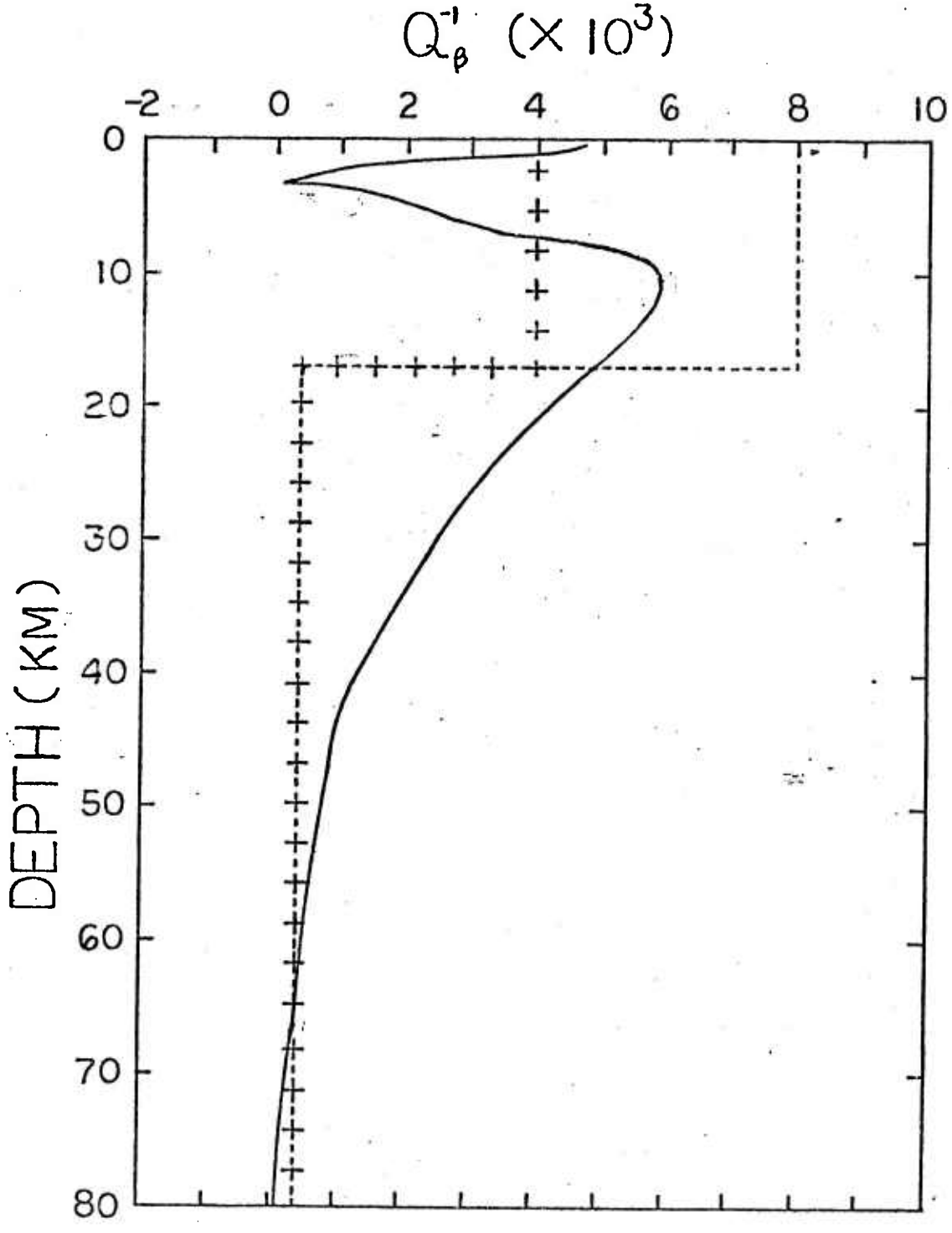

Figure 6. Q_β^{-1} model for Tibetan plateau (solid line), western North America (dashed line), and east-central North America (cross line).

values at long periods, we will get negative Q_β^{-1} values, which are unreasonable.

Figure 6 also presents the Q_β^{-1} models for western North America (dotted line) and east-central North America (cross line). Our Tibetan model has extremely low Q_β^{-1} value at a depth of about 3 km.

It is possible to investigate how well the earth model and attenuation coefficients satisfy the Rayleigh wave data by generating synthetic seismograms. We are attempting to compute such seismograms.

A Tibetan earthquake which occurred on July 14, 1973 at 13^h 39^m 30.0^s GMT, with focal depth of 20 km and hypocentral coordinates of 35.3^oN, 86.6^oE, is going to be studied to determine its source-time function. The fault plane solution shown in Figure 7 tell us it has strike-slip and normal components of faulting, which is in agreement with geologic, seismic and gravity data. We are going to attempt to obtain its source-time function by the inversion method in the research to be done in the following months.

Table 4

Theoretical Attenuation Coefficient Values
for Tibetan Region

PERIOD (sec)	$\gamma \times 10^{-4}$ (km^{-1})
4.0	7.120
5.0	6.817
6.0	6.391
7.0	5.844
8.0	5.253
9.0	4.680
10.0	4.160
12.0	3.310
14.0	2.679
16.0	2.202
18.0	1.835
20.0	1.543
26.0	0.952
30.0	0.699
35.0	0.477
40.0	0.327
45.0	0.229
50.0	0.167

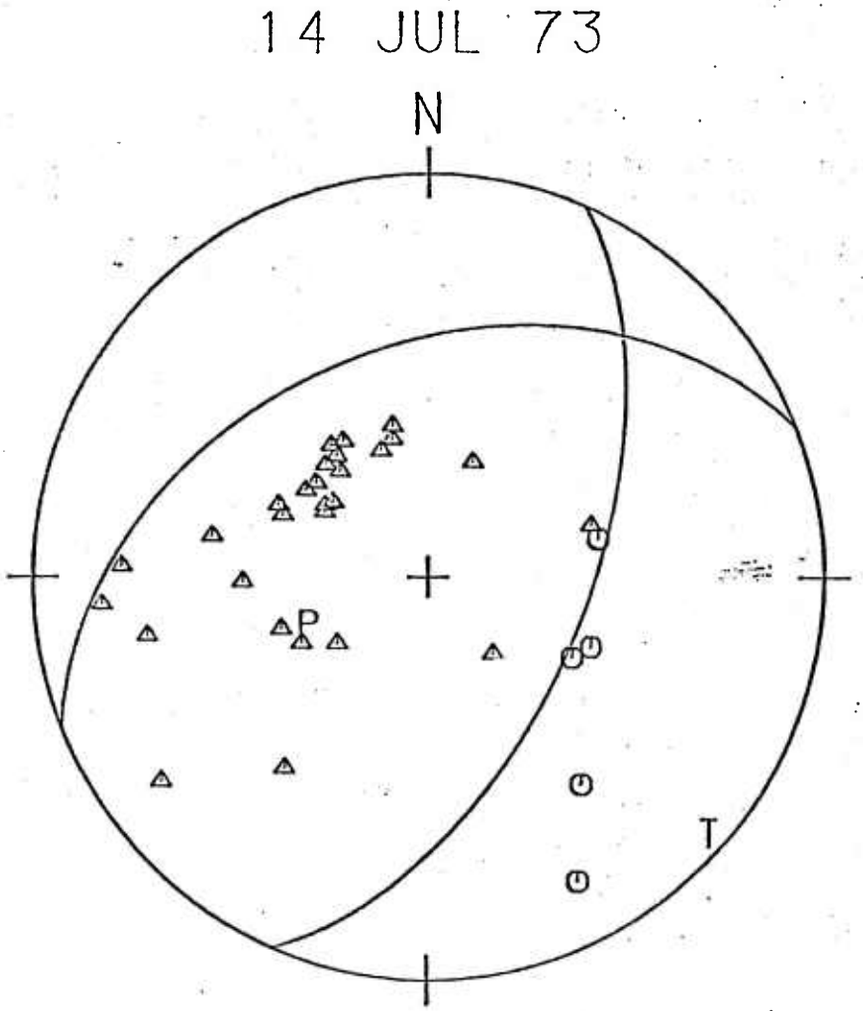

Figure 7. Fault-plane solution for the Tibetan earthquake of 14 July 1973. Triangles represent dilatational first motion, and octagons represent compressional first motion

REFERENCES

Anderson, D.L., A. Ben-Menahem and C.B. Archambeau, 1965. Attenuation of seismic energy in the upper mantle, J. Geophys. Res., 70, 1441-1448.

Backus. G. and F. Gilbert, 1970. Uniqueness in the inversion of gross earth data, Phil. Trans. Roy. Soc. (London), Ser. A, 266, 123-192.

Chun, K. and T. Yoshii, 1977. Crustal structure of the Tibetan plateau: A surface wave study by a moving window, Bull. Seism. Soc. Am., 67, 735-750.

Harkrider, D.G., 1964. Surface waves in multilayered elastic media, 1. Rayleigh and Love waves from buried sources in a multilayered elastic half space, Bull. Seism. Soc. Am., 54, 627-679.

Harkrider, D.G., 1970. Surface waves in a multilayered elastic media, 2. Higher mode spectra and spectral ratios from point sources in plane layered earth models, Bull. Seism. Soc. Am., 60, 1937-1967.

Haskell, N.A., 1953. The dispersion of surface waves in a multi-layered media, Bull. Seism. Soc. Am., 43, 17-34.

Rodi, W.L., 1977. A general linear inversion program for surface wave velocities, (personal communication).

Yacoub, N. and B. Mitchell, 1977. Attenuation of Rayleigh-wave amplitudes across Eurasia, Bull. Seism. Soc. Am., 67, 751-769.